MICROFLUIDIC SYSTEMS FOR INVESTIGATING AND MODULATING SINGLE-CELL CANCER INVASION DYNAMICS

A Dissertation

Presented to the Faculty of the Graduate School

of Cornell University

In Partial Fulfillment of the Requirements for the Degree of

Doctor of Philosophy

by

Michael Mak

January 2014

MICROFLUIDIC SYSTEMS FOR INVESTIGATING AND MODULATING SINGLE-CELL CANCER INVASION DYNAMICS

Michael Mak, Ph. D.

Cornell University 2014

My research entails the design and implementation of microfluidic systems to investigate the mechanical dynamics in cancer invasion at the single-cell level. Metastasis, the process of cancer spreading, is the leading cause of cancer related deaths, but the principles and dynamics that drive this process remain largely unknown. The challenge is in part due to the large spatial and temporal scales that the metastatic process spans, as it could involve single-cells transporting to distal sites across meters and over months to years. To address this challenge, my goal is to create microsystems that aim to recapitulate the critical steps in dissemination. Cell-scaled microchannels with subnucleus-scaled barriers are incorporated to elucidate the mechanical transition dynamics of invasive cancer cells. Single-cell – single-barrier interactions are induced and invasive behavior is elicited. Different regulators of invasion are explored, including molecular modulators of microtubules and actomyosin as well as mechanical factors such as dimensional, directional, and other engineered spatially asymmetric cues. Results of my work have shown that microtubule stabilization suppresses cell invasion across subnucleus-scaled barriers, physiologically ubiquitous mechanical cues such as dimensionality and directionality modulate migratory cell decision making, myosin IIa activity inhibition can alter invasion patterns, and certain mechanically asymmetric microenvironments can potentially suppress dissemination via the phenomenon *iteratio ad nauseam*.

BIOGRAPHICAL SKETCH

Michael Mak attended Brown University from 2004 to 2008 and completed a Bachelor of Science degree in Engineering and Physics with fulfillment of a Bachelor of Arts degree in Applied Mathematics. He became excited about biophysics and bioengineering and completed a senior thesis in biopolymer physics. He then joined the Biomedical Engineering Department at Cornell University in 2008 and subsequently became a member of the Erickson Lab, where he became actively involved in developing novel microfluidic technologies for cancer research. He was a National Science Foundation (NSF) Graduate Research Fellow from 2010 to 2013 and worked extensively with the National Cancer Institute (NCI) Physical Sciences in Oncology Centers (PS-OC), Cornell Nanofabrication Facility (CNF), and the Nanobiotechnology Center (NBTC). With support from the NSF and NCI, he created microfluidic systems aimed at elucidating the fundamental mechanical dynamics of cancer invasion. His goal is to continue uncovering the principles that drive metastasis and to develop and propagate new practical tools that can help find more effective strategies and therapies against cancer.

To family, friends, and humanity

ACKNOWLEDGMENTS

There are numerous factors that helped me through my Ph.D. research. Professor Erickson has been a wonderful advisor who has established an amazing intellectual environment in his lab that promotes innovative approaches to solve impactful problems. It is in this ambience and under his quality leadership that I was able to pursue and accomplish intellectually satisfying research. I am grateful for the support, guidance, and insights that Professor Erickson has provided throughout my graduate studies.

Professor Cynthia Reinhart-King has also been tremendously helpful in providing valuable discussions and openly offering insights and advice throughout our collaborative efforts and has helped guide my new found understanding and appreciation in cell mechanics and cancer research. She has been very encouraging of my continued pursuit in research and academia and I am grateful for her support. Professor Andrew Yen has continually offered excellent feedback for my work and provided helpful insights in leading my work towards exciting directions. Professor Zipfel has also given support and thoughtful advice on my research and future directions. I am very thankful for all of the valuable interactions that I have had with my supporting faculty members.

I also thank all of my friends and colleagues at the Erickson Lab. In particular, Bernardo Cordovez, Sudeep Mandal, Allen Yang, Aram Chung, Mekala Krishnan, Michael Kalontarov, Xavier Serey, Erica Jung, Matthew Mancuso, Li Jiang, Abdurrahman Gumus, Aadhar Jain, Pilgyu Kang and all other members of the Erickson lab have offered valuable feedback for my work and supported my

development since my early years in the lab. I am truly grateful for all of the discussions in our small and large group meetings, at random instances in the office, and outside of the lab. Furthermore, I thank the Reinhart-King lab for our collaborative efforts.

I acknowledge the funding sources and facilities that have made my research possible, specifically the National Science Foundation, the National Cancer Institute Physical Sciences in Oncology Centers, the Cornell Nanoscale Science and Technology Facility, and the Nanobiotechnology Center.

Finally, I thank my family for being supportive of all of my endeavors. My parents, grandparents, sister, aunts, uncles, and cousins have always believed in my capacity to succeed and have enabled me to always see the good in humanity.

TABLE OF CONTENTS

LIST OF FIGURES

CHAPTER 1

INTRODUCTION

1.1 Microfluidic Labs on Chips and Biology Applications

Microfluidics refers to fluidic systems and phenomena at the micrometer scale. These systems have been used widely in many different fields for many different applications, including biochemical analysis, particle manipulation and separation, drug delivery, drug screening, and cell-based assays [1-3]. The key advantages of using microfluidics include small sample size requirements, highly parallel and high throughput operations, and precise and controllable physical, geometric, and chemical profiles and interfaces [4-6].

1.1.2 Basic Considerations in Microfluidic Design and Operation

Here, a brief description of operational microfluidic principles is presented. In particular, I will focus mainly on pressure driven flow, which is the primary mode of fluid manipulation used in the research presented in this dissertation. The motion of an incompressible Newtonian fluid with no body forces is governed by the following form of the Navier-Stokes equation:

$$\rho\left(\frac{\partial \boldsymbol{v}}{\partial t} + \boldsymbol{v}\cdot\boldsymbol{\nabla v}\right) = -\nabla P + \mu\boldsymbol{\nabla^2 v} \qquad (1.1a)$$

where ρ is the fluid density, v is the velocity, P is the pressure, and μ is the dynamic viscosity. The left side of equation 1.1 contains the inertial terms and the right most element is the viscous term. The ratio of the inertial forces to the viscous forces in a fluidic system is known as the Reynolds number R_e, given by:

$$R_e = \frac{\rho v_m D_H}{\mu} \qquad (1.1b)$$

where v_m is the mean fluid velocity and D_H is the hydraulic diameter of the microfluidic channel. As a typical example for experiments here, for a microfluidic channel with a hydraulic diameter of 12μm and filled with water (μ ≈ 1mPa*s, ρ ≈ 1000kg/m^3) flowing at 500μm/s, R_e = 0.006. At low Reynolds number R_e << 1, inertial terms can be neglected, leaving a simplified version of equation 1.1a:

$$0 = -\nabla P + \mu \boldsymbol{\nabla^2 v} \qquad (1.1c).$$

In this regime and from equation 1.1c, it can be shown that the volumetric flow rate Q of a fluid with dynamic viscosity μ in a rectangular channel with height h, width w (w > h), and length L is related to the pressure drop across the channel ΔP by [2]:

$$Q = \frac{\Delta P}{R_H} \qquad (1.1d)$$

where R_H is the hydrodynamic resistance given by:

$$R_H = \frac{12\,\mu L}{w h^3} * \frac{1}{1 - O} \qquad (1.1e)$$

and O is the correction factor for microchannels with rectangular cross-sections, given by:

$$O = 0.627411 * \frac{h}{w} \qquad (1.1f).$$

For typical operations of devices used in my research, considering a microchannel with width = 15μm, height = 10μm, length = 1mm, and a pressure gradient across the channel of 100Pa, the average flow velocity if the solution is water is approximately

equal to 500μm/s. References on fluid mechanics and microfluidic system design considerations can be found in [2] and fluid mechanics textbooks.

1.1.3 Applications in Cell Dynamics

In this dissertation, the focus is the use of microfluidic systems for the analysis of cell mechanics and dynamics, particularly in the context of cancer metastasis and cell invasion. Well defined geometries spanning the subnucleus and cell scales are used to induce cell transition dynamics and behavioral phenomena that provide insights toward the fundamental physical principles that govern cell invasion [7, 8].

1.2 Cancer Metastasis and Mechanics

Metastasis is the leading cause of cancer related deaths. Once disseminated, cancer becomes a systemic disease that cannot be solved simply through surgical removal of the primary tumor. Existing standards for cancer therapies, however, are primarily aimed towards anti-growth rather than anti-spread targeting [9-13]. Additionally, studies have shown that a few cells, potentially as few as a single disseminated cancer cell, are sufficient for distal colonies to form [14, 15].

Recent work has demonstrated that cancer is a highly complex process that is likely beyond the scope of conventional biological approaches such as genomics. Many non-traditional factors come into play, such as cell to cell heterogeneity and cell-microenvironment interactions[16-19]. For instance, different parts of the same tumor can exhibit different gene expression profiles [17], suggesting that targeted therapy may leave subpopulations of tumor cells that do not express particular biomarkers

unaffected [20, 21]. Additionally, extracellular matrix (ECM) mechanics has been shown to modulate and even revert the invasive behavior of cancer cells [19, 22].

Many other mechanical factors are starting to emerge that may have important implications in cancer metastasis. For instance, microfluidics and optical forced-based tools have shown that metastatic cells tend to be more deformable. Traction force microscopy has shown that metastatic cancer cells tend to generate high contractile forces. Confined microchannel environments have been demonstrated to enable highly persistent unidirectional cell migration.

Cell mechanics is an intrinsic factor of the metastatic cascade, as cancer metastasis is ultimately a mechanical transport phenomena in which tumor cells break free from the primary tumor, invade through small pores in the ECM, intravasate into the vasculature, circulate and traffic in blood and lymphatic vessels, and extravasate and invade into other sites to form distal colonies [16, 23, 24]. While many biochemical factors and cell signaling events play important roles in driving this process, cancer cells must still mechanically transport from point a to point b across a series of mechanical barriers. Furthermore, research via conventional biology techniques has uncovered many of the critical signaling pathways that modulate cancer growth and dissemination [25]. The mechanical aspects, however, remain elusive and under-explored. One of the major challenges in understanding the mechanics of cancer and cancer metastasis in general is that these processes can span months to years over length scales from micrometers to meters. Thus, a comprehensive analysis of the dynamics of cancer require long term studies over large scales but with high spatial and temporal resolution, which is extremely impractical and further complicated by the resolution limits of medical imaging modalities such as computed tomography

(CT) and magnetic resonance imaging (MRI), which cannot resolve single-cell phenomena and thus cannot detect metastasis until sizable colonies have already formed.

Therefore, to understand the fundamental dynamics of cancer progression, it is necessary to create model systems that incorporate features that recapitulate the critical steps in metastasis. In my work, I have focused on mechanical environments and dimensional and geometric effects. This is particularly interesting because even in the presence of matrix metalloproteinase (MMP) inhibitors, which prevent cells from degrading their local environment to create paths for invasion, cancer cells are still able to mechanically remodel the ECM or mechanically squeeze through small gaps to invade [26-28]. Thus, the capacity to invade mechanically and the response to mechanical features in the microenvironment may be critical properties that fundamentally drive cancer dissemination.

1.3 Single-Cell Invasion Dynamics in Engineered Microfluidic Environments

To fully appreciate heterogeneity in cancer cells and the mechanical dynamics of invasion, I developed microfluidic systems that interface individual cells with individual mechanical barriers. The idea is to probe cell transition dynamics when encountering confined spaces, which is prevalent in the tumor microenvironment and along the metastatic cascade, from small pores of the ECM to tight endothelial junctions.

New device designs were prototyped and fabricated at the Cornell Nanoscale Facility (CNF) and soft lithography was performed to create polydimethysiloxane (PDMS)

microfluidic chips. To probe the impact of the rate-limiting steps in cell invasion, confined microchannels with subnucleus-scaled barriers were created. Since the nucleus is large, stiff, and the most obstructive element in mechanical invasion [8, 29], transition dynamics during invasion can be appreciated and higher order effects beyond cell velocities and displacements can be induced and visualized.

Previous studies have shown that cells spontaneously respond to physical and topographical cues, leading to persistent 1-D motion along straight microchannels and patterned lines [30, 31]. In my thesis work, I have developed more refined microgeometries with subnucleus-scaled features in order to probe transition dynamics and decision making in response to dimensional and polarization effects during invasion. In these environments, single cells encounter single barriers, and complex cell-barrier interactions are elicited. Asymmetry in the microenvironment induces symmetry breaking during cell migration and can bias the pattern of cell invasion. In my research, I have revealed the behavior of invading cancer cells, in particular the MDA-MB-231 highly metastatic breast adenocarcinoma cell line, under mechanical asymmetry and showed that dimensionality, directionality, and motor protein targeting, *e.g.* inhibiting non-muscle myosin IIa via blebbistatin, can all modulate the invasion behavior of cells. Additionally, microtubule targeting drugs, particularly Paclitaxel (taxol) can suppress the super-diffusive migratory behavior of typical invasive cells and prevent invasion across subnucleus-scaled barriers [8].

By understanding cell behavior in response to dimensional, mechanical, and geometric modulation, which are ubiquitous elements in the physiological environment that are currently under-appreciated, it may be possible to reveal new insights towards modulating cell invasive behavior and novel targets for therapy. Well-defined

geometries achievable in microfabricated devices can thus reveal subtle phenomenological events that are otherwise difficult to gauge in heterogeneous 3D ECM and gel-based models that are commonly used.

1.4 Research Overview and Dissertation Outline

Chapter 2 introduces the application of physical spatial gradients for studying cell transition dynamics during invasion. Many current studies are performed using symmetric environments, such as straight microchannels, which cannot probe the impact of physical changes in the microenvironment on cell invasion. During metastasis, however, cancer cells often encounter interfaces, *i.e.* a change in the local environment, and their responses in these encounters can reveal the responsivity of cells towards mechanical barriers. Three different cell lines were used in this study – bovine aortic endothelial cells, MCF-10a non-metastatic breast epithelial cells, and MDA-MB-231 highly metastatic breast adenocarcinoma cells. The results of the study demonstrate that cells respond physical spatial gradients and the response can be characterized by a two-state system – cells that permeate into the more confined region and cells that repolarize and turn around once the microchannel becomes more confining. Metastatic cells and non-metastatic cells exhibit different behaviors. Finally, cell transition dynamics are induced when cells encounter the spatial gradient, leading to multiple phases in the cell migratory response where the cell slows down, pauses, and gains speed again in both permeation and repolarization cases.

Chapter 3 emphasizes on the transition dynamics of MDA-MB-231 cells during invasion across serial subnucleus-scaled mechanical barriers. Transition dynamics are induced and cell nuclei are deformed during invasion. The effect of the degree of confinement on cell invasion is tested by using different barrier lengths - 10μm-long

barriers that are shorter than typical cells and 60μm barriers that are longer than typical cells in suspension. Transition dynamics are probed and multiple phases are revealed and their durations are characterized. Different strategies of mechanical invasion are also revealed, as phenomena such as back extensions, cell body rotations, and simple contractions are demonstrated that facilitate cell deformations across the subnucleus barriers. Next, taxol, a microtubule targeting drug conventionally used for its anti-mitotic effects, was tested for anti-invasion effects. I showed that taxol suppressed the super-diffusive behavior of invading cancer cells in microchannels and also abolished cell permeation across subnucleus-scaled barriers, demonstrating the anti-invasion capacity of this class of chemotherapeutic. Finally, I also revealed that mechanical asymmetry can induce asymmetry in cell division, particularly for the taxol-resistant variant of MDA-MB-231 cells.

Chapter 4 discusses a serial microfluidic micropipette system and its application in measuring cell deformation dynamics over sequential constrictions. Current methods for studying cell deformability include atomic force microscopy (AFM), micropipette aspiration (MPA), and novel micro and optofluidic systems such as inertial flow focusing and optical stretchers [32]. AFM and MPA require complex setups and laborious manual operations and existing microfluidic techniques often measure highly simplistic one-shot measurements such as cell aspect ratio. The serial microfluidic micropipette system developed here addresses some of these critical issues with a simple and automated operational workflow and the ability to perform multiple strain measurements per cell in a highly parallel format.

Chapter 5 describes the implementation of novel microfluidic designs aimed to uncover fundamental mechanical factors that govern migratory cell decision making

during invasion. Dimensional, directional, and biochemical modulations are used to control invasion behavior, and a new concept is introduced in using mechanical asymmetry to suppress cell dissemination by inducing the phenomenon *iteratio ad nauseam*.

Chapter 6 summarizes the dissertation and my contributions thus far in developing and implementing microfluidic systems for the study of single-cell cancer dynamics.

REFERENCES

1. P. S. Dittrich and A. Manz, *Nature Reviews Drug Discovery*, 2006, **5**, 210-218.
2. H. A. Stone, A. D. Stroock and A. Ajdari, *Annu. Rev. Fluid Mech.*, 2004, **36**, 381-411.
3. T. Thorsen, S. J. Maerkl and S. R. Quake, *Science*, 2002, **298**, 580-584.
4. G. M. Whitesides, *Nature*, 2006, **442**, 368-373.
5. N. L. Jeon, S. K. W. Dertinger, D. T. Chiu, I. S. Choi, A. D. Stroock and G. M. Whitesides, *Langmuir*, 2000, **16**, 8311-8316.
6. Y.-C. Tan, J. S. Fisher, A. I. Lee, V. Cristini and A. P. Lee, *Lab on a Chip*, 2004, **4**, 292-298.
7. M. Mak, C. A. Reinhart-King and D. Erickson, *Plos One*, 2011, **6**.
8. M. Mak, C. A. Reinhart-King and D. Erickson, *Lab on a Chip*, 2013, **13**, 340-348.
9. M. A. Jordan and L. Wilson, *Nature Reviews Cancer*, 2004, **4**, 253-265.
10. G. F. Weber, *Cancer Letters*, 2013, **328**, 207-211.
11. J. Sleeman and P. S. Steeg, *European Journal of Cancer*, 2010, **46**, 1177-1180.
12. N. Sethi and Y. Kang, *Nat Rev Cancer*, 2011, **11**, 735-748.
13. L. Chen, S. Yang, J. Jakoncic, J. J. Zhang and X.-Y. Huang, *Nature*, 2010, **464**, 1062-1066.
14. E. Quintana, M. Shackleton, M. S. Sabel, D. R. Fullen, T. M. Johnson and S. J. Morrison, *Nature*, 2008, **456**, 593-598.
15. M. Al-Hajj, M. S. Wicha, A. Benito-Hernandez, S. J. Morrison and M. F. Clarke, *Proc. Natl. Acad. Sci. USA.*, 2003, **100**, 3983-3988.
16. I. J. Fidler, *Cancer Research*, 1978, **38**, 2651-2660.
17. M. Gerlinger, A. J. Rowan, S. Horswell, J. Larkin, D. Endesfelder, E. Gronroos, P. Martinez, N. Matthews, A. Stewart, P. Tarpey, I. Varela, B. Phillimore, S. Begum, N. Q. McDonald, A. Butler, D. Jones, K. Raine, C. Latimer, C. R. Santos, M. Nohadani, A. C. Eklund, B. Spencer-Dene, G. Clark, L. Pickering, G. Stamp, M. Gore, Z. Szallasi, J. Downward, P. A. Futreal and C. Swanton, *The New England Journal of Medicine*, 2012, **366**, 883-892.
18. M. Shackleton, E. Quintana, E. R. Fearon and S. J. Morrison, *Cell*, 2009, **138**, 822-829.
19. M. J. Paszek, N. Zahir, K. R. Johnson, J. N. Lakins, G. I. Rozenberg, A. Gefen, C. A. Reinhart-king, S. S. Margulies, M. Dembo, D. Boettiger, D. A. Hammer and V. M. Weaver, *Cancer Cell*, 2005, **8**, 241-254.
20. R. J. Gillies, D. Verduzco and R. A. Gatenby, *Nat Rev Cancer*, 2012, **12**, 487-493.
21. X. Li, M. T. Lewis, J. Huang, C. Gutierrez, C. K. Osborne, M.-F. Wu, S. G. Hilsenbeck, A. Pavlick, X. Zhang, G. C. Chamness, H. Wong, J. Rosen and J. C. Chang, *Journal of the National Cancer Institute*, 2008, **100**, 672-679.
22. M. J. Bissell and D. Radisky, *Nat Rev Cancer*, 2001, **1**, 46-54.
23. A. F. Chambers, A. C. Groom and I. C. MacDonald, *Nature Reviews Cancer*, 2002, **2**, 563-572.
24. E. Sahai, *Nature Reviews Cancer*, 2007, **7**, 737-749.

25. D. Hanahan and R. A. Weinberg, *Cell*, 2011, **144**, 646-674.
26. E. Sahai and C. J. Marshall, *Nature Cell Biology*, 2003, **5**, 711-719.
27. K. Wolf, I. Mazo, H. Leung, K. Engelke, U. H. v. Andrian, E. I. Deryugina, A. Y. Strongin, E.-B. Bröcker and P. Friedl, *The Journal of Cell Biology*, 2003, **160**, 267-277.
28. P. Friedl and K. Wolf, *Nature Reviews Cancer*, 2003, **3**, 363-374.
29. P. Friedl, K. Wolf and J. Lammerding, *Current Opinion in Cell Biology*, 2011, **23**, 55-64.
30. D. Irmia and M. Toner, *Integrative Biology*, 2009, **1**, 506-512.
31. A. D. Doyle, F. W. Wang, K. Matsumoto and K. M. Yamada, *The Journal of Cell Biology*, 2009, **184**, 481-490.
32. G. Bao and S. Suresh, *Nature Materials*, 2003, **2**, 715-725.

CHAPTER 2

MICROFABRICATED PHYSICAL SPATIAL GRADIENTS FOR INVESTIGATING CELL MIGRATION AND INVASION DYNAMICS

2.1 Abstract

We devise a novel assay that introduces micro-architectures into highly confining microchannels to probe the decision making processes of migrating cells. The conditions are meant to mimic the tight spaces in the physiological environment that cancer cells encounter during metastasis within the matrix dense stroma and during intravasation and extravasation through the vascular wall. In this study we use the assay to investigate the relative probabilities of a cell 1) permeating and 2) repolarizing (turning around) when it migrates into a spatially confining region. We observe the existence of both states even within a single cell line, indicating phenotypic heterogeneity in cell migration invasiveness and persistence. We also show that varying the spatial gradient of the taper can induce behavioral changes in cells, and different cell types respond differently to spatial changes. Particularly, for bovine aortic endothelial cells (BAECs), higher spatial gradients induce more cells to permeate (60%) than lower gradients (12%). Furthermore, highly metastatic breast cancer cells (MDA-MB-231) demonstrate a more invasive and permeative nature (87%) than non-metastatic breast epithelial cells (MCF-10A) (25%). We examine the migration dynamics of cells in the tapered region and derive characteristic constants that quantify this transition process. Our data indicate that cell response to physical spatial gradients is both cell-type specific and heterogeneous within a cell population, analogous to the behaviors reported to occur during tumor progression. Incorporation

Reprinted with permission from PLoS, Michael Mak, Cynthia A. Reinhart-King, and David Erickson, "Microfabricated Physical Spatial Gradients for Investigating Cell Migration and Invasion Dynamics," *PLoS ONE* 6(6): e20825 (2011). doi:10.1371/journal.pone.0020825

of micro-architectures in confined channels enables the probing of migration behaviors specific to defined geometries that mimic *in vivo* microenvironments.

2.2 Introduction

Metastasis is the leading cause of cancer related deaths. The mechanisms and effects of metastasis often span large spatial and temporal scales, which make any experimental and analytical characterization difficult. To address the need for characterizing and screening the metastatic potential of cells, researchers have begun looking for mechanical markers at the single cell level [1-3]. This is particularly useful since metastasis has been characterized as an inefficient process that eventually works due to very small subpopulations of successfully invasive cells. This notable feature has also led to an emphasis on understanding the importance of heterogeneity within cancer cell populations, as certain subpopulations are speculated to be more apt to progress through the entire metastatic cascade. The importance of heterogeneity and the implications of different heterogeneous phenotypes on cancer metastasis, however, have not yet been fully resolved [4-9]. Of particular interest are phenotypes that promote motility and invasiveness, as these properties are often associated with metastasis.

In many instances during the metastatic process, cancer cells encounter spatial gradients. Examples include cells navigating through small pores in the extracellular matrix (ECM) during invasion through the stroma, intra- and extravasation across tight junctions of the endothelium, and migration through the microvasculature especially in vessel branch points [1,3,10,11] – all illustrated in Fig. 2.1. Essentially, in many scenarios in which a cell interacts with an interface where its degrees of freedom of

motion or effective mobility are changed, the local microenvironment exhibits a spatial gradient. Understanding the mechanical responsivity of a cell when encountering spatial gradients, particularly in the context of squeezing into tight spaces during invasion, can elucidate phenomenological attributes associated with metastatic cells.

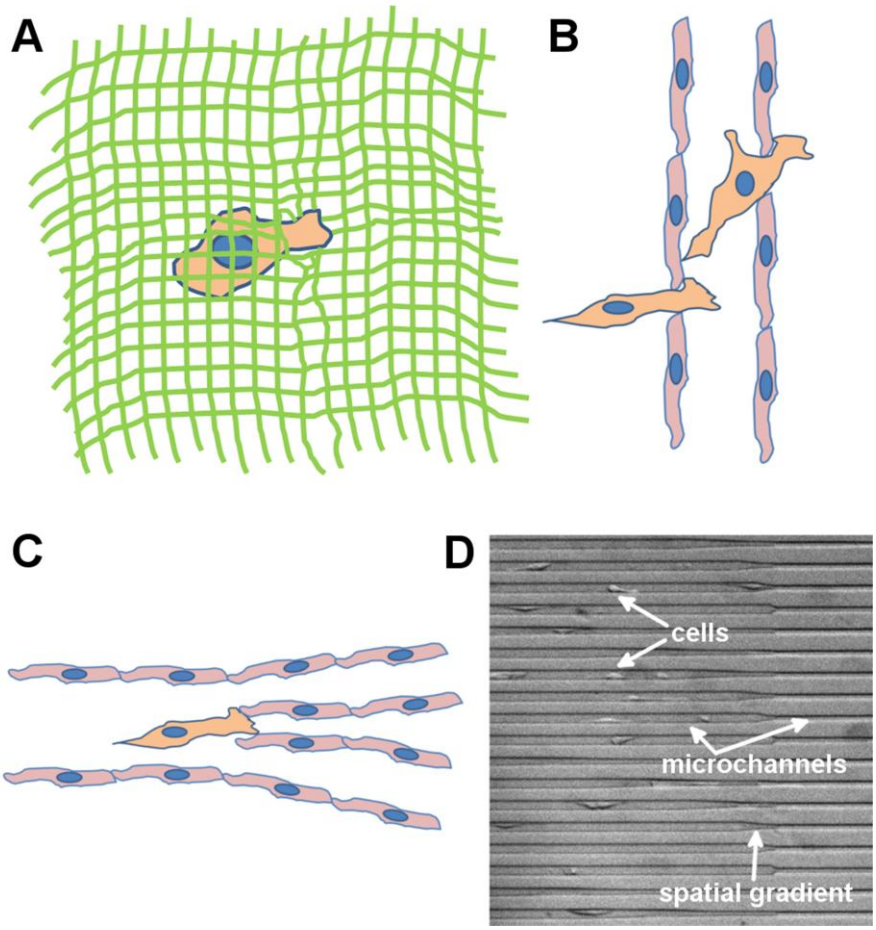

Figure 2.1. Cells encountering spatial gradients in physiological and simulated environments. A-C. A cancer cell (orange) is (A) navigating through small pores in the extracellular matrix (green) as it is invading through the tumor stroma, (B) squeezing through the endothelium (red cells) during intra- and extravasation, and (C) encountering vessel branch points upon migration in the microvasculature. D. Cells migrating in our tapered microchannel device, which simulates physiological spatial gradients encountered by cells during the metastatic process. The width of the larger channel is 15μm.

A number of recent studies have used microfluidic and micropatterning techniques to simulate microenvironments that may be relevant to cancer cell migration. Asymmetric patterns generated on 2D substrates via etching or microcontact printing have been shown to direct cell motion [12-14]. Studies using long and straight microchannels with small cross-sectional areas comparable to the cell size, which simulate confined paths in tissues, the microvasculature, and lymphatic vessels [10], have shown that in such environments, cells are able to move unidirectionally with unusually high persistence as compared to 2D studies on flat substrates with no confining boundaries [15,16]. The physiological microenvironment, however, is diverse and non-uniform. Therefore, straight microchannels, a zeroth order environment (i.e. no perturbations in the direction of cell migration), provide limited means of extracting information about a cell's responsivity. By introducing small perturbations, higher order effects can be examined that may allow one to better understand how individual cells respond to a perturbation to its steady-state.

To accomplish this, here we have developed and conducted cell migration experiments in spatially tapered microchannels with cross-sectional areas comparable to the cell size. This provides a good model for cell navigation through physical constraints and spatial gradients, which are important during metastasis. Typical experiments (Fig. 2.1 d) for weakly and strongly metastatic cells in these environments are shown in supplementary videos S2.1 and S2.2, respectively. We demonstrate and compare the mechanical responsivity of three cell types: 1) bovine aortic endothelial cells (BAECs), which are a primary cell culture used here to provide basic insights toward mechanical and migratory behavior of adherent cells in tapered microchannels, 2) MCF-10A, a non-transformed human mammary epithelial cell line

used here to represent non-metastatic cells, and 3) MDA-MB-231, a highly metastatic human cell line derived from metastatic breast carcinoma used in this study to model highly metastatic cells.

To date, most experiments involving engineered microenvironments and cell mechanics have been considered only in the steady-state. For instance, chemotactic responses, migration through straight confinement channels, and many other studies of cell migration, polarization, and morphology have only been characterized by average and steady-state velocities, directional persistence, and other ensemble averaged mechanical properties [15-18]. Cell behavior, however, is governed by both spatially and temporally varying molecular signals and feedback [19-23]. These transient dynamics, such as the activation of intracellular processes in response to external mechanical or chemotactic stimuli, have not been considered in great detail. In this study, we investigate the transient cell dynamics caused by spatial, physical gradients.

2.3 Results

2.3.1 Heterogeneity and Statistical Behavior

To investigate the migratory response of cells to physical spatial gradients, we designed an array of PDMS microchannels bonded to a glass substrate. The device design and fabrication procedure are shown in Fig. 2.2. Each channel consists of a tapered junction of variable spatial gradient that connects a large (cross-sectional area: 15μm x 10μm) channel with a small (4μm x 10μm) channel. Six different gradients are incorporated, and for the studies here they are categorized as either "high" (tapering angle larger than 7 degrees) or "low" (tapering angle smaller than 3 degrees) gradients (see Fig. 2.2 caption for more details). Cells migrate unidirectionally in the

large channel towards the small channel and their behavior in the tapered region is observed via timelapse microscopy (approximately 24hrs per experiment) and analyzed. See methods section for more details on the fabrication of the microfluidics.

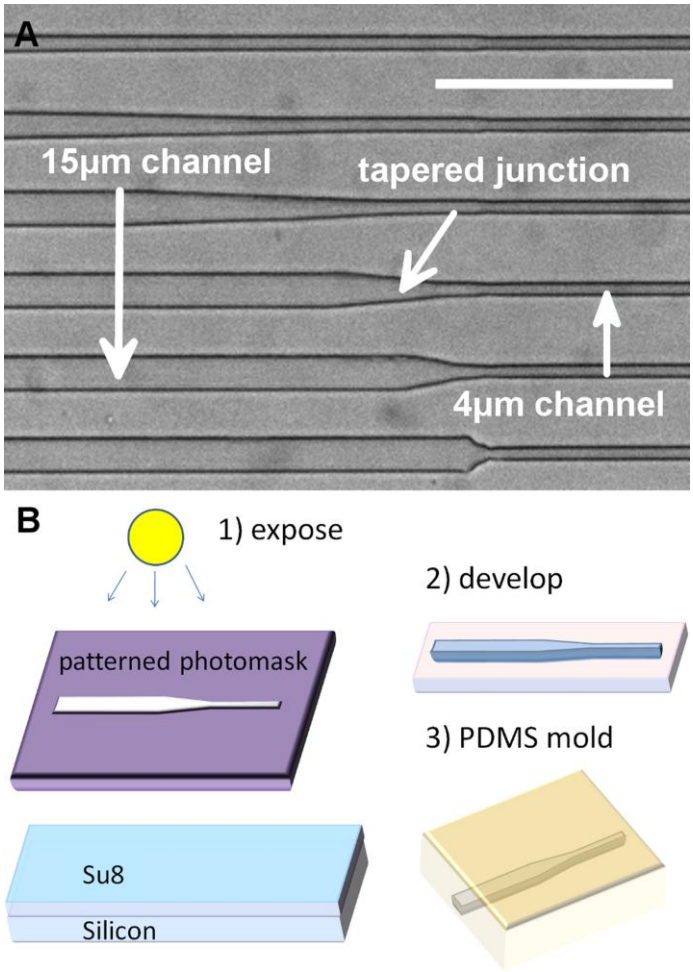

Figure 2.2. Design patterns and device fabrication process. A. Image of actual device tapered microchannels from brightfield microscopy. Larger channels (15µm x 10µm) are connected to smaller channels (4µm x 10µm) via a tapered junction. The tapering angles are 1, 2, 3, 7, 15, and 40 degrees from low to high. The first three junctions are considered "low gradients" and the last three are considered "high gradients." Scale bar 100µm. B. Schematic of fabrication procedure. Standard contact photolithography is used to pattern SU8 masters which are then used in PDMS soft lithography to generate microchannels.

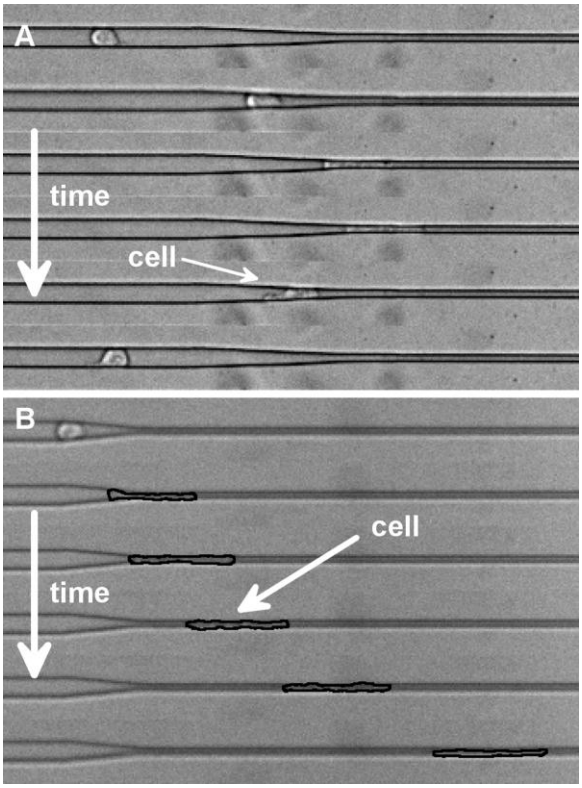

Figure 2.3. Heterogeneous cell behavior in tapered junctions. A-B. Timelapse montage of a cell (MCF-10A) (A) turning back once reaching the tapered region (each frame is 0.96hrs) and (B) permeating into the smaller channel (each frame is 2.5hrs). Width of larger channel is 15μm. See supplementary materials for timelapse videos of all 3 cell types studied.

We characterize the cell as a two-state system where each state corresponds to its polarization, which is determined here based on the direction of cell migration. Since the cell is confined to migrate in 1D, only two polarizations exist, forward and backward. We measure the probability of occurrence of each state upon a cell's interaction with the tapered geometry. Specifically, the two states are determined as: 1) a cell penetrating through the tapered junction and permeating into the smaller channel (*i.e.* the entire cell body is inside the smaller channel), and 2) a cell turning around (repolarizing) once reaching the tapered region and migrating in the backwards

direction. Sample experiments demonstrating both states are shown in Fig. 2.3, and supplementary Videos S2.3-S2.6 show timelapse movies of various cell types migrating in the devices and exhibiting various behaviors. All cells considered are initially migrating in the direction pointing from the larger channel to the smaller channel. To account for random repolarizations due to distance traveled and the different lengths of tapered junctions of different spatial gradients, a fixed interaction length (250μm between tapered region and start of small channel) is considered for each cell. All and only cells entering this region are considered, so random repolarizations due to distance traveled are weighted equally in all junctions. Furthermore, cells that die or have not made a conclusive decision by the end of each timelapse experiment are ignored. Cells interacting with other cells are also ignored.

First, our results demonstrate the non-trivial existence of these two states, as both have been observed with appreciable frequency. We have identified two distinct migratory phenotypes, permeating cells and repolarizing cells. Here, phenotype refers to any observable characteristic or behavior of the cell. The occurrence of these two states enables us to quantify migratory invasiveness both in the same cell population and across different cell types with a simple binary analysis. We characterize these events by their probability of occurrence and show that there is a significant dependence of this property on both the spatial gradient of the tapered junction and the cell type.

Fig. 2.4 shows the response of different cell types to the spatial gradient of the tapered junction. For BAECs, the probability of permeation (into the small channel once reaching the tapered region from the large channel) is greater for higher spatial gradients (60%, $n = 20$) than for lower gradients (12%, $n = 17$) ($p<.05$). In other words, more gradual transitions tend to induce cells to repolarize more often.

Furthermore, for the subset of cells that experience this more gradual transition, the probability of repolarization (88%) is statistically higher than permeation (12%) ($p<.05$). For MCF-10A's, the probability of permeation is 50% (n=10) for low gradients and 25% (n=8) for high gradients. For MDA-MB-231's, the probability of permeation is 86% (n=7) for low gradients and 87% (n=15) for high gradients.

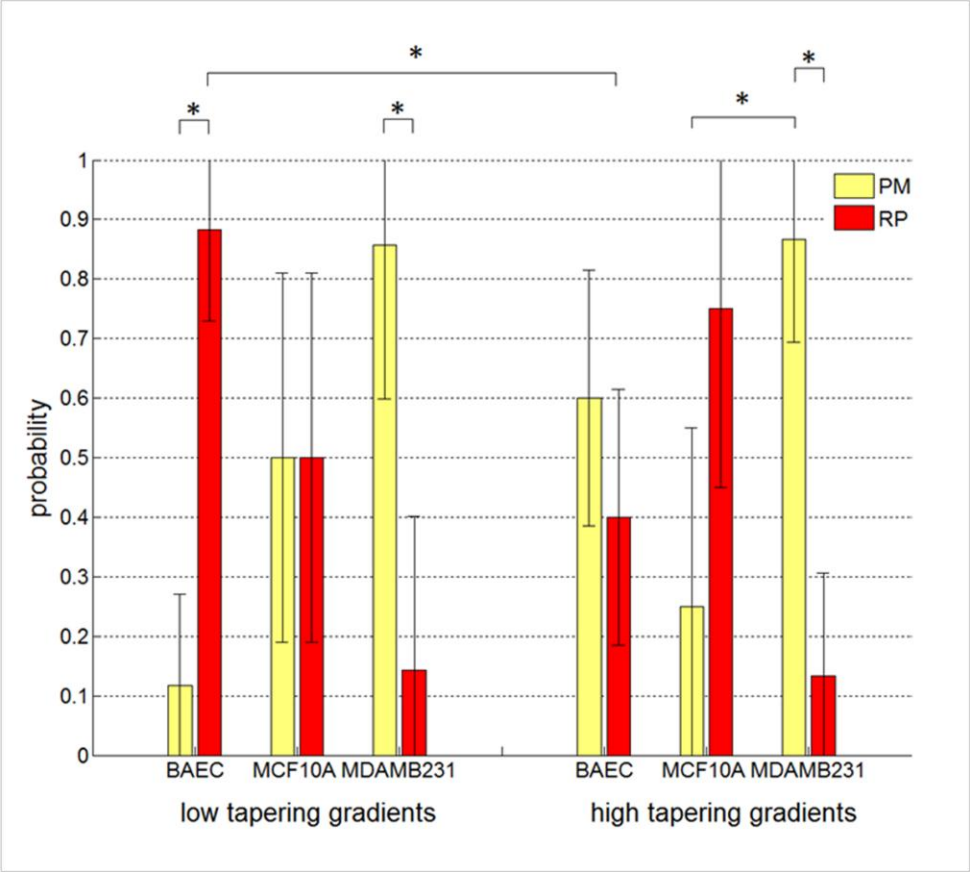

Figure 2.4. Cell behavior statistics at the tapered junction. Data plots showing the probability of cell permeation (PM, yellow) and repolarization (RP, red) for low and high gradient tapers for three different cell types. Error bars represent 95% confidence intervals calculated from the standard deviation of Bernoulli experiments. * denotes statistical difference, p-value <.05, between data at the nodes of each line.

The response of highly metastatic MDA-MB-231 cells shows several distinguishing features. First, the probability of permeation for both low and high gradients is statistically greater than the probability of turning around ($p<.05$). For low gradient tapers, this result is opposite to that of BAECs. Next, in comparison with non-metastatic breast epithelial cells (MCF-10A's), MDA-MB-231 cells exhibit a statistically higher ($p<.05$) probability of permeation for high gradient tapers. These differences, particularly the latter case, can potentially be distinguishing factors between highly metastatic cells and non-metastatic cells. A higher probability of permeation in a spatially tapered and highly confining microenvironment for a particular cell type may indicate greater invasiveness in the context of cancer metastasis.

It has been shown previously that small channels which force cells to deform significantly in order to enter have a much lower probability of cell permeation upon contact [16]. Our results, particularly for MDA-MB-231's, show that there is a substantial permeative population into the smaller channel despite such highly constrictive spatial domains. This may imply that once a cell has entered into a mode of 1D unidirectional migration, its permeative and invasive capabilities are enhanced, at least in the direction of motion. Physiologically this may suggest that there is a feedback mechanism that once a metastatic cancer cell has entered into a defined track in the extracellular matrix or microvasculature, it gains increased aggressiveness during invasion into more confining spaces.

2.3.2 Cell Transition Dynamics and Signaling Feedback on the Single Cell Level

The tapered channel assay presented above can also be used as a label-free method of quantitatively characterizing signaling feedback on the single cell level by analyzing the mechanical responsivity of cells and profiling cell migration transition dynamics. Responsivity is the factor that maps an external input to an output of interest. Here, the input is the transformation of space and the output is the induced cell migration dynamics. Cell dynamics involve intracellular signaling which entails feedback loops to ensure a robust and rapid cell response. Feedback (whether electrical, mechanical, or biological) can often manifest mathematically as an exponential (sigmoid) curve [20,21]. Therefore, we fit the velocity profile of cells migrating in the spatially tapered region into sigmoid curves and derive characteristic transient constants. We note the sequential activation of two feedback loops (one negative and one positive). The model we used for curve fitting is:

$$velocity = \frac{v_i - v_{f1}}{1 + \exp(c_1(t - t_{01}))} + \frac{v_f - v_{f1}}{1 + \exp(-c_2(t - t_{02}))} + v_{f1}$$

where v_i is the initial steady-state velocity, v_f is the final steady-state velocity, $1/c_1$ is the time constant of the first sigmoid, $1/c_2$ is the time constant of the second sigmoid, t_{01} is the time for the mid-point of the first sigmoid, t_{02} is the time for the mid-point of the second sigmoid, and v_{f1} is the final steady-state velocity if the second sigmoid is not present. By analyzing the temporal evolution of the cell's velocity, we can extract several key parameters of the transition process – 1) the time constants of the sigmoid curves (the net signaling feedback loops) and 2) the temporal delay between the activation of the two net signaling processes ($t_{02} - t_{01}$).

The first process is a negative feedback loop that diminishes the speed of the cell as it encounters additional spatial constraints (*i.e*. the spatial taper). The second process is a positive feedback loop that accelerates the cell to a steady-state velocity in the direction it has chosen to pursue after encountering the spatial gradient. The delay

in the activation of these two signaling processes is likely time used to reorganize the cell's cytoskeletal network for permeation into a more confining channel or repolarization for migration in a different direction.

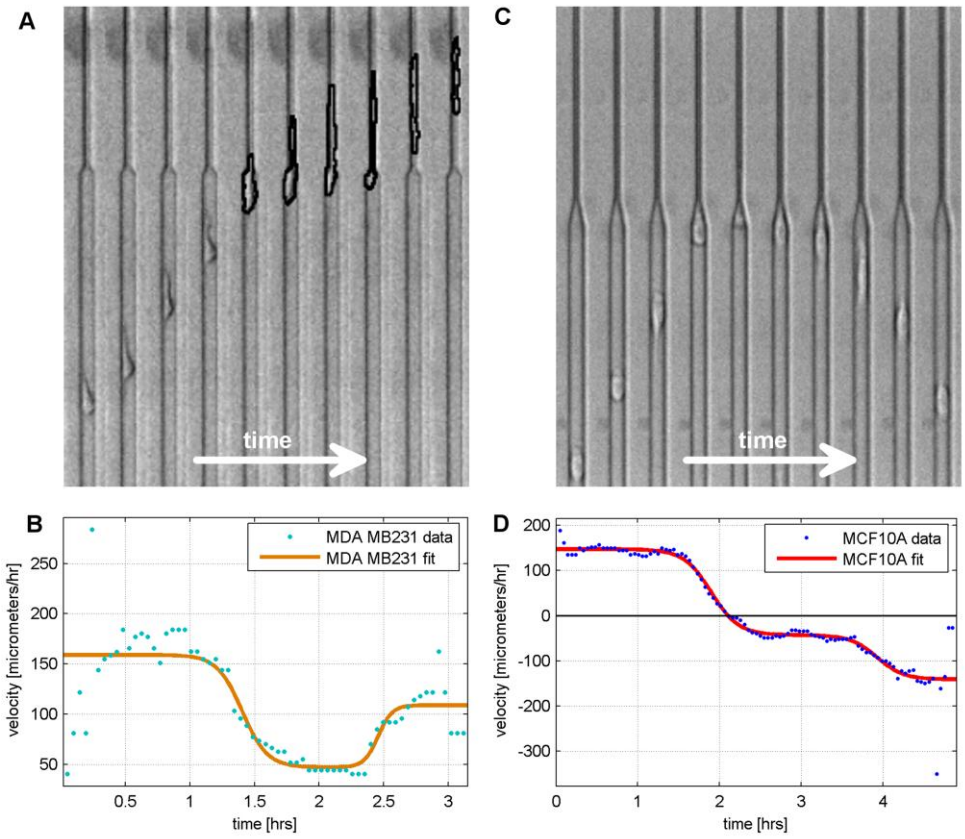

Figure 2.5. Migration dynamics of repolarizing and permeating cells. A-B. Timelapse image stack (A) juxtaposed on top of the data and sigmoid curve fit of the velocity profile on the same time interval (B) of a permeating MDA-MB-231 cell during transition in the tapered junction. The time constants for the first and second sigmoidal curves are approximately 6 and 3 minutes, respectively, and the delay constant is 1 hour. R^2 of the fit is 0.7. **C-D.** Timelapse image stack (C) juxtaposed on top of the data and sigmoid curve fit of the velocity profile on the same time interval (D) of a repolarizing MCF-10A cell during transition in the tapered junction. The time constants for the first and second sigmoidal curves are both approximately 10 minutes, and the delay constant is 2 hours. R^2 of the fit is 0.94.

Two time constants and a delay constant provide suitable curve fits for the velocity profile of cells undergoing this transition. For example, as shown in Fig. 2.5a for a permeating cell, the two time constants are 6 and 3 minutes, respectively, and the delay constant is 1 hour, and as shown in Fig. 2.5b for a repolarizing cell, the two time constants are both approximately 10 minutes and the delay constant is 2 hours. Time and delay constants for different cells can vary (from minutes to hours) indicating potentially diversity in signaling pathways at play and the cytoskeletal complex of individual cells. This illustrates the importance of considering single cell dynamics rather than ensemble averages, particularly for the analysis of cancer cell mechanics since metastatic potential may be dictated by heterogeneous subpopulations displaying more invasive characteristics [7-9]. This method presents a way of measuring the signaling of a net biological process which may be more meaningful than the expression of individual signaling molecules that may contribute to a multitude of pathways and phenotypes.

2.4 Discussion

In this study, we have investigated the migratory behavior of different cell types in response to physical spatial gradients. We focused on the transition region connecting a larger channel to a smaller channel and demonstrated the effect of varying the spatial gradient of the junction on cell responsivity. We also showed that the highly metastatic cells used here (MDA-MB-231's) have a statistically higher permeative nature into smaller regions than non-metastatic cells (MCF-10A's), at least when the spatial gradient is high.

Previous work that used highly confining environments to study cell migration and adhesion dynamics has primarily involved straight and symmetric microchannel structures. For example, Jacobelli *et al.* [24] demonstrated that myosin IIA regulates the crawling mode of T-cell migration by analyzing the "walking" and "sliding" adhesion dynamics of T-cells when migrating in straight confinement microchannels. Hawkins *et al.* [25] developed a mathematical model that addresses spontaneous motion in narrow channels based on actin polymerization within a model cell. Furthermore, Irmia and Toner [15] demonstrated that mechanical confinement can induce spontaneous unidirectional migration in cells, and migration rates are affected by microtubule-disrupting drugs such as Taxol and Nocodazole. These studies clearly showed the rich information about cell mechanics and motility that can be extracted by imposing physical constraints in the cells' local microenvironment. However, the data from these previous experiments were based on spontaneous cell reactions in a static environment with no perturbative features for stimulating cell responsivity. Very little information can be extracted about cell behavior at barriers and interfaces, which is especially important when considering metastasis, during which cancer cells are often transitioning across impeding junctions and into new environments. One such interface is the increase in physical constraint (as illustrated in Fig. 2.1), which our assay simulates. By introducing a spatially tapering region into microchannels, cells are stimulated at the interface and responses are induced. Therefore, stimulated dynamics rather than steady-state or spontaneous reactions can be studied.

Additionally, we elucidated the existence of behavioral differences within a common cell type in response to a tapered microgeometry; all cell types used here exhibited both permeating and repolarizing subpopulations. The existence of these two states demonstrates phenotypic heterogeneity in mechanical invasiveness among a

common population of cells. Whether this heterogeneity is static or dynamic (*i.e.* whether the same cells always exhibit the same phenotype or this phenotype fluctuates in time for all cells) and the implications of either are currently not known and further studies are required. Heterogeneous subpopulations in tumors have been shown [26,27], but the contributions to metastatic potential are not well understood [5,7,8]. Our technique presents a way of probing this heterogeneity based on mechanical properties on a single cell level.

Furthermore, migration dynamics under transition phases can provide insights into the mechanical responsivity of cells that can ultimately be mapped to intracellular signaling feedback mechanisms. For instance, one of the key contributors to cell locomotion is the actin machinery, where the polymerization and depolymerization of actin filaments provide force that drives cells in the direction of motion [28,29]. The velocity of cells then should be approximately proportional to the number of actively contributing actin filaments, and the velocity profile measured in this study should therefore be representative of actin signaling dynamics (*i.e.* the concentration profile of actin in the polarized edge of the cell, with negative values indicating that the polarization has changed directions).

Finally, our data indicate that metastatic MDA-MB-231 cells exhibit a more invasive phenotype (greater motility through the high gradient channels) than non-metastatic MCF-10A and BAECs. Because metastasis is a highly physical process that involves cell migration and deformation, our microfabricated system may have uncovered a novel mechanism by which metastatic cells enter narrow capillary beds of organs – cells may move through capillaries through active migration rather than simply passive flow transport. In our system, high and low gradient tapers may simulate vessel branch points and continuation along the main branch, respectively.

Overall, by introducing additional parameters, *e.g.* variable geometric constraints, in engineered microenvironments, more information can be deduced about cell-environment interactions, such as mechanical triggers for cell repolarization and stability and persistence of cell polarization when perturbed externally. Investigation of the migratory response of cells to spatial constrictions could be valuable in elucidating other mechanical markers of metastasis.

As with most *in vitro* experimental systems, there are important caveats to address. Two important properties are the compliance of the materials used and the dimensionality of the system compared with physiological environments. The boundaries of our microchannels are glass, which is effectively purely rigid, and PDMS (10:1 ratio of silicone elastomer to curing agent), which has an elastic modulus of around 10^3 kPa [30,31]. Typical physiological surfaces that cells adhere to are soft and viscoelastic tissues comprising of the extracellular matrix and other cells (with elastic moduli between 10-10000 Pa) [32-35], which can be deformable under cellular forces [30,32,36,37]. Strong connective tissue and blood vessel walls can have elastic moduli on the order of 1 MPa [31,33]. The complexity of the physiological environment, with such properties as non-uniform pore sizes and varying viscoelasticity in addition to dynamically regulated chemical signaling and proteolysis [35,38-42], makes it difficult to quantitatively analyze the fundamental principles of any physical processes. To begin to derive the governing properties of cell migration and invasion, it is important to simplify the experimental domain. With our assay, we are essentially considering a limiting case in which the compliance is low (relative to soft tissues) at the microchannel walls and infinite inside and along the channel. By reducing the width of the channel through physical tapering, we are reducing the "effective compliance" as experienced by the cells. Similarly, the dimensionality of

our microchannel system can be considered as either 1-D, since cells are primarily moving along one axis, or pseudo 3-D, since cells can adhere to and interact with the four surrounding walls. Typical experiments that are supposed to mimic more physiological 3-D environments are conducted with cells embedded in extracellular matrix-simulating gels [40,43,44]. Fraley *et al.* [45], for example, demonstrated that cell motility in these 3-D environments does not rely significantly on focal adhesion formation and depends on traction between cell protrusions and the surrounding matrix, both of which are different than 2-D motility. While 3-D experiments are excellent in elucidating more physiological mechanisms of cell motility, it is difficult to simulate and modulate interfaces, which as mentioned throughout this paper have important physiological consequences, in 3-D gels. Furthermore, the cell-in-gel model may not be the most accurate with regards to cell dynamics in microcapillaries, where the surrounding matter is the vessel wall and the interior is fluid (*e.g.* Yamauchi *et al.* [10] showed that cell dynamics in micro-vessels are relevant during the metastatic process). One of the main advantages of the confined microchannel approach is the ability to introduce and tune interface geometries. Ultimately, our tapered channel assay enables the quantitative analysis of the ability of a cell to transition from a region with higher degrees of freedom in movement to a region with lower degrees of freedom. Extensions of this assay could incorporate extracellular matrix components and multiple cell types in the channels to simulate more physiological conditions.

2.5 Methods

2.5.1 Cell Culture

BAECs (VEC Technologies) were maintained at 37^{o} C and 0% CO_2 in Leibovitz L-15 media supplemented with 10% Fetal Bovine Serum and 1% Pen/Strep. Experimentation was conducted using the same media under the same condition.

MDA-MB-231 cells from the American Type Culture Collection (ATCC, HTB-26) were maintained at 37^{o} C and 5% CO_2 in DMEM supplemented with 10% Fetal Bovine Serum. Experimentation was conducted in the same condition except with DMEM replaced by L-15 and at 0% CO_2.

MCF-10A cells from the ATCC (CRL-10317) were maintained at 37^{o} C and 5% CO_2 in DMEM/F12 supplemented with 5% Horse serum, 0.5 μg/ml Hydrocortisone, 20ng/ml hEGF, 10 μg/ml Insulin, 100 ng/ml Cholera toxin, 100 units/ml Penicillin, and 100 μg/ml Streptomycin. Experimentation was conducted in the same condition except with the addition of 10mM HEPES buffer and at 0% CO_2. During experiments, the pH of cell culture media was monitored periodically by observing the color of the media due to the phenol red dye. No significant changes were seen. Furthermore, fresh media with the addition of 10mM HEPES buffer for pH stabilization were replenished every 24 hours.

Note: The media used for each cell type are based on the ATCC (American Tissue Culture Collection) or National Institutes of Health Physical-Sciences and Oncology Center specifications, also delineated by Debnath *et al.* [46] and Guise *et al.* [47].

2.5.2 Microchannel Fabrication

As shown in Fig. 2.2b, standard contact photolithography is used to generate an SU8 (MicroChem, Newton, MA) on silicon master that is used to create PDMS (10:1

silicone elastomer to curing agent ratio) (Dow Corning, Midland, MI) molded microchannels, which are bonded to a glass slide. In the designed pattern, as shown in Fig. 2.2a, a tapered junction of variable spatial gradient connects a large (cross-sectional area: 15μm x 10μm) channel with a small (4μm x 10μm) channel.

2.5.3 Cell Loading and Preparation for Experiments

Two fluidic injection ports are incorporated into the microchannel device – one on the side of the larger channels (inlet) and one on the side of the smaller channels (outlet). Cells are loaded into the inlet and allowed to proliferate and migrate into the larger channels. During experiments, devices are placed on top of a heating stage maintained at 37^{o} C.

2.5.4 Cell Migration Trajectory and Velocity Tracing

Timelapse microscopy conducted on an inverted microscope with a 10x objective, with a temporal resolution of 2.88 min/frame, was used to record cell migration in microchannels. The center of mass of cells was tracked manually through image stacks using ImageJ, and velocities were calculated by linear approximation with adjacent frames. Each velocity data point was then averaged with the neighboring 10 points for smoothening and noise filtering.

2.5.5 Statistical Analysis of Cell Permeation Vs. Repolarization

Since we are considering a binary system and assuming the behavior of each cell represented by the data can be considered as an independent event, the statistics should follow the Bernoulli distribution. The statistical variance v of the cell behavior is then pq, where p and q are the probabilities of cell permeation and repolarization, respectively. By the central limit theorem [48] for a sample of size n, the error of estimating p (and q) from our experimentally acquired value of p_e (and q_e) should follow a normal distribution. Mathematically:

$$N(0,1) = \frac{n \times (p_e - p)}{\sqrt{n \times v}}$$

where N(0,1) is notation for the standard normal distribution. To calculate confidence intervals:

$$p_e - N(0,1) \times \sqrt{\frac{v}{n}} \leq p \leq p_e + N(0,1) \times \sqrt{\frac{v}{n}}$$

and N(0,1) is 1.96 for 95% confidence and v is approximated by our experimental values as $p_e q_e$. For further details see [48].

2.6 Acknowledgements

We thank Dr. Teresa Porri and Joseph Califano for helpful discussions on cell culture. The work described was supported by the Cornell Center on the Microenvironment and Metastasis through Award Number U54CA143876 from the National Cancer Institute. This work was performed in part at the Cornell NanoScale Facility, a member of the National Nanotechnology Network, which is supported by the NSF (Grant ECS-0335765). Michael Mak is a NSF Graduate Research Fellow.

2.7 Supporting Information

Video S2.1. Sample high-throughput (multichannel) experiment of MCF-10A cells migrating in tapered microchannel device. The frame rate is 10000 times faster than real-time (every second in the video corresponds to 2.78 hours). The widths of the larger and smaller channels are 15 and 4 μms, respectively.

Video S2.2. Sample high-throughput (multichannel) experiment of MDA-MB-231 cells migrating in tapered microchannel device. The frame rate is 10000 times faster than real-time (every second in the video corresponds to 2.78 hours). The widths of the larger and smaller channels are 15 and 4 μms, respectively.

Video S2.3. BAEC permeating through the tapered microchannel. The frame rate is 10000 times faster than real-time (every second in the video corresponds to 2.78 hours). The widths of the larger and smaller channels are 15 and 4 μms, respectively.

Video S2.4. BAEC turning around (repolarizing) once reaching the tapered region. The frame rate is 10000 times faster than real-time (every second in the video corresponds to 2.78 hours). The widths of the larger and smaller channels are 15 and 4 μms, respectively.

Video S2.5. MCF-10A cell permeating through the tapered microchannel. The frame rate is 10000 times faster than real-time (every second in the video corresponds to 2.78 hours). The widths of the larger and smaller channels are 15 and 4 μms, respectively.

Video S2.6. MCF-10A cell turning around (repolarizing) once reaching the tapered region. The frame rate is 10000 times faster than real-time (every second in the video

corresponds to 2.78 hours). The widths of the larger and smaller channels are 15 and 4 μms, respectively.

REFERENCES

1. Chambers A F, Groom A C, and MacDonald I C (2002) Dissemination and growth of cancer cells in metastatic sites. Nature reviews 2: 563-572.
2. Paszek M J, Zahir N, Johnson K R, Lakins J N, Rozenberg G I, et al. (2005) Tensional homeostasis and the malignant phenotype. Cancer Cell 8: 241-254.
3. Sahai E (2007) Illuminating the metastatic process. Nature Reviews Cancer 7: 737-749.
4. Altschuler S J, and Wu L F (2010) Cellular Heterogeneity: Do Differences Make a Difference? Cell 141: 559-563.
5. Kelly P N, Dakic A, Adams J M, Nutt S L, and Strasser A (2007) Tumor Growth Need Not Be Driven by Rare Cancer Stem Cells. Science 317: 337.
6. Stratton M R, Campbell P J, and Futreal P A (2009) The cancer genome. Nature 458: 719-724.
7. Visvader J E, and Lindeman G J (2008) Cancer stem cells in solid tumours: accumulating evidence and unresolved questions. Nature Reviews Cancer 8: 755-768.
8. Shackleton M, Quintana E, Fearon E R, and Morrison S J (2009) Heterogeneity in Cancer: Cancer Stem Cells versus Clonal Evolution. Cell 138: 822-829.
9. Fidler I J (1978) Tumor Heterogeneity and the Biology of Cancer Invasion and Metastasis. Cancer Research 38: 2651-2660.
10. Yamauchi K, M. Yang K H, P. Jiang N Y, Tsuchiya H, Tomita K, et al. (2008) Induction of cancer metastasis by cyclophosphamide pretreatment of host mice: an opposite effect of chemotherapy. Cancer Research 68: 516-520.
11. Friedl P, and Wolf K (2003) Tumour-Cell Invasion and Migration: Diversity and Escape Mechanisms. Nature Reviews Cancer 3: 363-374.
12. Jiang X, Bruzewicz D A, Wong A P, Piel M, and Whitesides G M (2005) Directing cell migration with asymmetric micropatterns. Proc Natl Acad Sci USA 102: 975-978.
13. Kumar G, Ho C C, and Co C C (2007) Guiding Cell Migration Using One-Way Micropattern Arrays. Advanced Materials 19: 1084-1090.
14. Mahmud G, Campbell C J, Bishop K J M, Komarova Y A, Chaga O, et al. (2009) Directing cell motions on micropatterned ratchets. Nature Physics 5: 606-612.
15. Irmia D, and Toner M (2009) Spontaneous migration of cancer cells under conditions of mechanical confinement. Integrative Biology 1: 506-512.
16. Rolli C G, Seufferlein T, Kemkemer R, and Spatz J P (2010) Impact of Tumor Cell Cytoskeleton Organization on Invasiveness and Migration : A Microchannel-Based Approach. PLoS ONE 5.
17. Petrie R J, Doyle A D, and Yamada K M (2009) Random versus directionally persistent cell migration. Nature Reviews: Molecular Cell Biology 10: 538-549.
18. Abhyankar V V, Toepke M, Cortesio C L, Lokuta M A, Huttenlocher A, et al. (2008) A platform for assessing chemotactic migration within a spatiotemporally defined 3D microenvironment. Lab Chip 8: 1507-1515.

19. Dieterich P, Klages R, Preuss R, and Schwab A (2008) Anomalous dynamics of cell migration. Proc Natl Acad Sci USA 105: 459-463.
20. Brandman O, and Meyer T (2008) Feedback Loops Shape Cellular Signals in Space and Time. Science 322: 390-395.
21. Kholodenko B N (2006) Cell-signalling dynamics in time and space. Nature Reviews: Molecular Cell Biology 7: 165-176.
22. Parsons J T, Horwitz A R, and Schwartz M A (2010) Cell adhesion: integrating cytoskeletal dynamics and cellular tension. Nature Reviews: Molecular Cell Biology 11: 633-643.
23. Ridley A J, Schwartz M A, Burridge K, Parsons J T, Firtel R A, et al. (2003) Cell Migration: Integrating Signals from Front to Back. Science 302: 1704-1709.
24. Jacobelli J, Friedman R S, Conti M A, Lennon-Dumenil A-M, Piel M, et al. (2010) Confinement-optimized three-dimensional T cell amoeboid motility is modulated via myosin IIA–regulated adhesions. Nature Immunology 11: 953-961.
25. Hawkins R J, Piel M, Faure-Andre G, Lennon-Dumenil A M, Joanny J F, et al. (2009) Pushing off theWalls: A Mechanism of Cell Motility in Confinemen. Physical Review Letters 102: 058103.
26. Al-Hajj M, Wicha M S, Benito-Hernandez A, Morrison S J, and Clarke M F (2003) Prospective identification of tumorigenic breast cancer cells. Proc Natl Acad Sci USA 100: 3983-3988.
27. Li C, Heidt D G, Dalerba P, Burant C F, Zhang L, et al. (2007) Identification of Pancreatic Cancer Stem Cells. Cancer Research 67: 1030-1037.
28. Theriot J A, and Mitchison T J (1991) Actin microfilament dynamics in locomoting cells. Nature 352.
29. Barak L S, Yocum R R, Nothnagel E A, and Webb W W (1980) Fluorescence staining of the actin cytoskeleton in living cells with 7-nitrobenz-2-oxa- 1,3-diazole-phallacidin. Proc Natl Acad Sci USA 77: 980-984.
30. Balaban N Q, Schwarz U S, Riveline D, Goichberg P, Tzur G, et al. (2001) Force and focal adhesion assembly: a close relationship studied using elastic micropatterned substrates. Nature Cell Biology: 466-472.
31. Brown X Q, Ookawa K, and Wong J Y (2004) Evaluation of polydimethylsiloxane scaffolds with physiologically- relevant elastic moduli: interplay of substrate mechanics and surface chemistry effects on vascular smooth muscle cell response. Biomaterials 26: 3123-3129.
32. Bao G, and Suresh S (2003) Cell and molecular mechanics of biological materials. Nature Materials 2: 715-725.
33. Wakatsuki T, Kolodney M S, Zahalak G I, and Elson E L (2000) Cell Mechanics Studied by a Reconstituted Model Tissue. Biophysical Journal 79: 2353-2368.
34. Yeung T, Georges P C, Flanagan L A, Marg B, Ortiz M, et al. (2005) Effects of Substrate Stiffness on Cell Morphology, Cytoskeletal Structure, and Adhesion. Cell Motility and the Cytoskeleton 60: 24-34.
35. Discher D E, Janmey P, and Wang Y-l (2005) Tissue Cells Feel and Respond to the Stiffness of Their Substrate. Science 310: 1139-1143.

36. Califano J P, and Reinhart-King C A (2010) Substrate Stiffness and Cell Area Predict Cellular Traction Stresses in Single Cells and Cells in Contact. Cellular and Molecular Bioengineering 3: 68-75.
37. Kraning-Rush C M, Carey S P, Califano J P, Smith B N, and Reinhart-King C A (2011) The role of the cytoskeleton in cellular force generation in 2D and 3D environments. Physical Biology 8: 015009.
38. Pathak A, and Kumar S (2011) Biophysical regulation of tumor cell invasion: moving beyond matrix stiffness. Integrative Biology 3: 267-278.
39. Friedl P, and Wolf K (2009) Proteolytic interstitial cell migration: a five-step process. Cancer Metastasis Rev 28: 129-135.
40. Zaman M H, Trapani L M, Sieminski A L, MacKellar D, Gong H, et al. (2006) Migration of tumor cells in 3D matrices is governed by matrix stiffness along with cell-matrix adhesion and proteolysis. Proc Natl Acad Sci USA 103: 10889-10894.
41. Bloom R J, George J P, Celedon A, Sun S X, and Wirtz D (2008) Mapping Local Matrix Remodeling Induced by a Migrating Tumor Cell Using Three-Dimensional Multiple-Particle Tracking. Biophysical Journal 95: 4077-4088.
42. Suresh S (2007) Biomechanics and biophysics of cancer cells. Acta Materialia 55: 3989-4014.
43. Wolf K, and Friedl P (2009) Mapping proteolytic cancer cell-extracellular matrix interfaces. Clin Exp Metastasis 26: 289-298.
44. Shields J D, Fleury M E, Yong C, Tomei A A, Randolph G J, et al. (2007) Autologous Chemotaxis as a Mechanism of Tumor Cell Homing to Lymphatics via Interstitial Flow and Autocrine CCR7 Signaling. Cancer Cell 11: 526-538.
45. Fraley S I, Feng Y, Krishnamurthy R, Kim D-H, Celedon A, et al. (2010) A distinctive role for focal adhesion proteins in three-dimensional cell motility. Nature Cell Biology 12: 598-604.
46. Debnath J, Muthuswamy S K, and Brugge J S (2003) Morphogenesis and oncogenesis of MCF-10A mammary epithelial acini grown in three-dimensional basement membrane cultures. Methods 30: 256-268.
47. Guise T A, Yin J J, Taylor S D, Kumagai Y, Dallas M, et al. (1996) Evidence for a Causal Role of Parathyroid Hormone–related Protein in the Pathogenesis of Human Breast Cancer–mediated Osteolysis. J Clin Invest 98: 1544-1549.
48. Feller W (1945) The Fundamental Limit Theorems in Probability. Bull Amer Math Soc 51: 800-832.

CHAPTER 3

ELUCIDATING MECHANICAL TRANSITION EFFECTS OF INVADING CANCER CELLS WITH A SUBNUCLEUS-SCALED MICROFLUIDIC SERIAL DIMENSIONAL MODULATION DEVICE

3.1 Abstract

Mechanical boundaries that define and regulate biological processes, such as cell-cell junctions and dense extracellular matrix networks, exist throughout the physiological landscape. During metastasis, cancer cells are able to invade across these barriers and spread to distant tissues. While transgressing boundaries is a necessary step for distal colonies to form, little is known about interface effects on cell behavior during invasion. Here we introduce a device and metric to assess cell transition effects across mechanical barriers. Using MDA-MB-231 cells, a highly metastatic breast adenocarcinoma cell line, our results demonstrate that dimensional modulation in confined spaces with mechanical barriers smaller than the cell nucleus can induce distinct invasion phases and elongated morphological states. Further investigations on the impact of microtubule stabilization and drug resistance reveal that taxol-treated cells have reduced ability in invading across tight spaces and lose their super-diffusive migratory state and taxol-resistant cells exhibit asymmetric cell division at barrier interfaces. These results illustrate that subnucleus-scaled confinement modulation can play a distinctive role in inducing behavioral responses in invading cells and can help reveal the mechanical elements of non-proteolytic invasion.

3.2 Introduction

Reproduced by permission of the Royal Society of Chemistry, Michael Mak, Cynthia A. Reinhart-King, and David Erickson, "Elucidating mechanical transition effects of invading cancer cells with a subnucleus-scaled microfluidic serial dimensional modulation device," *Lab Chip*, 13, 340-348 (2013). doi: 10.1039/C2LC41117B

Metastasis is the process by which cancer invades and spreads to different parts of the body. It is a difficult phenomenon to study because of its expansive spatiotemporal scales – it can involve a single cell's journey over meters and years [1-3]. While new technologies in genomics and proteomics, computational models, and advanced microscopy have facilitated our understanding of the many altered molecular pathways and mutations that occur in cancer [4], very little is understood about the mechanical properties that are characteristic of cancer, particularly at the single-cell level. Single-cell mechanics is important because metastasis is intrinsically a mechanical transport phenomenon in which individual cells must break from the primary tumor, squeeze and invade through small pores of the extracellular matrix (ECM) of the tumor stroma, intra- and extravasate across endothelial junctions, and circulate and traffic in the vasculature [1, 2, 5]. Additionally, cell mechanics is rich with many characteristic properties such as traction stress [6, 7], morphological responsivity to force, and material properties. All of these features may potentially impact the capabilities and behavior of cancer cells during invasion [8-11]. Moreover, the connections between many important phenomenological events associated with cancer – such as morphological phenotypes, cell division asymmetry, and drug resistance – and the mechanical features of the microenvironment – *e.g.* geometry, dimensionality, and confinement on a subnucleus length scale – are not well understood. The subnucleus length scale is of particular interest because the nucleus is one of the stiffest and largest organelles in the cell [12]. Therefore, intuitively, across the most confined spaces, the nucleus is likely to limit invasion rates and be forced to undergo deformations and potential conformational changes, which could have implications in mechanotransduction and altered cell phenotypes [12-14].

Current experimental systems for understanding cell-level mechanical phenomena can be categorized into two general types: passive and active systems from the frame of reference of the cell. In a passive system, the experimentalist is manipulating cells and obtaining measurements, such as material properties of the cytoskeleton and nucleus, often in real-time. Cells are passively being probed and cell signaling is generally not studied in detail. In an active system, cells are seeded in an engineered environment and allowed to interact (actively and holistically) with their surroundings. Timelapse video microscopy is used to record the interactions for later processing.

Examples of passive systems for cell mechanics studies include microfluidic inertial focusing, optical force deformation, microrheology, atomic force microscopy (AFM), and micropipette aspiration [10, 11, 15-17]. The advantage of these systems is that they can be very precise, as in piezo-electric positioning in AFM measurements, with many parameters that are highly tunable (such as flow rate, optical power, electric and magnetic field modulation, and micropipette suction force). Measurements can also be fast on a per cell basis; upwards of thousands of cells can be sampled per second [11]. The drawback is that these systems measure passive and/or bulk biological characteristics, such as cell deformability and viscoelasticity. While these properties are useful and can be correlated with important phenomena such as disease state, stem cell differentiation, and possibly metastatic potential [10, 11], they are usually a reductionist description of biological systems that are infinitely more complex. As such, phenomena attributable to dynamic behavior and functional abilities associated with the integrated system of a cell (which is a complex coordination of signaling events from a multitude of biomolecules and pathways) typically cannot be assessed.

The advantage of active systems is that they interrogate system-level biological processes and cell responses. The results are then more translatable and tangible toward cell behavior and capabilities in dynamic physiological events, which may help identify targetable elements for therapeutics [18-20]. Current state-of-the-art active systems include 3D cell-in-gel models, 2D micropatterning techniques, and microfluidic devices for cell migration [16, 21-24]. In these systems, aspects of cell motility and mechanics can be studied, such as the cell's ability to remodel and navigate through extracellular matrix (ECM) fibers, the migration behavior and morphology on a predefined substrate pattern, and motility characteristics in highly confined spaces. One main drawback is that thus far such active systems generally are not well equipped with features and metrics to facilitate the study of complex cell behavior. Dynamic single-cell events and characteristics are important towards our understanding of cancer progression, particularly in light of current themes of interest including heterogeneity, plasticity, and drug-resistance [25-28]. Existing methods tend to measure lower-order properties such as cell displacements and velocities. If we consider the complex displacement function of a typical cell, those properties are simply the 0^{th} and 1^{st} order terms of its Taylor expansion. Fundamentally, there is no reason why we should be reduced to those terms. Practically, however, there are limitations. 3D gels are viscoelastic and heterogeneous on the scale of the cell [2, 26, 29], so environmental dispersion is likely to reduce measurable elements to lower order properties – such as displacements and velocities. Microfluidic motility assays with no localized stimulatory features enable only the measurement of spontaneous cell behavior, so any transition dynamics would be difficult to quantify. Even techniques like traction force microscopy that measure more complex mechanical phenomena are often acquired at fixed points in time. Only recently have experimental studies started

alluding to mechanical cell transition dynamics, investigating active shape changes of cell nuclei in hydrogels and induced patterns of velocity change in microchannels [14, 30].

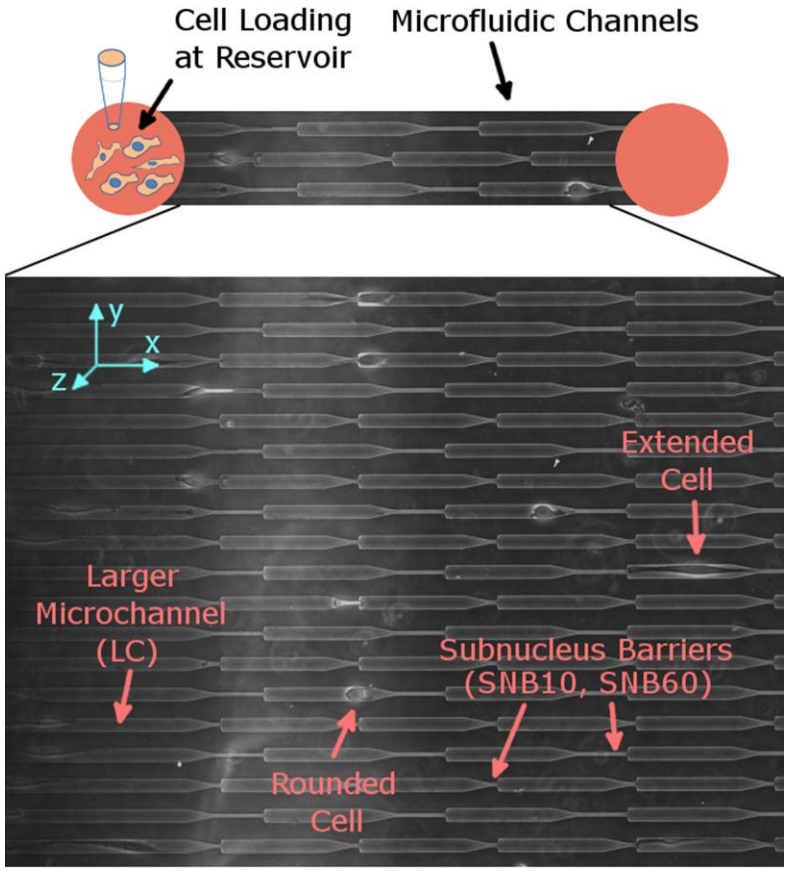

Fig. 3.1: Device design. Microfluidic channels connect two port reservoir regions. Cells are seeded into the reservoir and allowed to invade into the channels. In the actual device, the two ports are connected to the same larger reservoir in order to allow for pressure equilibration and a larger volume of media to be supplied. Expanded view: the multi-stage serial invasion channels (M.U.S.I.C.) device consists of repeating patterns of a larger channel (LC) with width (15μm) on the scale of the cell connected to a smaller channel (the subnucleus barrier) with width (3.3μm) smaller than the typical cell nucleus. There are two designs for the subnucleus barrier (SNB) – one is shorter than a typical cell (SNB10) and one is longer (SNB60), with lengths 10μm and 60μm, respectively. Transition dynamics occur when cells squeeze across the subnucleus barriers.

Here, we develop an active microfluidic system with complex, well-defined features to study the dynamics and mechanical properties of actively invading cells. As shown in Fig. 3.1, we incorporate patterns and repetitions along a dimensionally-confined microfluidic channel. Specifically, the dimensions are modulated and confinement features smaller than the cell nucleus are incorporated, which stimulate cell transition dynamics both in motility and morphology. Such highly confined geometries mimic the dimensionality of the smallest physiological spaces relevant in metastasis, for example small pores in the dense ECM of the tumor stroma, endothelial junctions during intravasation, and traffic-inducing microvessels [2, 19, 31, 32]. Additionally, the periodic barrier design imposes multiple interfaces per cell, which is a first step in better quantifying the effects of more complex physiological boundaries that mimic the spatial heterogeneities found in the tumor stroma. The periodic barriers along a single channel also enable the sampling of individual cells multiple times. The goal of our study is to develop a device designed to test the effects of subnucleus-scaled spatial confinement modulation on the dynamics of cell invasion and the specific roles of cell mechanical plasticity and cell-to-cell heterogeneity in tumor progression. Currently there does not exist a standardized technique that can probe into the connections between these important parameters in cancer metastasis, particularly on a single high-throughput platform.

In what follows, we quantify higher order mechanical dynamics, interface induced morphological effects, and the impacts of microtubule stabilization and drug resistance during invasion. Our results reveal several key findings – 1) cell transition across spaces smaller than the cell nucleus can be segmented into multiple distinct phases, 2) multiple functional strategies are employed by the cell during invasion, 3) a more extended morphological state is induced by the modulation of confined spaces, 4)

microtubule stabilization impairs cell transition across mechanical barriers and alters the motile state of the cell, and 5) taxane-resistance is correlated with geometrically induced asymmetric cell division.

3.3 Results and Discussions

3.3.1 Multi-staged Serial Invasion Microchannels (MUSIC) for Investigating Cell Mechanics and Dynamics

To develop an assay that can directionally focus the cell invasion program for high throughput quantitative analysis, we designed and fabricated a microfluidic device that induces serial dimensional modulation on the cell and nucleus scale (Fig. 3.1). We refer to this herein as a MUlti-staged Serial Invasion Channels (MUSIC) device. To perform the assay, first we induce spontaneous cell migration into confinement microchannels with cross-sectional area comparable to the cell size – the y and z dimensions are bound such that the cell is forced to move primarily along the x-direction. Then we incorporate a spatially tapering interface that connects the confinement channel to another even smaller channel (referred to as the subnucleus barrier (SNB)) with width smaller than the cell nucleus, which is one of the largest and stiffest organelles in the cell [14]. Fig. S3.1 shows fluorescently stained nuclei at different sections of the device, revealing nuclei morphology and deformation. This device design in essence directs and reduces the 3-D invasion program into a 2-component process – 1) the cell migrates in the x-direction while 2) necessarily altering its y-dimensions. Because the migration vector points in one direction (x) and the primary induced region of change is in the orthogonal direction (y), high throughput quantitative analysis can now be accomplished in 1-D, thus increasing the feasibility of experiments and enabling predetermined axes of interest. Furthermore, repeating patterns of the subnucleus barrier are placed along the length of the

microchannel, enabling serial effects and multiple sampling of individual cells, therefore providing a way to elucidate the plasticity of mechanisms of invasion for each cell. In our experiments, we consider both 1) cell invasion in only the larger confinement channel region (referred to as LCI) and 2) invasion from the larger channel across the subnucleus barrier (referred to as SNI). Our device design incorporates two different lengths for the SNB – 10μm (SNB10) and 60μm (SNB60), which are shorter and longer than a typical MDA-MB-231 cell, respectively.

3.3.2 Invasion Dynamics across the Subnucleus Barrier

To understand higher order effects of cell invasion, we first identified the nonlinearity in the cell displacement function during SNI. Then we segmented the process into 4 distinct phases and measured the time constants of each phase. This is important because SNI is a transition process, so an average velocity approximation does not reveal the transition dynamics. In our analysis, four SNI phases are distinguished by distinct mechanical characteristics as shown in Fig. 3.2. Phase 1 – the cell migrates in the larger channel (LC) and slows down as it approaches the subnucleus barrier interface. Phase 2 – the body (bulge region) of the cell starts permeating into the subnucleus barrier. Phase 3 – the cell stops monotonic forward motion and either pauses or moves back and forth. Phase 4 – the body of the cell exits the subnucleus barrier in a monotonic forward motion. We quantified the invasion time constants for the MDA-MB-231 cell line that models highly invasive breast cancer cells, and we parameterized the subnucleus barrier length (Fig. 3.2b, Video S3.1). By dissecting the measurements into phases, we are able to describe the steps and timeframe for a cell to organize into a conformation that is conducive for subnucleus barrier invasion. Phase 3 is of particular interest in this study because it is a phase that is neglected in conventional assays that score cells based on net cell velocities or average directional

persistence. It appears to be a transient reorganization phase, which we will discuss in more detail below.

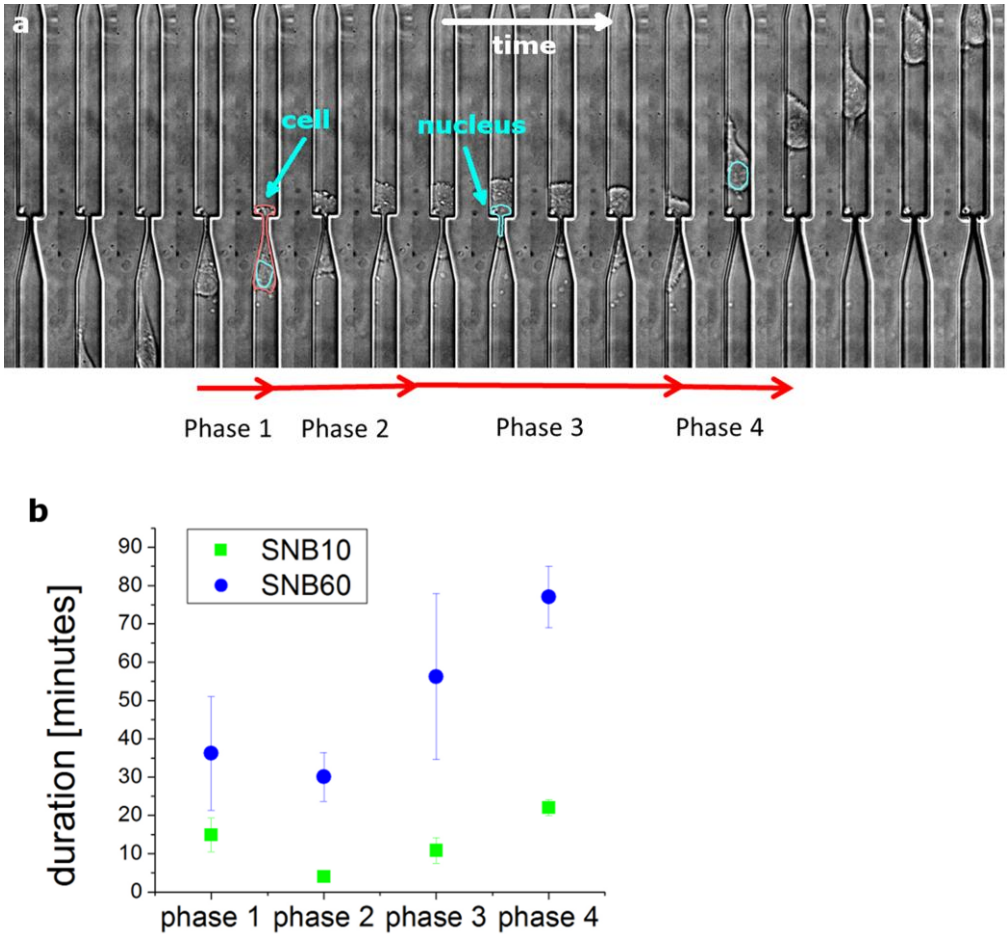

Fig. 3.2: Cell invasion phases. a) The dynamics of a cell invading across subnucleus barriers can be segmented into 4 phases, as shown in the timelapse image stack (17 min/frame). The cell slows down as it reaches the barrier (phase 1), the cell body starts permeating into the barrier (phase 2), the cell pauses or otherwise stops monotonic forward motion (phase 3), and the cell resumes monotonic forward motion and exits the barrier (phase 4). b) The average time constants for these phases are measured for invasions across the subnucleus barriers SNB10 (n = 62) and SNB60 (n = 20), where n is the number of invasion events observed. The width of the larger channel is 15μm.

3.3.3 Multiple mechanical strategies are employed during invasion

The probability data in Fig. 3.3a shows that not all of the invasion phases are exhibited by all cells, and the barrier length can modulate the expression of these mechanical phases. Specifically, the longer subnucleus barrier SNB60 has a higher probability of inducing invasion phase 3, whereas many cells do not exhibit this phase in the shorter barrier SNB10. We take a closer look into the mechanistic steps in cell invasion across a confined area and consider the functional role of the dynamic mechanical processes that take place. Here, we qualitatively describe some of the strategies used by the cell in order to modulate its width and squeeze through the subnucleus barrier. Fig. 3.3 b-d demonstrates several scenarios in which the cells squeeze across the barrier. In Fig. 3.3b, the cell simply contracts and the nucleus of the cell is deformed enough via the contractile force for the cell to move across the constriction. In Fig. 3.3 c-d, the cell undergoes phase 3 as described previously. Fig. 3.3c shows a cell stuck at the barrier due to a stiff intracellular aggregate. A back extension is protruded which tensionally elongates the cell body and reduces the width of the aggregate, thus facilitating intracellular trans-barrier transport. In Fig. 3.3d, the cell moves backwards and forward, during which there are cytoplasmic rotational dynamics. The cell body permeates into the confined region in a rolling motion, which potentially enables the sampling of different energy landscapes and deformable configurations and may reduce the energy required to deform the cell nucleus. Therefore, through dimensional modulation at the length scale of the cell nucleus, we have more clearly identified some of the mechanical and functional phenomena that are active during the invasion process. Recent studies have demonstrated that lamin b1 and dynein help regulate rotations of and force transduction onto the cell nucleus [33, 34], so further investigations would be interesting to investigate their contributions to the invasion program.

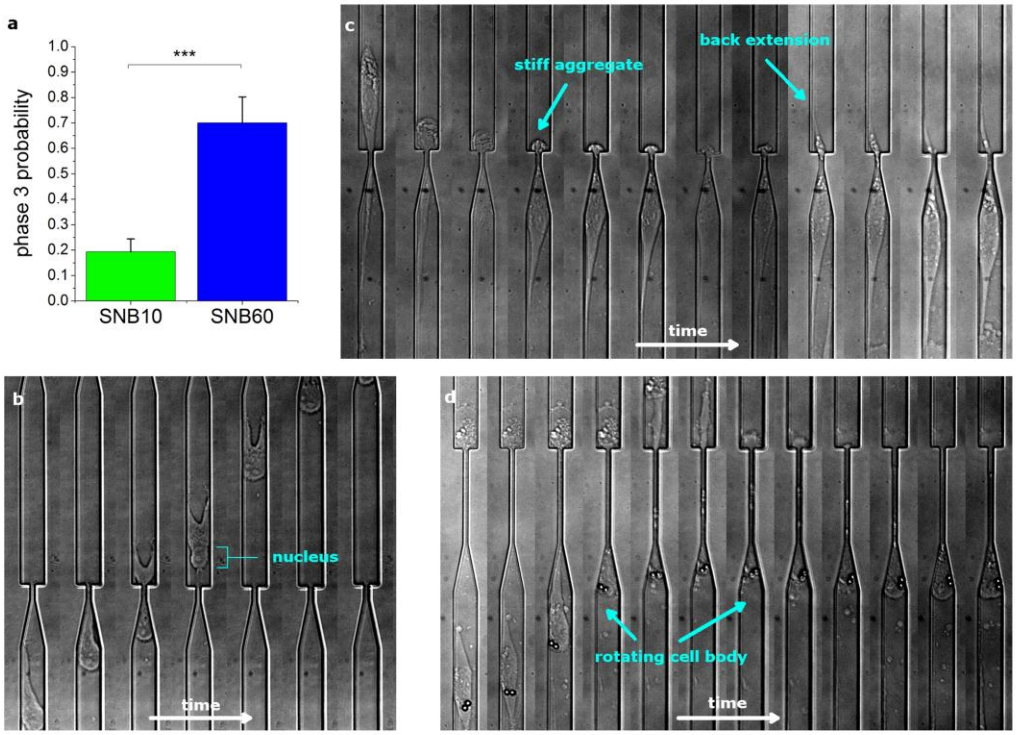

Fig. 3.3: Functional strategies during mechanical invasion. a) The probability of phase 3 existing for the two different subnucleus barriers SNB10 and SNB60. SNB60 induces a higher probability of phase 3 existing (70%, n = 20) than SNB10 (19.4%, n = 62). Error bars represent standard error of the mean (s.e.m.) from Bernoulli statistics and *** indicates $p < 0.001$ (Chi-squared test). b) A timelapse image stack (17 min/frame) showing a cell invading across SNB10 with no phase 3 observed. The contractile force of the cell is enough to deform the cell nucleus across the barrier in a monotonic forward motion. c) As this cell invades from top to bottom across SNB60, a stiff aggregate at the rear of the cell is stuck at the barrier interface. A back extension is protruded, which tensionally reduces the width of the aggregate and facilitates intracellular trans-barrier transport. 34 minutes elapsed between subsequent frames. d) As this cell is invading from the LC into SNB60, cell body rotations, with visualization facilitated by endocytosed particles, can be seen in the timelapse image stack during the invasion process. These rotational dynamics may help position the cell more favorably and/or sample more energetically favorable conformations as the cell is invading across the subnucleus barrier. 34 minutes elapsed between subsequent frames. The width of the larger channel is 15μm.

3.3.4 Microtubule stabilization decreases cell invasiveness, but not simply by reducing cell speed

Microtubule dynamics are important in many aspects of cell mechanics, including cell division and polarization [35-38]. Previous studies have demonstrated that microtubule stabilization reduces asymmetric distribution of cell motor proteins and reduces asymmetry in microtubule instability in the cell [38]. These properties are necessary for leading and trailing edges of the cell to form, which in turn lead to polarized cell migration. Here, we consider the invasion dynamics of the cell as a result of microtubule stabilization. We compare MDA-MB-231 cells that are either untreated or treated with 16μM taxol, which stabilizes microtubule dynamics [39] (Video S3.2). We show that taxol-treated cells spend a significantly longer time at the interface of the subnucleus barrier, as shown in Fig. 3.4a. For instance, for a 10μm long subnucleus barrier, cells typically take less than 1 hour for permeation. Taxol-treated cells, however, spend t > 20hrs at the interface. Many cells actually spend more than the duration of our timelapse experiments before permeation, so the times specified for taxol-treated cells represent a lower-bound of the actual SNI time.

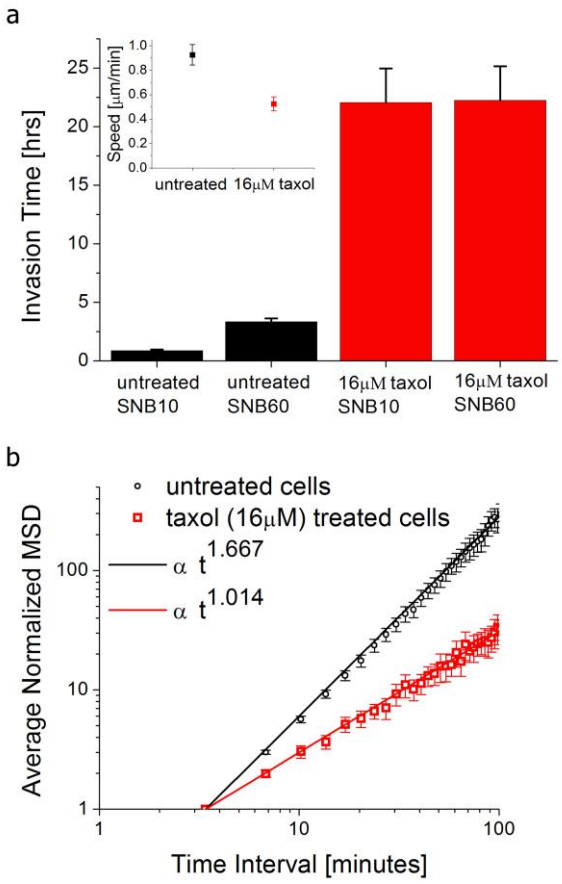

Fig. 3.4: Effects of Microtubule Stabilization. a) Taxol-treated (16μM) MDA-MB-231 cells take much longer to permeate across the subnucleus barriers than untreated MDA-MB-231 cells. The total invasion times are 0.86hrs (n = 62 invasion events), 3.33hrs (n = 20 invasion events), 22hrs (n = 42 invasion events), 22hrs (n = 31 invasion events), for untreated cells across SNB10, untreated cells across SNB60, taxol-treated cells across SNB10, and taxol-treated cells across SNB60, respectively. Many of the taxol-treated cells have yet to permeate through the subnucleus barrier by the end of the experiments, so the data represents a lower-bound measurement. Cells that have not permeated by the end of the experiments were only accounted for if they have spent at least 4hrs at the barrier. This way we have disregarded arbitrarily short lower-bound measurements for data that was truncated too early (less than 4hrs). Inset: the average speed of untreated (0.93μm/min, n = 12) and 16μM taxol-treated (0.53μm/min, n = 10) MDA-MB-231 cells in the larger channel LC during a 3.4 minute time interval. Error bars are s.e.m. b) Log-log plot of the average normalized mean-squared displacements (MSD) vs. time for untreated (black circles, n = 12 cells) and taxol-treated cells (red squares, n = 10 cells) in the larger channel LC. Normalization is with respect to the first data point (3.4 minute time interval) of each cell. Error bars are s.e.m. A non-linear least squares fit to a power-law model shows a dependence of $t^{1.667}$ (R^2: 0.996, 95% confidence [1.66, 1.673]) and $t^{1.014}$ (R^2: 0.9829, 95% confidence [1.006, 1.022]) for untreated and taxol-treated MDA-MB-231 cells, respectively. For Brownian motion, MSD $\propto$ t.

To explain these results from a mechanical standpoint, we consider migration dynamics of the cells in the larger channel region LC (before reaching the subnucleus barrier interface). In this region, the average cell speed differs by only a factor of ~2 between treated and untreated cells (Fig. 3.4a (inset)). We consider this to be low compared to the factor of >20 in total SNI time over a barrier that is only 10μm long. To investigate the possible reasons for this phenomenon, we analyze the second moment of the cell displacement function (*i.e.* the mean-squared displacement (MSD)). As shown in Fig. 3.4b, the MSD vs. time interval relation can be fitted well to a power-law model. For untreated cells MSD $\propto t^{1.67}$, whereas for microtubule-stabilized cells MSD $\propto t^{1}$, where t is the time interval. To help understand the consequence of these results, consider the two limiting cases. If a particle moves at a constant velocity v, MSD = v^2t^2, and if a particle is undergoing 1-D Brownian motion (pure random walk), MSD = 2Dt, where D is the diffusion coefficient. The power-law dependence on time will manifest on the log-log MSD vs. t curve as the slope. Our results demonstrate that untreated cells are super-diffusive, as consistent with previous 2D studies [40], but microtubule stabilized cells exhibit a purely random motion behavior, indicating that microtubule dynamics contribute to adding a "memory effect" to cell motility.

Since microtubules play an important role in cell polarization, motility, and division, in addition to being a well-targeted molecule in anticancer treatments [37], it is particularly interesting to understand their role during mechanical invasion. Microtubule stabilization drastically reduces the ability of MDA-MB-231 cells to invade across subnucleus barriers, and one potential cause is that the cells' natural super-diffusive nature is abolished, reducing them to Brownian movers. Previous studies have shown that signaling through the Rho family of GTPases help stabilize

microtubules at the leading edge of cells and can determine migration persistence, phenomenologically distinct from phosphoinositide 3-kinase (PI3K) signaling in chemotaxis [41, 42]. Concentrations of the GTPase Rac1 are modulated through the dimensionality of the microenvironment (1D lines, 2D flat surfaces, and 3D matrices), and a naturally occurring reduction in Rac1 expression in 1D and 3D as compared to 2D environments leads to fewer peripheral protrusions which results in more persistent migratory behavior [42]. Rho-GTPase signaling may therefore explain the persistent migration in these confined microchannels, and by diminishing this persistence through uniform rather than localized microtubule stabilization, the cell invasion ability across subnucleus barriers is also impaired. This suggests that microtubule stabilization may prevent cells from permeating across tight spaces, which when used together with matrix metalloproteinases (MMP)-inhibitors to prevent proteolytic invasion, may produce a synergistic effect in suppressing invasion across tight physiological spaces (some of which are degradable by MMPs). A previous study used protease inhibitors together with Y27632 (which inhibits Rho-associated protein kinase ROCK) and demonstrated synergistic effects in preventing cell invasion [18]. One difference here is that microtubule targeting drugs are approved and readily available in cancer treatments. These drugs have been applied traditionally for their anti-mitosis and apoptosis effects in addition to potential anti-metastasis properties [37, 43]. However, it is unclear how they affect single-cell invasion. Our results suggest that for viable cells after treatment, anti-invasion effects from taxol may manifest in the impediment of polarization-dependent permeation across subnucleus barriers (rather than on simply altering cell speed). These details can potentially help in the design of new combination chemotherapeutics.

3.3.5 Dimensional modulation induces differential cell extension lengths

With the MUSIC device, we demonstrate that dimensional modulation on the scale of the cell and cell nucleus and interface effects from subnucleus barriers can induce morphological changes in invading cells. As demonstrated in Fig. 3.5 and Video S3.3, when a cell interacts with a region smaller than the cell nucleus, significantly longer extensions are protruded. These extensions can be hundreds of micrometers long. Interestingly, K20T cells, the taxol resistant derivative of MDA-MB-231 cells, are longer even without interface effects. Furthermore, the cell length distribution data shown in Fig. 3.5b demonstrates the diversity of morphological states exhibited during the invasion process.

These results suggest that mechanical barriers can cause cells to have a larger, more extended region of influence, which may facilitate nutrient-finding and homing towards the vasculature in conjunction with other mechanisms such as chemotaxis [44]. Certain cell morphologies have been linked to more potent cancer phenotypes. Compressive forces in 2D experiments for instance lead to a "leader cell" phenotype that is elongated and spindle-shaped and leads neighboring cells in the invasion process [9]. Substrate stiffness and tensional forces can induce larger cell areas and activate integrin mediated signaling pathways that lead to more malignant phenotypes [8]. The sidewalls of the subnucleus barriers in the MUSIC device essentially impose compression in the form of normal forces onto the cell and its nucleus during invasion, and the induced cell elongation process likely causes higher tension along the cell. Subnucleus barrier confinements therefore may contribute towards driving metastatic phenotypes.

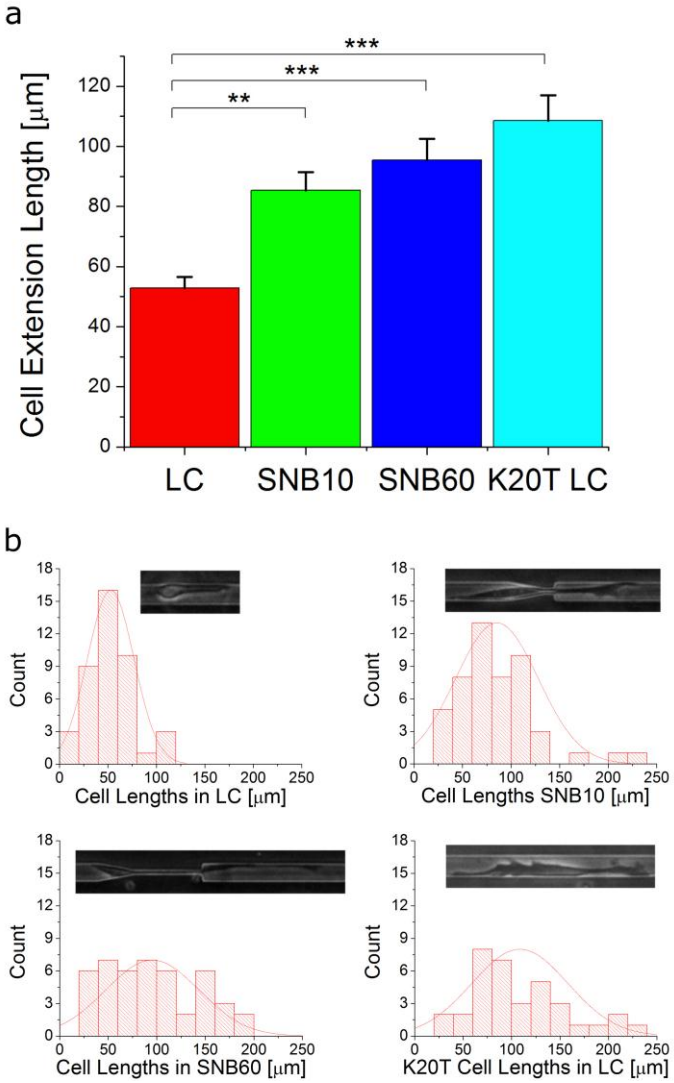

Fig. 3.5: Cell extension lengths. a) The average cell extension length measured at a random point in time for MDA-MB-231 cells in the larger channel LC (53μm, n = 42 cells), while interacting with SNB10 (85μm, n = 50 cells), while interacting with SNB60 (95μm, n = 45 cells), and K20T cells in the LC (109μm, n = 35 cells). Extension lengths are measured from the center of the cell body to the end of the longest extension. The subnucleus barrier induces longer cell extensions and K20T cells also have longer cell extensions. ** represents $p < 0.01$ and *** represents $p < 0.001$ from ANOVA statistics. b) Histograms and typical cell morphologies at each scenario. The width of the larger channel is 15μm.

3.3.6 Taxol resistant cells are more susceptible to asymmetric cell division during invasion

K20T cells are taxol-resistant MDA-MB-231 cells selected as described in [45]. As shown in Fig. 3.6 and Video S3.4, K20T cells that divide while moving from left to right into the subnucleus barrier interface exhibit geometric asymmetry in its axis of division, with the daughter cell closer to the confinement region being 50% larger. This phenomenon is not as pronounced in control MDA-MB-231 cells or in K20T cells that divide in the symmetric straight region of the device. Calculations of area ratios are determined by the following methodology: in symmetric large channel regions, the area ratio AR = $A_{\text{smaller cell}}/A_{\text{larger cell}}$; in the interface region, only cells moving from left to right into the interface are considered, and the area ratio is determined by AR = $A_{\text{left cell}}/A_{\text{right cell}}$. Asymmetric cell division has been linked to aneuploidy and genomic instability, which can potentially lead to accelerated and gain of function mutations [46-48]. Our results here could imply that the resistant cell line is intrinsically more ready to mutate and that geometric effects during invasion can have an impact on cell division, mutations, and directed evolution. Further investigations into cell ploidy and phenotypic differences between cells that have divided asymmetrically will be necessary to investigate the connections between drug and taxane-resistance and tumor cell evolution during invasion. Previous efforts in 2D protein micropatterning techniques have demonstrated that the axis of cell division and mitotic spindle positioning can be regulated by geometric constraints [49, 50]. However, connections between cell behavior (migration and division) in 2D geometric patterns and cancer progression and evolution due to invasion, inherently a 3D process, are unclear. Confinement in 3D mechanically simulates tight physiological spaces relevant during invasion, and physiological cell division also usually occurs in 3D, so a transition from 2D engineered patterns to 3D engineered patterns can reveal insights

of dimensionality on cell division mechanics. Additionally, the probability of a cell dividing at any given region of fixed length should be higher if there is a mechanical barrier there because the cell spends more time in that region due to the transition dynamics described earlier. Therefore, understanding cell division effects caused by different mechanical barriers during invasion may provide insights towards potential driving elements of cell evolution. This is particularly interesting for cancer cells since they are notorious for their ability to acquire new abilities [4] and they typically do not exhibit contact inhibition [51, 52], so their cell cycle is likely not influenced by external elements such as mechanical confinement. We note here that the throughput of these experiments in this design of the MUSIC device is lower in comparison to the invasion studies since only a fraction of the invading cells will divide at the SNB interface. A next generation device design incorporating more frequent SNBs can increase experimental throughput by increasing the probability that a cell is positioned in a geometrically asymmetric location during division.

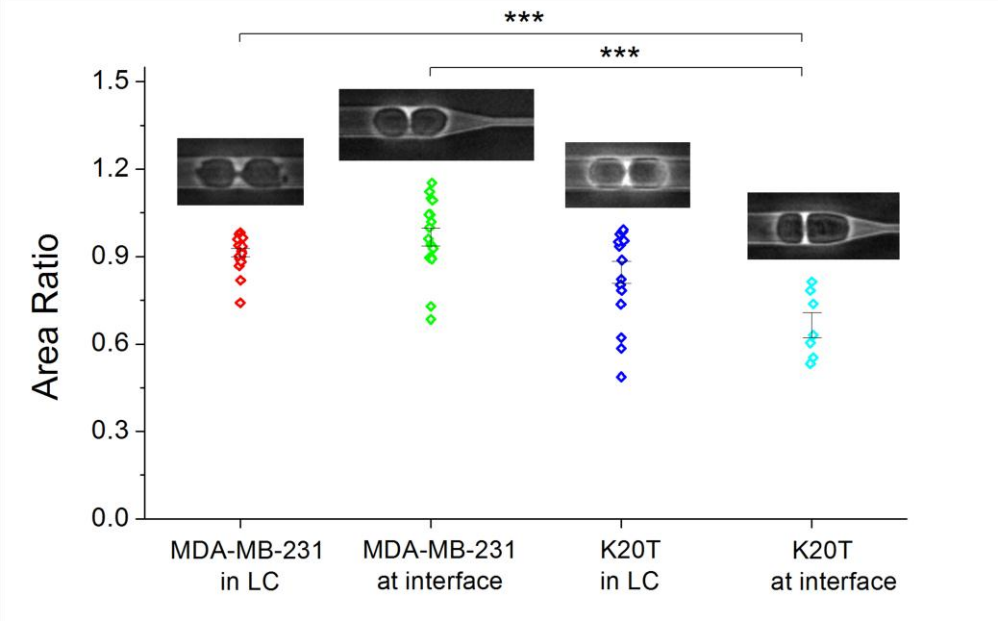

Fig. 3.6: Cell division asymmetry. MDA-MB-231 cells tend to divide symmetrically both in the larger channel LC and at the barrier interface. K20T cells, however, tend to divide asymmetrically at the subnucleus barrier interface. The daughter cell closer to the barrier is larger. AR = area ratio between daughter cells. In the symmetric larger channel LC, AR = smaller cell/larger cell. At the interface, AR = left cell/right cell, and only cells dividing while invading from left to right into the SNB are taken into account. The area ratios measured are (mean = 0.91, median = 0.92, n = 19) for MDA-MB-231 in LC, (mean = 0.97, median = 0.96, n = 17) for MDA-MB-231 at SNB interface, (mean = 0.85, median = 0.94, n = 17) for K20T in LC, and (mean = 0.67, median = 0.63, n = 7) for K20T at SNB interface. *** indicates $p < 0.001$ from ANOVA statistics. Error bars are s.e.m. The width of the larger channel is 15μm.

3.4 Conclusion

There are many instances when cells exhibit modulation from their environment. Sometimes the external stimulation exists as chemical cues as in chemotaxis, and sometimes it is presented as mechanical cues, such as during contact inhibition or durotaxis [44, 52-54]. Often times the signal is both physical and chemical, as in cell-cell

or cell-ECM interactions [8, 54-56]. Here we presented a different form of mechanical modulation – modulation in the confinement dimensions of invading cells. This is of particular interest towards cancer progression and metastasis because tumor growth can lead to increased confinement sensed by the cells and cell invasion can involve permeation across tight spaces, from tumor stroma to basement membranes to endothelial junctions [1, 2, 9]. We have created a platform – serial dimensional modulation at the subnucleus length scale – and device (MUSIC) that enable new phenomenological events associated with mechanical cell invasion and boundary effects to be elucidated and quantified. We focused on higher order invasion dynamics, morphologies, division, and pharmacologic effects and thus have demonstrated the details and wide range of biological phenomena on the single-cell scale that can be interrogated with our approach. Our analysis revealed some important characteristics, such as elongated morphologies, cell division asymmetry, and super-diffusivity, that suggest potential mechanical elements during invasion that can drive cancer metastasis and progression. Our previous work [30] has also shown that more subtle geometric effects such as barrier angles could impact invasion behavior and that cancer cells of different metastatic grades exhibit differential invasion capacities across mechanical barriers. Further studies using the MUSIC device for different cancer cell lines with different external chemotactic inputs can help elicit and establish characteristic behavioral signatures of mechanical invasion and identify modulation effects from chemokines. Therefore, our platform has potential applications in uncovering subtle properties of cell invasion, drug screening, and discovering mechanical biomarkers. The portable and versatile lab-on-a-chip form-factor of and the label free properties measureable by our technique also facilitate implementation in clinical and commercial settings.

3.5 Methods

3.5.1 Cell culture and reagents

MDA-MB-231 cells were obtained from the NCI PS-OC and the ATCC. They were cultured in Leibovitz L-15 media (Life Technologies) supplemented with 10% fetal bovine serum (Atlanta Biologicals) and 1% Penicillin-Streptavidin (Life Technologies). K20T cells were obtained from the Giannakakou lab at Weill Cornell Medical College. They are a taxol-resistant derivative of MDA-MB-231 cells [45]. They were cultured in L-15 media supplemented with 10% fetal bovine serum, 1% Penicillin-Streptavidin, and 15nM paclitaxel (taxol) (Cytoskeleton, Inc). All cells were incubated at 37^{o} C without supplemented CO_2.

3.5.2 Device Fabrication

Device masters were fabricated at the Cornell Nanofabrication Facility (CNF). Standard stepper photolithography was used on SU8 resist on a silicon substrate followed by PDMS-soft lithography, similarly described in [30]. Briefly, SU8 was spun onto a Si wafer, exposed to UV with a stepper under a patterned photomask, and developed to create patterned master substrates. PDMS was then molded over the master and crosslinked to create microchannels. The channels were bonded to glass slides to create microfluidic devices.

3.5.3 Experiments and Analysis

Cells were loaded into the inlet reservoir regions at the ends of the microchannels and allowed to spontaneously migrate into the three-dimensionally confined channels. Devices with cells were incubated as in regular cell culture as described above. Timelapse experiments were performed once the cells were in the channels. For each experiment, devices were placed on top of a heating plate maintained at 37^{o}C. Typical

durations for timelapse experiments were around 1-2 days at a temporal resolution of 3.4 minutes. Cell tracking and measurements were performed by manual tracing via ImageJ. Data processing and analysis were performed via custom programs on MATLAB. The height of the microchannels used for all experiments with quantitative analysis was 10μm. 5μm high channels were used in Fig. 3.2a and 3.3 only for demonstrative purposes and qualitative presentation. The reason was that mechanical features were very clear for 5μm high channels, but the experimental throughput was low because many cells did not permeate subnucleus barriers that were 5μm high. For statistical analysis, the Chi-squared test was used for probability measurements, and ANOVA statistics were used for all other measurements, unless otherwise specified. Error bars are standard error of the mean (s.e.m.). Standard DAPI staining was used for fluorescence imaging in Fig. 3.S1. For cell viability in these devices, we found in a typical timelapse experiment of ~23hrs that less than 10% (5 out of 54) of the cells died while occupying the experimental field of view.

3.6 Acknowledgements

We thank Professor Paraskevi Giannakakou for the K20T cells. The work described was supported by the Cornell Center on the Microenvironment and Metastasis through Award Number U54CA143876 from the National Cancer Institute. This work was performed in part at the Cornell NanoScale Facility, a member of the National Nanotechnology Network, which is supported by the National Science Foundation (Grant ECS-0335765). Michael Mak is a NSF Graduate Research Fellow. The funders had no role in study design, data collection and analysis, decision to publish, or preparation of the manuscript.

3.7 Supplementary Information (SI)

Fig. S3.1: Two fixed MDA-MB-231 cells with nuclei counterstained with DAPI in the MUSIC device (fluorescence with brightfield illumination). The morphology and deformation of the cell nuclei in the larger channel and during invasion across the subnucleus barrier are demonstrated. The width of the larger channel is 15μm.

Video S3.1: A sample experiment showing cell invasion in the MUSIC device. The video frame rate is 10000x real-time.

Video S3.2: A taxol-treated cell fails to invade across the subnucleus barrier. The video frame rate is 10000x real-time.

Video S3.3: As the cell invades across the subnucleus barrier, long extensions are protruded. The video frame rate is 10000x real-time.

Video S3.4: A K20T cell divides asymmetrically at the subnucleus barrier interface. The daughter cells have unequal projected areas. The video frame rate is 10000x real-time.

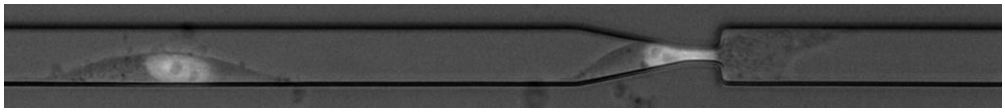

Fig. S3.1: Two fixed MDA-MB-231 cells with nuclei counterstained with DAPI in the MUSIC device (fluorescence with brightfield illumination). The morphology and deformation of the cell nuclei in the larger channel and during invasion across the subnucleus barrier are demonstrated. The width of the larger channel is 15μm.

REFERENCES

1. A. F. Chambers, A. C. Groom and I. C. MacDonald, *Nature reviews*, 2002, **2**, 563-572.
2. E. Sahai, *Nature Reviews Cancer*, 2007, **7**, 737-749.
3. E. Quintana, M. Shackleton, M. S. Sabel, D. R. Fullen, T. M. Johnson and S. J. Morrison, *Nature*, 2008, **456**, 593-598.
4. D. Hanahan and R. A. Weinberg, *Cell*, 2011, **144**, 646-674.
5. S. Kumar and V. M. Weaver, *Cancer Metastasis Rev*, 2009, **28**, 113-127.
6. C. M. Kraning-Rush, S. P. Carey, J. P. Califano, B. N. Smith and C. A. Reinhart-King, *Physical Biology*, 2011, **8**, 015009.
7. C. M. Kraning-Rush, J. P. Califano and C. A. Reinhart-King, *PLoS ONE*, 2012, **7**, e32572.
8. M. J. Paszek, N. Zahir, K. R. Johnson, J. N. Lakins, G. I. Rozenberg, A. Gefen, C. A. Reinhart-king, S. S. Margulies, M. Dembo, D. Boettiger, D. A. Hammer and V. M. Weaver, *Cancer Cell*, 2005, **8**, 241-254.
9. J. M. Tse, G. Cheng, J. A. Tyrrell, S. A. Wilcox-Adelman, Y. Boucher, R. K. Jain and L. L. Munn, *PNAS*, 2012, **109**, 911-916.
10. J. Guck, S. Schinkinger, B. Lincoln, F. Wottawah, S. Ebert, M. Romeyke, D. Lenz, H. M. Erickson, R. Ananthakrishnan, D. M. J. Kas, S. Ulvick and C. Bilby, *Biophysical Journal*, 2005, **88**, 3689-3698.
11. D. R. Gossett, H. T. K. Tse, S. A. Lee, Y. Ying, A. G. Lindgren, O. O. Yang, J. Rao, A. T. Clark and D. D. Carlo, *Proc. Natl. Acad. Sci. USA*, 2012, **109**, 7630-7635.
12. K. N. Dahl, A. J. S. Ribeiro and J. Lammerding, *Circulation Research*, 2008, **102**, 1307-1318.
13. D. T. Butcher, T. Alliston and V. M. Weaver, *Nature Reviews Cancer*, 2009, **9**, 108-122.
14. P. Friedl, K. Wolf and J. Lammerding, *Current Opinion in Cell Biology*, 2011, **23**, 55-64.
15. G. Bao and S. Suresh, *Nature Materials*, 2003, **2**, 715-725.
16. D. Wirtz, K. Konstantopoulos and P. C. Searson, *Nature Reviews Cancer*, 2011, **11**, 512-522.
17. M. J. Rosenbluth, W. A. Lam and D. A. Fletcher, *Biophysical Journal*, 2006, **90**, 2994-3003.
18. E. Sahai and C. J. Marshall, *Nature Cell Biology*, 2003, **5**, 711-719.
19. P. Friedl and K. Wolf, *Nature Reviews Cancer*, 2003, **3**, 363-374.
20. A. Albini and D. M. Noonan, *Current Opinion in Cell Biology*, 2010.
21. S. I. Fraley, Y. Feng, R. Krishnamurthy, D.-H. Kim, A. Celedon, G. D. Longmore and D. Wirtz, *Nature Cell Biology*, 2010, **12**, 598-604.
22. D. Irmia and M. Toner, *Integrative Biology*, 2009, **1**, 506-512.
23. G. Mahmud, C. J. Campbell, K. J. M. Bishop, Y. A. Komarova, O. Chaga, S. Soh, S. Huda, K. Kandere-Grzybowska and B. A. Grzybowski, *Nature Physics*, 2009, **5**, 606-612.

24. X. Jiang, D. A. Bruzewicz, A. P. Wong, M. Piel and G. M. Whitesides, *Proc. Natl. Acad. Sci. USA.*, 2005, **102**, 975-978.
25. M. Gerlinger, A. J. Rowan, S. Horswell, J. Larkin, D. Endesfelder, E. Gronroos, P. Martinez, N. Matthews, A. Stewart, P. Tarpey, I. Varela, B. Phillimore, S. Begum, N. Q. McDonald, A. Butler, D. Jones, K. Raine, C. Latimer, C. R. Santos, M. Nohadani, A. C. Eklund, B. Spencer-Dene, G. Clark, L. Pickering, G. Stamp, M. Gore, Z. Szallasi, J. Downward, P. A. Futreal and C. Swanton, *The New England Journal of Medicine*, 2012, **366**, 883-892.
26. K. Wolf, I. Mazo, H. Leung, K. Engelke, U. H. v. Andrian, E. I. Deryugina, A. Y. Strongin, E.-B. Bröcker and P. Friedl, *The Journal of Cell Biology*, 2003, **160**, 267-277.
27. P. C. Hermann, S. L. Huber, T. Herrler, A. Aicher, J. W. Ellwart, M. Guba, C. J. Bruns and C. Heeschen, *Cell Stem Cell*, 2007, **1**, 313-323.
28. G. A. O. P. Verdier-Pinard, H. McDai and S. B. Horwitz, *Oncogene*, 2003, **22**, 7280-7295.
29. D. Velegol and F. Lanni, *Biophysical Journal*, 2001, **81**, 1786-1792.
30. M. Mak, C. A. Reinhart-King and D. Erickson, *PLoS ONE*, 2011, **6**, e20825.
31. F. Sabeh, R. Shimizu-Hirota and S. J. Weiss, *Journal of Cell Biology*, 2009, **185**, 11-19.
32. Y. Kienast, L. v. Baumgarten, M. Fuhrmann, W. E. F. Klinkert, R. Goldbrunner, J. Herms and F. Winkler, *Nature Medicine*, 2010, **16**, 116-122.
33. J. R. Levy and E. L. F. Holzbaur, *Journal of Cell Science*, 2008, **121**, 3187-3195.
34. J. Y. Ji, R. T. Lee, L. Vergnes, L. G. Fong, C. L. Stewart, K. Reue, S. G. Young, Q. Zhang, C. M. Shanahan and J. Lammerding, *Journal of Biological Chemistry*, 2007, **282**, 20015-20026.
35. A. Takesono, S. J. Heasman, B. Wojciak-Stothard, R. Garg and A. J. Ridley, *PLoS ONE*, 2010, **5**, e8774.
36. K. E. Rankin and L. Wordeman, *Journal of Cell Biology*, 2010, **190**, 35-43.
37. M. A. Jordan and L. Wilson, *Nature Reviews Cancer*, 2004, **4**, 253-265.
38. S. Kapoor and D. Panda, *Biochemical Pharmacology*, 2012, **83**, 1495-1506.
39. P. B. Schiff and S. B. Horwitz, *Proc. Natl. Acad. Sci. USA*, 1980, **77**, 1561-1565.
40. P. Dieterich, R. Klages, R. Preuss and A. Schwab, *Proc. Natl. Acad. Sci. USA.*, 2008, **105**, 459-463.
41. R. J. Petrie, A. D. Doyle and K. M. Yamada, *Nature Reviews: Molecular Cell Biology*, 2009, **10**, 538-549.
42. R. Pankov, Y. Endo, S. Even-Ram, M. Araki, K. Clark, E. Cukierman, K. Matsumoto and K. M. Yamada, *Journal of Cell Biology*, 2005, **170**, 793-802.
43. M. E. Stearns and M. Wang, *Cancer Research*, 1992, **52**, 3776-3781.
44. J. D. Shields, M. E. Fleury, C. Yong, A. A. Tomei, G. J. Randolph and M. A. Swartz, *Cancer Cell*, 2007, **11**, 526-538.
45. K. M. Wiesen, S. Xia, C.-P. H. Yang and S. B. Horwitz, *Cancer Letters*, 2007, **257**, 227-235.

46. Z. Storchova and D. Pellman, *Nature Reviews Molecular Cell Biology*, 2004, **5**, 45-54.
47. J. A. Knoblich, *Nature Reviews Molecular Cell Biology*, 2010, **11**, 849-860.
48. H. Rajagopalan and C. Lengauer, *Nature*, 2004, **432**, 338-341.
49. J. Fink, N. Carpi, T. Betz, A. Bétard, M. Chebah, A. Azioune, M. Bornens, C. Sykes, L. Fetler, D. Cuvelier and M. Piel, *Nature Cell Biology*, 2011, **13**, 771-778.
50. M. Thery, A. Jimenez-Dalmaroni, V. Racine, M. Bornens and F. Julicher, *Nature*, 2007, **447**, 493-497.
51. S. Suresh, *Acta Materialia*, 2007, **55**, 3989-4014.
52. L. Liu, B. Sun, J. N. Pedersen, K.-M. A. Yong, R. H. Getzenberg, H. A. Stone and R. H. Austin, *Proc. Natl. Acad. Sci. USA*, 2011, **108**, 6853-6856.
53. B. C. Isenberg, P. A. DiMilla, M. Walker, S. Kim and J. Y. Wong, *Biophysical Journal*, 2009, **97**, 1313-1322.
54. E. T. Roussos, J. S. Condeelis and A. Patsialou, *Nature Reviews Cancer*, 2011, **11**, 573-587.
55. M. H. Zaman, L. M. Trapani, A. L. Sieminski, D. MacKellar, H. Gong, R. D. Kamm, A. Wells, D. A. Lauffenburger and P. Matsudaira, *Proc. Natl. Acad. Sci. USA.*, 2006, **103**, 10889-10894.
56. Y. Zheng, J. Chen, M. Craven, N. W. Choi, S. Totorica, A. Diaz-Santana, P. Kermani, B. Hempstead, C. Fischbach-Teschl, J. A. López and A. D. Stroock, *Proc. Natl. Acad. Sci. USA*, 2012.

CHAPTER 4

A SERIAL MICROPIPETTE MICROFLUIDIC DEVICE WITH APPLICATIONS TO CANCER CELL REPEATED DEFORMATION STUDIES

4.1 Abstract

Cells are complex viscoelastic materials that are frequently in deformed morphological states, particularly during the cancer invasion process. The ability to study cell mechanical deformability in an accessible way can be enabling in many areas of research where biomechanics is important, from cancer metastasis to immune response to stem cell differentiation. Furthermore, phenomena in biology are frequently exhibited in high multiplicity. For instance, during metastasis, cells undergoing non-proteolytic invasion squeeze through a multitude of physiological barriers, including many small pores in the dense extracellular matrix (ECM) of the tumor stroma. Therefore, it is important to perform multiple measurements of the same property even for the same cell in order to fully appreciate its dynamics and variability, especially in the high recurrence regime. We have created a simple and minimalistic micropipette system with automated operational procedures that can sample the deformation and relaxation dynamics of single-cells serially and in a parallel manner. We demonstrated its ability to elucidate the impact of an initial cell deformation event on subsequent deformations for untreated and Paclitaxel treated MDA-MB-231 metastatic breast cancer cells, and we examined contributions from the cell nucleus during whole-cell micropipette experiments. Finally we developed an empirical model that characterizes the serial factor, which describes the reduction in cost for cell deformations across sequential constrictions. We performed experiments

Reproduced by permission of Michael Mak and David Erickson, "A Serial Microfluidic Micropipette Device with Applications to Cancer Cell Repeated Deformation Studies" (2013).

using spatial, temporal, and force scales that match physiological and biomechanical processes, thus potentially enabling a qualitatively more pertinent representation of the functional attributes of cell deformability.

4.2 Introduction

Cell mechanics is an emerging field that is becoming more relevant in many different areas in biology, from cancer to hematology to stem cell biology. Many specialized techniques, including atomic force microscopy (AFM), micropipette aspiration (MPA), optical tweezers, and magnetic twisting cytometry, have been developed or tailored to enable researchers to study the mechanical properties of cells [1]. One particular property – deformability – has become increasingly popular, as cell deformations have important functional roles in a broad spectrum of biological phenomena. As an important example, cancer metastasis involves a series of mechanical events at the single-cell level. In order to invade to distal sites, aggressive cells must be able to squeeze across small spaces in the extracellular matrix (ECM) of the tumor stroma and endothelial barrier and circulate and traffic through microvessels smaller than the size of the cell [2-4]. Under such confined microenvironments, these cells must acquire deformed morphologies. There have been many studies on cell deformability, with techniques ranging from more conventional AFM [5, 6] and MPA [7] to more recent microfluidic systems with active (optical forces, hydrodynamic inertial focusing) [8-10] and passive (microconstrictions) [11-13] deformation actuators. In particular, we are interested in deformations in the most extreme form observed in physiological systems – deformations at the subnucleus scale. This is important because such large deformations with strained and elongated nuclei, which are not fully understood from current approaches, are often observed in cell invasion through the ECM, across endothelial junctions, and in microcirculation from various cell-in-

gel and animal metastasis models as well as in histological slides of tumor slices [4, 14-18]. These events in the metastatic process suggest that cell deformability is an important property in the context of cancer.

Recent work using microfluidic techniques has shown that deformability may be correlated with disease states in cells, metastatic potential, and stem cell differentiation [8, 10, 13]. Deformability in these cases is often measured by the aspect ratio of a cell under a fixed stress, such that more deformable cells exhibit a higher aspect ratio. Another common metric is the amount of time it takes a cell to flow through a microconstriction under pressure. While these metrics are simple in nature, they nonetheless are proving to have clinical implications [10]. Additionally, these assays are typically high throughput and automated, requiring minimal manual operations, during measurements, which offer appeal towards clinical applications.

A key disadvantage of these high throughput microfluidic assays is that the information content is typically simplistic and does not fully appreciate the complexity of a biological phenomenon. In particular, the mechanical properties of cells are intrinsically complex in nature and heterogeneous. Not only does heterogeneity exist between different components of the cell, such as the cytoplasm, cytoskeleton, and nucleus, but heterogeneity exists even within the cytoskeletal and nucleoskeletal networks. Additionally, the cytoskeleton and nucleoskeleton are viscoelastic and their response under stress is dynamic [7, 19]. These dynamics have rich mathematical representations [7, 20], and the structural subcellular components, such as actin and intermediate filament networks, also have complex and dynamic behaviors when perturbed [21, 22]. As a result, a simple one-shot measurement of each cell (*i.e.* aspect ratio under asymmetric stress or average transit time across a barrier), while offering

an appealing and simple assay, is a reductionist characterization of biological cells. Fundamental properties, such as creep strain dynamics, that are pertinent to the deformability of viscoelastic materials are difficult to measure with such techniques. As such, conventional, high resolution and more comprehensive measurements from traditional techniques such as AFM and MPA offer more detailed information about the state and fundamental properties of individual cells.

Micropipette aspiration and atomic force microscopy have been used to elucidate more complex phenomena associated with the mechanical properties of cells and nuclei. For instance, micropipette studies were able to produce high resolution data that revealed and enabled the development of mathematical models of the viscoelasticity of different cell types, which as an example characterized the distinction between solid like cells (endothelial cells) and liquid like cells (neutrophils) [7]. Additionally, MPA of isolated cell nuclei identified the contributions of different subnucleus structures on force bearing properties under different conditions (swollen and unswollen nuclei) and further revealed that the creep compliance of the nucleus follows a power-law temporal dependence over time scales from 0.1 to 1000 seconds [19]. AFM studies have also been critical in revealing local cell stiffness as well as cell forces and stress under compression and extension [6, 23].

In these existing methods, there is a tradeoff between 1) experimental simplicity and automation and 2) the complexity of the measurable properties. More complex material properties such as cell strain dynamics during deformation and relaxation require more complicated procedures that are practicable typically only in labor intensive and bulky apparatuses (MPA and AFM) [5-7], while more automated systems such as microfluidic constriction assays, optical stretchers, and inertial focusing

methods [8-12] produce static and reductionist measurements and are currently limited to simple experimental procedures. The incorporation of more functionality in microfluidic assays often requires more manual labor or additional components such as robotic actuators for image-assisted flow modulation, thus reducing their automation or adding to their already bulky systems that require external pressure pumps and optical components (*e.g.* high power lasers). These tradeoffs limit the adoptability of the mentioned techniques and thus the practicability of the field of cell biomechanics to select experts in select settings. Mechanical properties such as cell deformability and viscoelasticity, however, are critical and complementary to many areas in cell biology, with implications in cancer metastasis, immune cell responses, tissue homeostasis, blood diseases, and stem cell differentiation [23-31]. Therefore there is a need for multifunctional, procedurally adept, and automated systems that require minimal labor and components in order to promote accessibility and technology adoption.

To address this need, to eliminate the tradeoff, and to simplify labor for complex experimental procedures – we considered several factors. In order to fully appreciate the biomechanical properties of cells but in a high throughput and automated manner, it is necessary to develop a scalable microfluidic design that incorporates scale matching in important experimental parameters, such as spatial, temporal, and force properties. Not only is it important for feature sizes of the device to be on the order of the cell and nucleus size, but the time scale of measurements should match biomechanical time scales as in strain and relaxation events. It may also be important for externally applied forces onto cells to be comparable in magnitude to those present in biological systems in order to appreciate physiological responses, as in migration and invasion driven by cell generated forces. For instance, if the flow rate used in

microfluidic techniques is too high, which is typically the case in previous studies aimed at high throughput operations, relaxation dynamics cannot be studied and appreciated since they are slower. If the flow rate is too low, experiments would be impractical as cells would not deform sufficiently. Additionally, in vivo flow velocities are on the order of 0.5μm/s and tumor interstitial pressures are around 1000pa [32, 33]. By performing time-scale matching, we can appreciate the properties conferred upon the cell by the coupling of relaxation and deformation dynamics. This is particularly interesting in the context of cancer metastasis, in which cells undergo frequent squeezing and recovery events during and after invasion across highly confined physiological spaces (*e.g.* constricted gaps in the ECM, endothelial junctions, microvessels) [4, 14, 34-36]. Furthermore, while typical experiments especially in microfluidics can sample many cells, individual cells are usually sampled only once. Because each cell is a highly complex system, a single sample per cell may not provide details about the diversity of and dynamics associated with the responses of a single cell. Thus, such data, while high throughput, are limited by their inability to distinguish the variability between different cells in a population and the variability of a property within an individual cell.

The device we present here is a parallel array of serial micropipettes capable of performing both deformation and relaxation measurements of individual cancer cells. Each cell is sampled multiple times for the assessment of consequential effects, which enables us to answer questions such as 1) how does one deformation event impact subsequent deformation events and 2) what are the key dynamics that govern serial deformations? Addressing these questions is important because it offers a more comprehensive assessment of a complex cell mechanical property (deformability) over a one-shot measurement (*e.g.* the aspect ratio of a cell under a fixed stress). This is

also important for physiological relevance because, for instance, during the metastatic cascade, cells typically undergo a multitude of deformation events, from active invasion across confined spaces of the ECM in the tumor stroma to circulation across small blood and lymphatic vessels. Cancer cells therefore undergo constant deformations. Because cells are viscoelastic, their deformability is impacted by their conformational states conferred from their previous deformation events. However, the dynamics of serial deformations are unclear, and our device enables these dynamics to be elucidated. By understanding if and how a cell is conditioned by deformations in subsequent events, we can begin to gain potential insights toward the mechanical elements that govern cancer metastasis.

For our experiments, we used the MDA-MB-231 cell line, which model highly metastatic breast adenocarcinoma. Their metastatic nature and previous studies [8, 37, 38] indicate that their deformation dynamics are of particular interest. Our results demonstrate several key findings. An initial deformation event facilitates subsequent serial deformations of the same cell, and this mechanical conditioning is dependent on the initial and remaining strain on the cell. The strain dynamics during deformation are dependent on both the viscoelastic cell body and nucleus. These experiments were performed in a simple microfluidic design with an automated experimentation scheme, which increases the capacity of practicable experiments and provides an instantly enabling technology to any basic biology lab setting in a small self-reliant form factor requiring no external equipment or micromanagement.

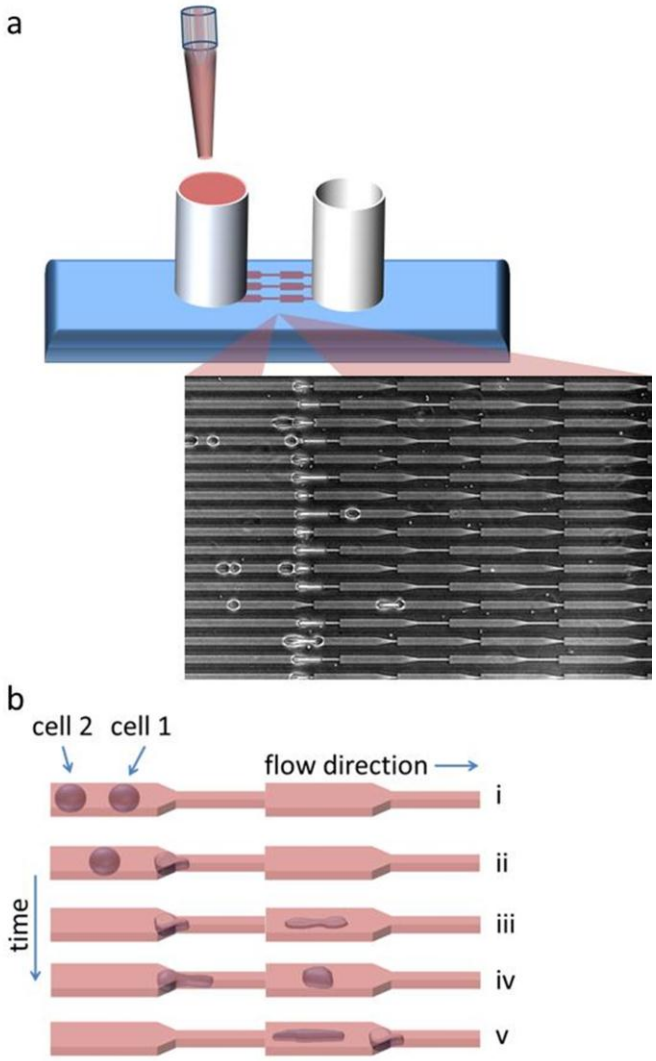

Figure 4.1: Schematic of device and operations. a) The user simply pipettes the sample of interest into the inlet reservoir (left) and gravity drives the flow, enabling the device to operate without any external pressure actuators. Cells are automatically driven to the micropipette constrictions (inset). b) After sample loading, the multi-step serial cell deformation experiments are performed automatically with no manual input required. 5 main steps are performed in an automated manner: i) multiple cells flow through the channels and into the constriction region, ii) cell 1 enters the constriction and clogs the flow as it undergoes deformation under a fixed pressure gradient, iii) cell 1 fully transits across the barrier and cell 2 subsequently clogs the flow, enabling iv) cell 1 to relax towards equilibrium at a fixed position, v) cell 2 fully transits across the barrier and cell 1 clogs the flow at the next constriction, allowing cell 2 to relax at a fixed position while cell 1 undergoes a secondary deformation. The width of the larger channel region is 15μm, the width of the smaller channel (constriction) region is 3.3μm, and two different lengths are incorporated at the constrictions (10μm and 60μm), as shown in Figure 4.1a inset. The height of the channels is a constant 10μm.

4.3 Results and Discussion

4.3.1 Device design and operations

The device consists of parallel microchannels. Each channel contains a series of microconstrictions to serve as a serial micropipette capable of deforming objects multiple times via pressure driven flow. The larger region of the channel has a width of 15μm, which is on the order of the size of a cell. The smaller constriction region is 3.3μm, which is smaller than the cell nucleus, thus ensuring that the cell undergoes a substantial deformation that samples a key organelle in the cell that often limits cell squeezing in physiological landscapes due to its size and stiffness. Additionally, two different lengths of the constriction region are incorporated, one that is 10μm-long (shorter than a typical cell) and one that is 60μm-long (longer than a typical cell), mimicking short physiological barriers such as ECM-pores and long physiological barriers such as microvessels, respectively (Figure 4.1a inset). A pressure gradient is induced on-chip across each channel by applying a difference in liquid height between the inlet and the outlet of the device. This enables device operation without external pressure sources. For the experiments here, we applied a pressure gradient of around 400pa, which is comparable to interstitial pressures in tumors [33]. Our device design and operations facilitate more conventional micropipette studies than existing microfluidic constriction or deformation schemes, enabling multifaceted studies in an automated manner as shown in Figure 4.1 and described in the following:

Strain rate at fixed pressure: Cells that enter the constriction region essentially clog the flow, inducing in that channel zero volumetric flow rate and infinite hydrodynamic resistance [39], so the pressure drop (400pa) across the channel is entirely across the cell. In considering the cross-sectional area of the channel and thus the area of the cell that the pressure is acting on, this translates into an applied force across the cell of around

60nN, which is on the scale of the forces that an individual cell generates [40-42]. Timelapse microscopy enables the tracking of the cell strain over time under this fixed pressure. In our experiments, since each cell flows in one direction (longitudinal) and is stretched along that direction, the strain J that we measure is defined to be the length that the cell is stretched from its equilibrium ΔL divided by its equilibrium length L_0 as measured by the cell length in the larger channel before reaching the constriction. This is the definition used throughout this paper and is consistent with conventional micropipette studies [7, 19].

Release and relaxation after an initial strain: After an initial strain is applied to the cell during constriction transit, cell relaxation dynamics can be assessed. This is accomplished in an automated manner in this device as subsequent cells will plug the constrictions as they undergo transits, stopping the flow, and enabling the previously deformed cell to relax at a fixed position for tracking.

Tracking serial cell deformations: Every micropipette channel is designed with multiple constrictions in series to enable the multiple sampling of each transiting cell. This is important because each cell is dynamic and heterogeneous, and a static measurement of a cell property does not provide insights into its full capacity. The serial design induces cells to necessarily transit across multiple barriers to probe dynamic effects. However, even at relatively low pressures, subsequent transit times can be fast due to a mismatch in the relaxation rates and flow speeds (the cell is still in a highly deformed state in subsequent transits), thus masking the dynamic regime in the behavior of serial deformations. With our device, because each serial micropipette consists of a single channel, intermittent flow pauses are automatically generated as multiple cells are transiting across the same micropipette channel, as shown in Figure

4.1 and SI video 4.1, thus enabling cells to relax back towards its initial conformation before the next deformation event. This enables us to probe into the dynamics that govern multiple cell deformations and cell mechanical properties that result from the coupling between relaxation and deformation.

4.3.2 Repeated Cell Transits and Taxol Treatment

Using the procedure demonstrated previously, we measured the transit times of the same cell across 5 sequential constrictions. Here, we considered situations in which only one cell was present in the serial micropipette channel, so cell 2 from Figure 4.1 was not present, and we examined experiments from the 10μm-long constriction design. Because cell 2 was not present, cell relaxation between constrictions is typically less than 1 second. We investigated the serial deformations of both untreated cells and cells treated with 10μM Paclitaxel (taxol), a chemotherapeutic drug that stabilizes microtubules and inhibits cell division [43-45], for 1 day. As shown in Figure 4.2a, the transit times across constrictions decrease after the first transit. The transit time across the first constriction is larger for taxol treated cells, which we may expect as the size of these cells is significantly larger than untreated cells (Figure 4.2a inset) due to mitotic inhibition. Here, the size is defined by the length of the cells in the microchannel, since the cell width generally fills the channel width. As the cells transit across subsequent barriers, however, the transit times collapse between the two cell groups, demonstrating that once the cells are under sufficient deformation, cell size becomes less important in determining transit times. Interestingly, we also found that cell permeation across constrictions is further facilitated after the second transit, as illustrated in Figure 4.2b. For each cell, we normalized the transit times across the third, fourth, and fifth constrictions to the transit time across the second constriction of

the same cell, and our results show that cells can transit across the later constrictions more quickly.

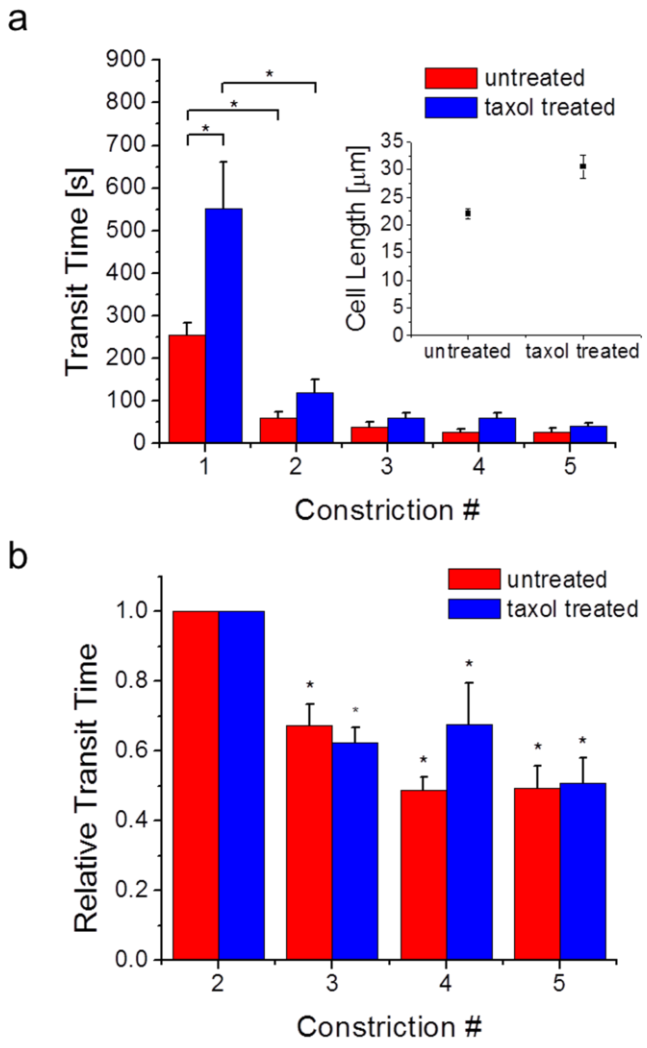

Figure 4.2: Cell permeation across sequential micropipette constrictions and the effects of taxol treatment. a) Individual untreated and taxol treated cells were driven via pressure driven flow to permeate across sequential subnucleus-scaled constrictions. Taxol treated cells are larger (length = 31 ± 2μm, n = 26) (inset) and require a longer transit time across the first constriction (550 ± 109s, n = 26) than untreated cells (length = 22 ± 0.9μm, n = 36; transit time 1 = 254 ± 59s, n = 34). For both cell groups, the initial transit requires the longest time. Subsequent transits are faster and the difference between the two cell groups is reduced. The number of cells n examined in subsequent transit events ranged from 20 to 40. * denotes $p < 0.01$. b) The transit times across the third, fourth, and fifth constrictions are normalized by the transit time across the second constriction of the same cell. Transit times are further reduced at subsequent constrictions after the second permeation. * denotes $p < 0.01$ when compared to unity. Error bars are s.e.m.

These findings suggest that cells that undergo perpetual deformations exhibit less difficulty in permeating across highly confining subnucleus-scaled mechanical barriers. Since aggressive cancer cells are constantly undergoing deformations, particularly across dense ECM networks with subnucleus-scaled pore sizes, it may be easier for them to invade than more static cells. In nutrient-deprived regions, as in locations where large tumors are forming, energetic efficiency may be important in tumor activity, and invasion becomes more efficient for more aggressively invasive cells. Additionally, we showed that taxol treatment, which is a common therapeutic for metastatic breast cancer, increases the size of the cell and the initial transit time. Once the cell is conditioned after the initial deformation event, the relative difference in cell transit times becomes less distinguishable, suggesting that for aggressive cells, size may not be critical in the cost of invasion. Taxol, however, also reduces directionally polarized migratory behavior [46, 47], which makes persistent invasion across confined barriers more difficult. This suggests that anti-invasion properties of taxol [46, 48] may result from a synergy of cell size increase and decreased directional persistence in migration, which would decrease the probability of occurrence of the initial deformation event and thus inhibit subsequent easier invasions. Taxol treatment for 1 day also has the impact of increasing the size of cell nuclei (SI Figure 4.1), as cells fail to divide during cytokinesis. Since the nucleus, due to its size and stiffness, is mechanically the most obstructive intracellular component during invasion [4], its size increase likely also plays an important role in impeding the initial deformation event. Finally, since microtubule disruption and taxol are known not to have a significant impact on the rigidity of cells [49-52], our results show that passive anti-invasive effects of taxol are most likely caused by the increase in cell and nucleus size.

4.3.3 The Strain Dynamics of Serial Deformations

Next we examined the serial deformation dynamics of cells in which cell 2 in the configuration in Figure 4.1 was present. This allowed for more substantial cell relaxation over longer durations, on average over 3 minutes as shown in SI Figure 4.2, between subsequent deformations. The results for the remainder of this paper will be based on this coupled-cell configuration in order to better appreciate both deformation and relaxation dynamics. In the previous section we considered short recovery times during which cells remained in highly deformed states after the first transit and here we considered substantially longer recovery times during which many cells recovered their equilibrium shapes. Thus our study covers a large range in the spectrum of recovery times and relaxation states that may occur in vivo.

Our experiments show that even after prolonged relaxation, an initial deformation event facilitates subsequent deformations, as demonstrated in Figure 4.3a. The initial deformation requires the longest time, and the strain vs. time curve displays several phases. Here, strain refers exclusively to the strain of each cell along the long axis of the channel, *i.e.* the length that the cell is stretched from equilibrium divided by the cell's equilibrium length. With respect to the strain rate of the cell, the three main phases identifiable are 1) the initial shortest and fastest phase followed by 2) a longer, stagnant phase then followed by 3) a moderately fast phase. Deformations across subsequent barriers have reduced or eliminated phases 2 and 3, enabling the cell to deform and transit across the barrier more easily.

To better gauge the nature of these phases, we stained the nuclei of live cells and performed simultaneous phase contrast and fluorescence imaging to distinguish relative contributions from the cell body (*i.e.* primarily the cytoskeleton) and the largest and stiffest organelle, the cell nucleus. Figure 4.3b and SI video 4.2 show the

kymograph and video, respectively, of a typical cell transit event, and the transit phases are now more apparent. The first phase is when part of the cell can easily deform into the constriction, likely due to a simple force balance between the applied pressure and the initial elastic response of the cell [53, 54]. This can be seen from the rapid increase in the longitudinal boundaries of the cell, outlined in red in the kymograph, at the very beginning under the label "1." Phase 2 is when the nucleus is obstructed and its stiffness is too high to transit further into the constriction, as demonstrated by the nucleus being stuck at the constriction interface. However, a slow creep from its viscoelastic nature enables gradual permeation. This creep deformation can be interpreted from the increase in the length of the boundaries of the nucleus, represented by the blue outline, in the kymograph. Phase 3 is when the nucleus has deformed entirely into the constriction, leaving the remaining (less obstructive) portion of the cell to deform more quickly into the constriction. The cell body and nucleus are now highly deformed and the longitudinal boundaries are substantially longer than initially. We note here that phase 3 in the initial transit is much longer than the entirety of the transit period of the subsequent transits shown in Figure 4.3a. This shows that while the nucleus appears to be the most obstructive element in cell transit, the serial deformation effect is a reflection of the conditioning of both the nucleus and the cytoskeleton. Once the cell is conditioned, its subsequent transit dynamics have an altered behavior that is faster than both phase 2 and phase 3. Figure 4.3c shows the kymograph of the same cell as in Figure 4.3b deforming across a second barrier. The strain dynamics of the whole cell as well as that of the nucleus are altered; there is no nucleus obstruction phase and the cell transits through the entire constriction much more quickly. Figure 4.3d shows a representative spatial slice from which the kymographs were taken.

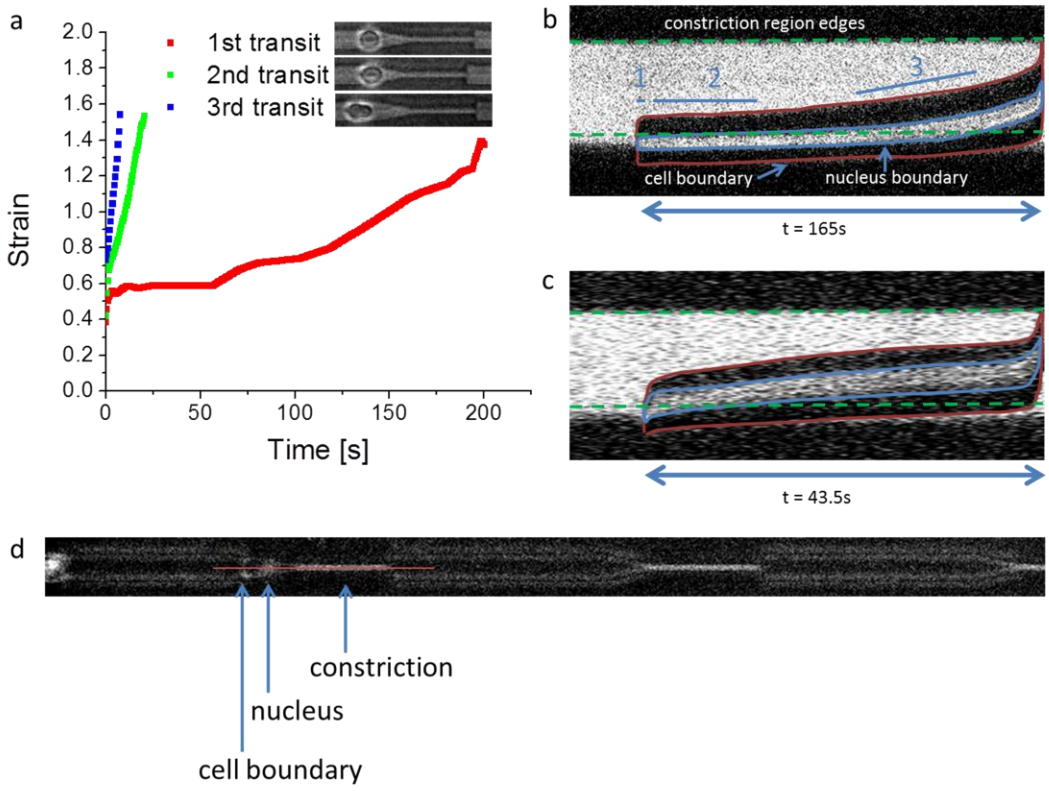

Figure 4.3: Serial deformation dynamics. a) The same MDA-MB-231 cell is deformed across multiple microconstrictions (3.3μm x 10μm x 60μm) in series in the serial micropipette device. Subsequent transits are faster and display altered strain dynamics. The cell is allowed to relax before subsequent deformations, as described in the text, and the extent of their relaxed state right before the next deformation event is displayed in the corresponding pictures (on the label). In the first transit, multiple phases are exhibited in the strain dynamics- an initial rapid phase, followed by a stagnant phase, and a moderate rate final phase. b) More details about the strain dynamics of the first transit are elucidated when considering the transit dynamics of the cell nucleus, as shown here with a live nucleus stain. The image is a kymograph along the center of the micropipette constriction (longitudinal axis vs. time). Simultaneous phase contrast and fluorescence imaging help display the cell boundaries, the nucleus, and the constriction. This enables a more comprehensive consideration of the contributing elements in the phases of cell deformation dynamics. As shown, phase 1 is the initial cell response to a fixed stress from the external pressure, phase 2 is when the stiff cell nucleus is obstructed at the entry of the constriction due to insufficient pressure but viscoelastic creep enables slow permeation, and during phase 3 the nucleus has sufficiently deformed (partially) into the constriction leading to an increase in subsequent strain rate. c) The subsequent transit for the same cell as in b) displays a faster strain rate without prolonged nucleus obstruction at the constriction interface. Both the cell boundaries and the nucleus deform into the constriction more quickly. d) A representative image illustrating the slice, indicated by the red line, where the kymographs were taken. For scale reference, the length of the constriction is 60μm.

It is noteworthy here that under a fixed cell-scaled force of 60nN (via 400pa of applied pressure completely dropped across the cell at the constriction), the cells examined in our experiments deformed and transited completely across the constriction within a matter of minutes (4.2 ± 0.5 and 7.3 ± 2 minutes for the first and thus longest deformation event through 10μm-long and 60μm-long constrictions, respectively). The times were even shorter for subsequent transits. This translates into comparable cell migration velocities in 3D gel studies [55, 56], suggesting that simple creep strain dynamics under consistent force loads could play a basic role in cell invasion across subcellular-scaled confinements. For instance, even if an applied force from the cell is not sufficient to enable it to squeeze across a constriction instantaneously, the cell simply needs to wait while consistently applying a forward force, *e.g.* through actin polymerization, and viscoelastic creep will confer the cell a sufficiently deformed state to pass through the constriction. Thus, cell invasion may characteristically exhibit the coupling between both active (force generation) and passive (creep strain) processes. It is also notable that the phases observed here in the strain dynamics of flowing cells have qualitative similarities to the phases observed when cells are actively migrating across subnucleus-scaled barriers [4, 37, 46].

4.3.4 The Serial Factor

To assess and appreciate the impact of repeated deformations on cells, we need a way to measure a factor, which we will now call the "serial factor" SF, that quantifies the relative degree of difficulty for a cell to transit across constrictions after it squeezes across an initial constriction. A good candidate for SF is the ratio of the transit times $SF = t_s/t_i$, where t_i is transit time across the first constriction and t_s is the transit time across a subsequent constriction.

First, our results show in Figure 4.4 that the average SF is larger for serial transits across shorter constrictions. The average SF is 0.40 ± 0.04 (n = 20) and 0.20 ± 0.05 (n = 13) for 10μm-long serial constrictions and 60μm-long serial constrictions, respectively, where n is the number of single-cell serial transit events. We note here that in this data, the strains on the cells before subsequent transits for the 10μm-long and 60μm-long serial micropipette experiments are 0.24 ± 0.03 (n = 20) and 0.25 ± 0.05 (n = 13), respectively, and they are not statistically different. This indicates that longer constrictions, which induce larger overall deformations on the cell, facilitate subsequent deformations to a larger degree, even after the cell is allowed to relax back towards equilibrium.

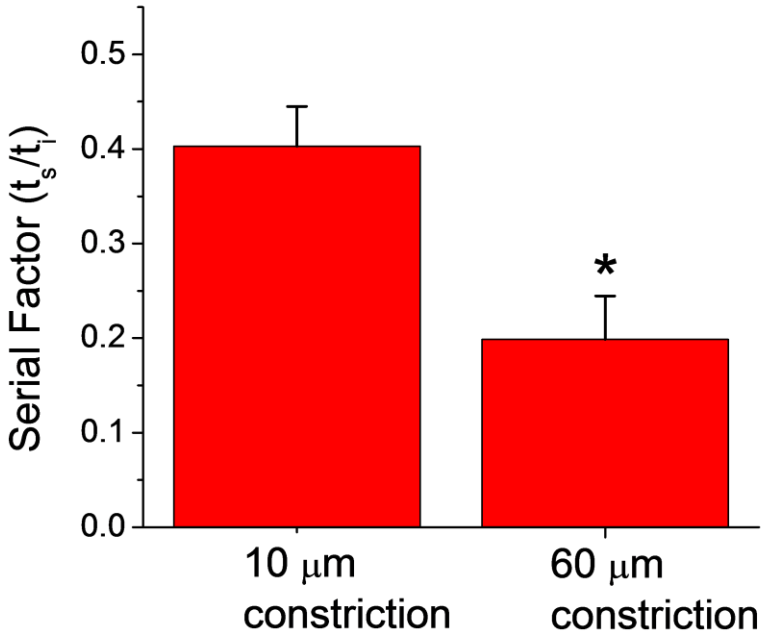

Figure 4.4: The serial factor vs. constriction length. Shorter constrictions (10μm) that only span a fraction of the total cell length exhibit a longer normalized transit time in subsequent constrictions (t_s/t_i = 0.40 ± 0.04, n = 20) than longer constrictions (60μm) that span most if not the entire deformed cell length (t_s/t_i = 0.20 ± 0.05, n = 13). The serial factor is thus larger for cells experiencing larger initial strains. Error bars represent standard error of the mean, and * indicates $p < 0.01$.

Next, we were interested in measuring SF as a function of the conformation of the cell after deformation in order to gauge how the shape or morphology of a previously deformed cell translates into its ability to deform across a subsequent constriction. Therefore, since we were conducting deformation and relaxation experiments on these cells, we were interested in the function $SF(J_r)$, where J_r is the remaining strain on an initially deformed cell after it is given time to relax towards equilibrium. To derive this function, we considered previous micropipette studies that empirically characterized cells to exhibit a power-law creep under a fixed applied pressure, such that the creep strain is $J(t) = At^{\alpha}$, where A is a constant scaling prefactor, t is the time the cell is under the applied pressure, and α is the power-law scaling exponent. We note that this simple power-law relation does break down over the entirety of the cell and may be impacted by our simultaneous sampling of the nucleus and the cytoskeleton with subnucleus-scaled constrictions [19, 53]. However, for simplicity and in order to derive an empirical effective model, here we adopted the power-law approximation. Next we also assumed that A remains constant for the same cell under serial deformations such that all changes in cell strain behavior are then attributed to α, which helps simplify our effective model. For our experiments, since most of the time the cell spends transiting across the barrier is time spent for the strain to increase until the cell reaches a conformation (*i.e.* when the cell is thin enough) that enables the cell to flow easily and rapidly through the constriction, we approximated t_i and t_s to be effectively the time when the cell strain is increasing under a constant applied pressure gradient. From this we derived SF as follows:

Since serial deformations are easier, the power-law scaling factor α is altered in subsequent deformations in comparison to the initial, such that there are two different strain dynamics relations:

$$J_1(t) = At^{\alpha_1} \tag{4.1a}$$

$$J_2(t) = At^{\alpha_2} \tag{4.1b}$$

where the indices 1 and 2 correspond to initial and subsequent strains, respectively. From this, we obtain:

$$J_i = J_1(t_i) = At_i{}^{\alpha_1} \tag{4.2a}$$

$$J_s = J_2(t_r + t_s) = A(t_r + t_s)^{\alpha_2} \tag{4.2b}$$

$$J_r = J_2(t_r) = At_r{}^{\alpha_2} \tag{4.2c}$$

where J_i is the total strain from the initial deformation (1st transit), J_s is the total strain in a subsequent deformation (the following serial transits), J_r is the remaining strain on the cell after relaxation and before the next deformation event, and t_r is the virtual time that it would require the cell to strain from 0 to J_r. The total strains on the cells are the same for each transit since they are deforming across identical subsequent constrictions so J_i equals J_s and it follows that:

$$t_i{}^{\alpha_1} = (t_r + t_s)^{\alpha_2} \tag{4.3a}$$

$$SF = \frac{t_s}{t_i} = t_i^{\frac{\alpha_1}{\alpha_2}-1}\left(1 - \left(\frac{J_r}{Ji}\right)^{\frac{1}{\alpha_2}}\right) \tag{4.3b}$$

which gives an analytical form of SF. Next, we impose the condition that as the cell is allowed to relax completely to its equilibrium state after deformation, α_2 would recover to α_1:

$$\alpha_2 = \alpha_1(1 + C * F[J_r/J_i]) \tag{4.4}$$

where C is a scaling coefficient and F is the normalized relaxation function that decays from 1 to 0 when the cell fully recovers (when $J_r/J_i = 0$). From the data, SF decays sharply initially and then plateaus near 0, so therefore we choose a simple function that displays that form:

$$F = 1 - e^{-\frac{Jr}{k*J_i}} \tag{4.5}$$

where $k*J_i$ is the characteristic decay length of F.

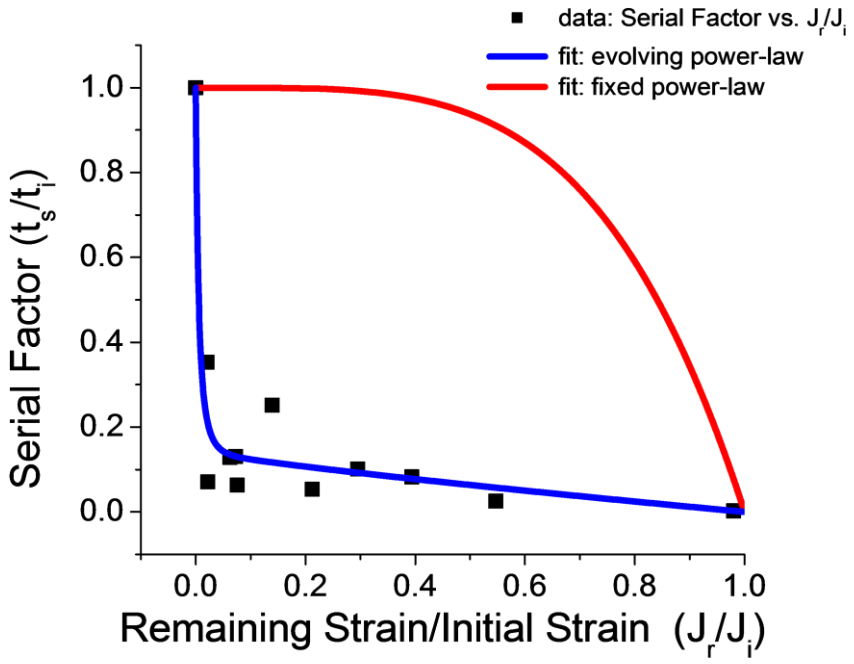

Figure 4.5: The serial factor vs. normalized remaining cell strain. After an initial cell deformation across a 60µm long subnucleus-scaled (3.3µm x 10µm cross-sectional area) constriction, it becomes easier for cells to deform across subsequent (identical) constrictions. The relative degree of difficulty between subsequent and initial deformation processes can be interpreted from the relative transit times across the constrictions (t_s/t_i), *i.e.* the serial factor SF. As the remaining strain J_r is increased (relative to the total initial strain J_i) signifying less relaxation before the subsequent deformation, the transit process becomes faster. Moreover, SF exhibits a sharp initial decay, which our modified power-law based model for SF captures (blue fitted curve, $R^2 = 0.92$). The conventional low strain, weak power-law model ($\alpha = 0.25$) exhibits a different behavior (red curve).

Figure 4.5 shows the SF vs. J_r/J_i plot for the micropipette experiments with 60μm-long constrictions. Only experiments from 60μm-long constrictions were analyzed here because for 10μm-long constrictions, since the constriction is shorter than the cell, there is non-uniform relaxation after cell transit (parts of the cell starts relaxing earlier than others), which complicates any analytical comparisons, particularly with our simple model. As shown in Figure 4.5 by the blue fitted curve, the experimental data fits to our model for SF ($R^2 = 0.92$). Previous studies focusing on the low strain regime have shown that the strain dynamics exhibit a weak power-law dependence with $\alpha < 1$ [19, 53, 57]. We calculated and plotted the red curve in Figure 4.5 that assumes a constant $\alpha = 0.25$, a typical value in the low strain regime. As demonstrated, the curvatures of the two calculated curves are different with one that is concave and one that is convex. The actual SF data is concave, illustrating that in the serial deformation scenario, it is applicable to consider an evolving α that becomes larger than 1. Without considering the serial effect, it would be difficult to fully appreciate the details and degree to which subsequent deformations are facilitated, which are especially relevant to physiological phenomena that require cells to deform repeatedly such as in migration and invasion. Using our model for an evolving α that is dependent on the remaining strain before subsequent cell deformations, we can recover the typical characteristics of J(t) for differentially relaxed cell states, as shown in Figure 4.6.

The results here show that unless a cell is allowed to relax completely back to its equilibrium state after a deformation event, any remaining strain indicates that the cell is in an enhanced "serial mode" that enables it to deform across subsequent constrictions more easily, in accordance to the serial factor. As illustrated in Figure 4.7, this could have implications in the metastatic process in cancer, as non-proteolytic

invasion induces cells to squeeze across narrow gaps that are often smaller than the cell nucleus, *i.e.* through constriction rings in the ECM [4, 34]. An initial invasion event would thus confer upon the cell faster strain dynamics that facilitate subsequent invasion through confining physiological barriers.

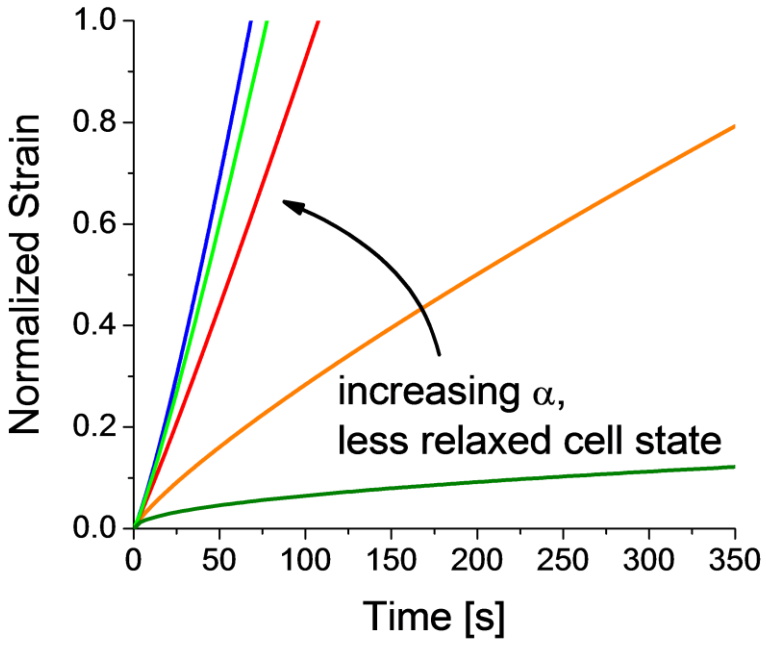

Figure 4.6: Strain dynamics under fixed pressure from the evolving power-law model. By assuming that the power-law scaling exponent α evolves based on the degree of relaxation of the cell state after an initial deformation, we plotted the normalized strain $J_N(t) = At^{\alpha}/J_i = t^{\alpha}/t_i^{\alpha 1}$ for different α's and recovered the typical behavior in serial strain dynamics under fixed pressure.

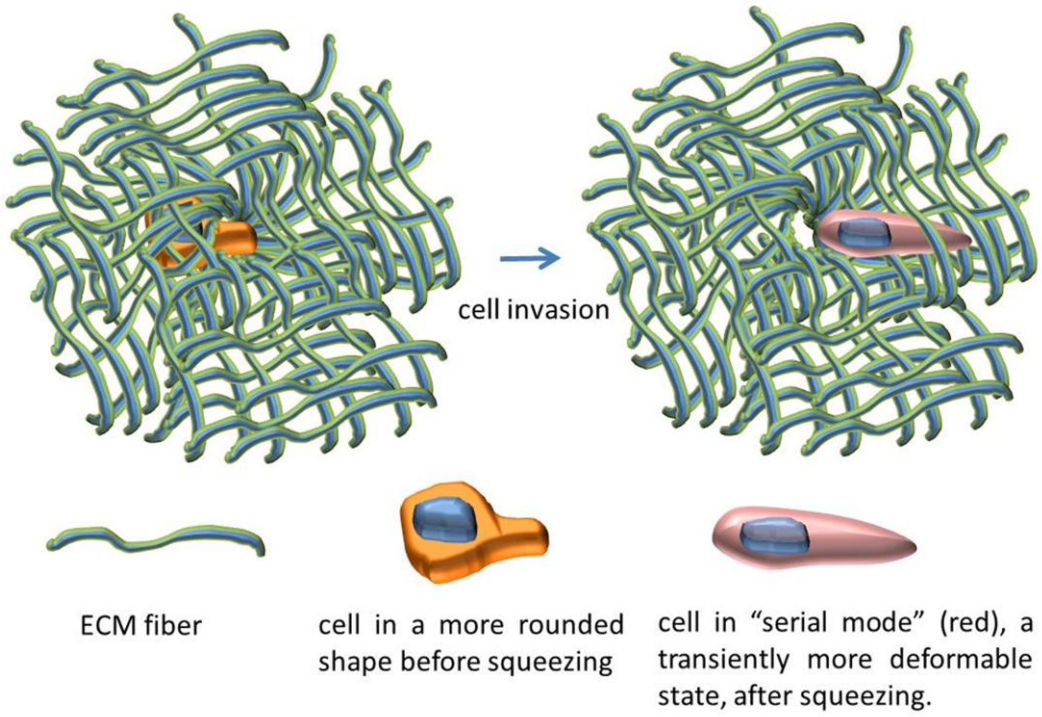

Figure 4.7: Illustration of the serial effect during cancer invasion. When a cell is in a more relaxed state and invades (non-proteolytically) across a constriction ring in the ECM, the cell is deformed and transiently enters a "serial mode" that exhibits a higher power-law scaling exponent in its strain dynamics, making the subsequent invasion events easier in accordance to the serial factor.

4.4 Conclusion

We developed a simple self-reliant system with no external parts or sources (syringe pumps, pressure manifolds, or other bulky connections that drive microfluidic devices) that requires only the loading of the cell samples of choice and performs multifaceted experiments in an automated manner without robotic assistance from programmable microscope stages, motorized parts, or other robotic actuators. We have demonstrated using this device that an initial cell deformation event, via a fixed cell-scaled force, conditions the cell for easier subsequent deformations, as the strain dynamics are altered. This conditioning is a function of the initial and remaining strain on the cell

and may have physical implications for biological phenomena that require a multitude of deformation events, such as cancer invasion or immune cell diapedesis. We also gauged the contribution to the deformation strain dynamics from both the whole-cell body and the nucleus, which complements previous work that primarily considered only whole-cell boundaries or isolated nuclei or other intracellular components. Finally, we believe that the simplicity, form factor, automation, and multiple capabilities of this device can facilitate in a highly adoptable manner a broad array of cell mechanobiology studies, from measuring cell viscoelastic properties to disease diagnostics.

4.5 Experimental Section

4.5.1 Cell Culture

MDA-MB-231 cells were obtained from the NCI Physical-Sciences and Oncology Center. They were cultured in Leibovitz L-15 media (Life Technologies) with 10% fetal bovine serum (Atlanta Biologicals) and 1% Penicillin-Streptavidin (Life Technologies) at 37^{o}C without CO_2.

4.5.2 Device Fabrication

Device masters were fabricated at the Cornell NanoScale Facility (CNF). Standard photo- and soft-lithography techniques were used to create devices. Briefly, SU8 was spun onto a silicon wafer and exposed under a photomask with the micropipette patterns in a stepper. The patterned wafer was then developed to create a negative image of the device. PDMS was cast onto the master and crosslinked to create the micropipette channels. The channels were then bonded to glass slides to create the finished microfluidic device.

4.5.3 Experiments and Analysis

Devices were treated with 1% bovine serum albumin (BSA) (Sigma-Aldrich) in serum-free media (L-15) for several hours before experiments in order to prevent stiction. Additionally, cells used in experiments were resuspended in serum-free media, as serum is a major contributor to cell adhesion [58]. Cells were loaded into the inlet reservoir of the device and experiments were automatically conducted as described in the design and operations section of this paper. Gravity drives the flow with an applied pressure gradient equal to $\rho g \Delta h$, where ρ is liquid density, g is the coefficient of gravity, and Δh is the difference in liquid height between the inlet and outlet. A fixed volume difference, which is directly proportional to a fixed liquid height difference, was set between the inlet and outlet reservoirs via pipetting. The volume difference for these experiments was 1.4mL with a pipette resolution of 0.02mL. The device was placed and kept on a heating plate set at 37^{o}C. Videos were recorded at 500ms per frame under a microscope, which produced the data of the experiments. Experiments typically lasted 1-2hrs, after which the device inlet is usually clogged by excessive cells. Next generation designs that incorporate larger channels between the inlet and outlet to allow excessive cells to flow through instead of clog the device would likely extend the operational lifetime. Experimental analysis and cell tracking were performed using ImageJ and custom MATLAB programs. For statistical analysis, one-way ANOVA was used to determine statistical significance. Error bars on data represent standard error of the mean (s.e.m.). For taxol experiments, cells were incubated in 10μM taxol (Cytoskeleton, Inc.) for 1 day prior to experiments. For fluorescence experiments, NucBlue (a live nucleus counterstain that is formulated from Hoechst 33342) (Life Technologies) was used and cells were incubated in the dye in complete growth media for 15 minutes.

4.6 Acknowledgements

The work described was supported by the Cornell Center on the Microenvironment and Metastasis through Award Number U54CA143876 from the National Cancer Institute. This work was performed in part at the Cornell NanoScale Facility, a member of the National Nanotechnology Network, which is supported by the National Science Foundation (Grant ECS-0335765). Michael Mak is a NSF Graduate Research Fellow.

4.7 Supporting Information (SI)

SI Video 4.1: A video showing the operation of the serial micropipette device. A pressure gradient is applied from left to right. Two cells in the same channel are repeatedly deformed and allowed to relax in place to enable the measurement of the coupling between deformation and relaxation dynamics. The cells are able to transit across subsequent constrictions much more quickly than the initial constriction even after substantial relaxation of their initial strains. The frame rate of the video is 100x faster than real time, and the width of the wider channel region is 15μm.

SI Video 4.2: A superposed phase contrast and fluorescence imaging video showing serial deformations of cells treated with a live nucleus counterstain (NucBlue/Hoechst 33342). This enables the relative contributions of the cell nucleus and the whole cell body in the cell deformation process across constrictions to be distinguished. The frame rate of the video is 100x faster than real time, and the width of the wider channel region is 15μm.

SI Figure 4.1: Distribution of nuclei sizes for a) untreated and b) taxol-treated (1 day) MDA-MB-231 cells with fluorescently stained representative nuclei images (insets).

c) Untreated cells have an average area of 130 ± 4μm (n = 200) and taxol-treated cells have an average area of 217 ± 16μm (n = 62). Error bars are s.e.m. *** indicates p < 0.001. The scale bar is 20μm.

SI Figure 4.2: Distribution of relaxation times used in multi-cell relaxation-deformation experiments. The average relaxation time used was 3.3 minutes.

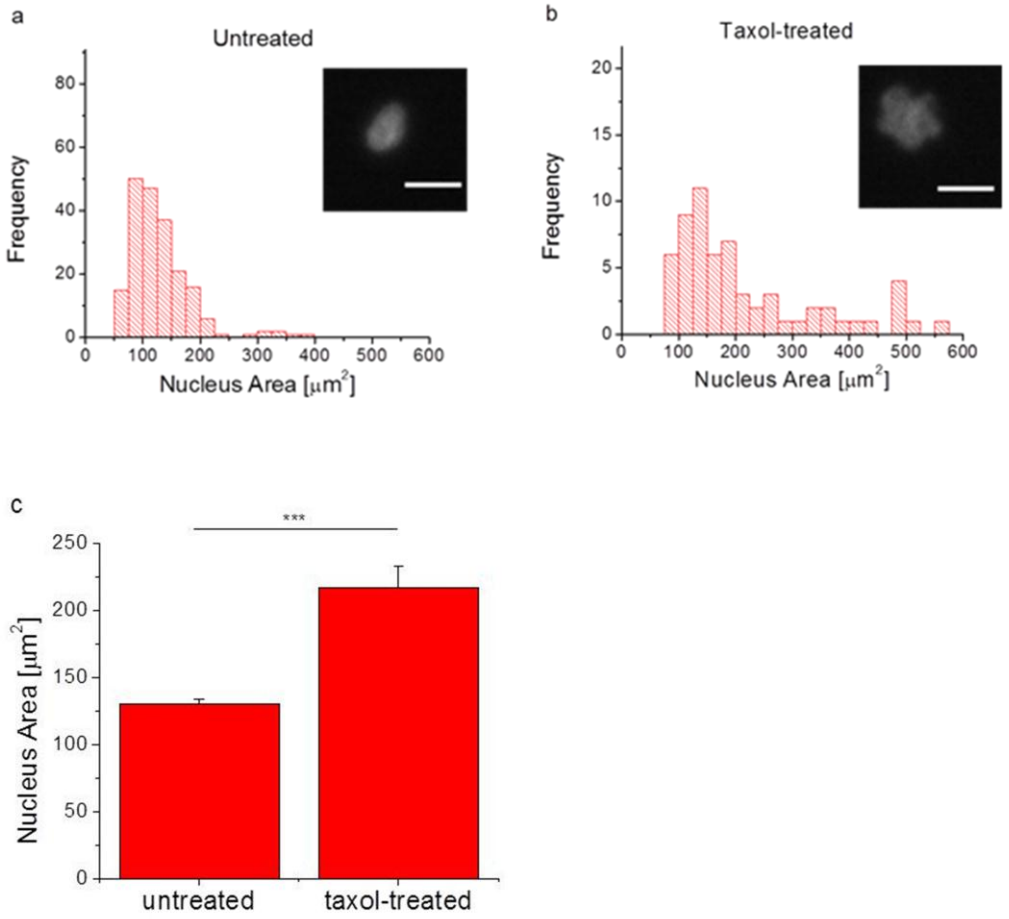

SI Figure 4.1: Distribution of nuclei sizes for a) untreated and b) taxol-treated (1 day) MDA-MB-231 cells with fluorescently stained representative nuclei images (insets). c) Untreated cells have an average area of 130 ± 4μm (n = 200) and taxol-treated cells have an average area of 217 ± 16μm (n = 62). Error bars are s.e.m. *** indicates p < 0.001. The scale bar is 20μm.

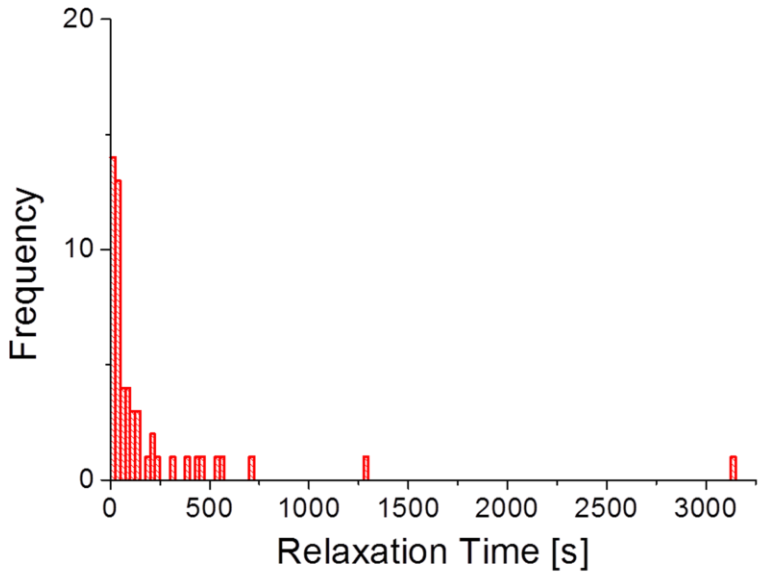

SI Figure 4.2: Distribution of relaxation times used in multi-cell relaxation-deformation experiments. The average relaxation time used was 3.3 minutes.

REFERENCES

1. G. Bao and S. Suresh, Cell and molecular mechanics of biological materials, *Nature Materials*, 2003, 2, 715-725.
2. A. F. Chambers, A. C. Groom and I. C. MacDonald, Dissemination and growth of cancer cells in metastatic sites, *Nature Reviews Cancer*, 2002, 2, 563-572.
3. P. Friedl and K. Wolf, Tumour-Cell Invasion and Migration: Diversity and Escape Mechanisms, *Nature Reviews Cancer*, 2003, 3, 363-374.
4. P. Friedl, K. Wolf and J. Lammerding, Nuclear mechanics during cell migration, *Current Opinion in Cell Biology*, 2011, 23, 55-64.
5. M. J. Rosenbluth, W. A. Lam and D. A. Fletcher, Force Microscopy of Nonadherent Cells: A Comparison of Leukemia Cell Deformability, *Biophysical Journal*, 2006, 90, 2994-3003.
6. M. P. Stewart, Y. Toyoda, A. A. Hyman and D. J. Muller, Tracking mechanics and volume of globular cells with atomic force microscopy using a constant-height clamp, *Nat. Protocols*, 2012, 7, 143-154.
7. R. M. Hochmuth, Micropipette aspiration of living cells, *Journal of Biomechanics*, 2000, 33, 15-22.
8. J. Guck, S. Schinkinger, B. Lincoln, F. Wottawah, S. Ebert, M. Romeyke, D. Lenz, H. M. Erickson, R. Ananthakrishnan, D. Mitchell, J. Kas, S. Ulvick and C. Bilby, Optical Deformability as an Inherent Cell Marker for Testing Malignant Transformation and Metastatic Competence, *Biophysical Journal*, 2005, 88, 3689-3698.
9. I. Sraj, C. D. Eggleton, R. Jimenez, E. Hoover, J. Squier, J. Chichester and D. W. M. Marr, Cell deformation cytometry using diode-bar optical stretchers, *Journal of Biomedical Optics*, 2010, 15, 047010-047010.
10. D. R. Gossett, H. T. K. Tse, S. A. Lee, Y. Ying, A. G. Lindgren, O. O. Yang, J. Rao, A. T. Clark and D. D. Carlo, Hydrodynamic stretching of single cells for large population mechanical phenotyping, *Proc. Natl. Acad. Sci. USA*, 2012, 109, 7630-7635.
11. S. Gabriele, A.-M. Benoliel, P. Bongrand and O. Théodoly, Microfluidic Investigation Reveals Distinct Roles for Actin Cytoskeleton and Myosin II Activity in Capillary Leukocyte Trafficking, *Biophysical Journal*, 2009, 96, 4308-4318.
12. A. Adamo, A. Sharei, L. Adamo, B. Lee, S. Mao and K. F. Jensen, Microfluidics-Based Assessment of Cell Deformability, *Analytical Chemistry*, 2012, 84, 6438-6443.
13. W. Zhang, K. Kai, D. S. Choi, T. Iwamoto, Y. H. Nguyen, H. Wong, M. D. Landis, N. T. Ueno, J. Chang and L. Qin, Microfluidics separation reveals the stem-cell–like deformability of tumor-initiating cells, *Proceedings of the National Academy of Sciences*, 2012, 109, 18707-18712.
14. K. Yamauchi, M. Yang, P. Jiang, N. Yamamoto, M. Xu, Y. Amoh, K. Tsuji, M. Bouvet, H. Tsuchiya, K. Tomita, A. R. Moossa and R. M. Hoffman, Real-

time In vivo Dual-color Imaging of Intracapillary Cancer Cell and Nucleus Deformation and Migration, *Cancer Research*, 2005, 65, 4246-4252.
15. P. Friedl, E. Sahai, S. Weiss and K. M. Yamada, New dimensions in cell migration, *Nat Rev Mol Cell Biol*, 2012, 13, 743-747.
16. A. Pathak and S. Kumar, Biophysical regulation of tumor cell invasion: moving beyond matrix stiffness, *Integrative Biology*, 2011, 3, 267-278.
17. S. Petushi, F. U. Garcia, M. M. Haber, C. Katsinis and A. Tozeren, Large-scale computations on histology images reveal grade-differentiating parameters for breast cancer, *BMC Medical Imaging*, 2006, 6, 14.
18. P. Jiang, K. Yamauchi, M. Yang, K. Tsuji, M. Xu, A. Maitra, M. Bouvet and R. M. Hoffman, Tumor cells genetically labeled with GFP in the nucleus and RFP in the cytoplasm for imaging cellular dynamics, *Cell Cycle*, 2006, 5, 1198-1201.
19. K. N. Dahl, A. J. Engler, J. D. Pajerowski and D. E. Discher, Power-Law Rheology of Isolated Nuclei with Deformation Mapping of Nuclear Substructures, *Biophysical Journal*, 2005, 89, 2855-2864.
20. A. Vaziri and M. R. K. Mofrad, Mechanics and deformation of the nucleus in micropipette aspiration experiment, *Journal of Biomechanics*, 2007, 40, 2053-2062.
21. S. Yamada, D. Wirtz and S. C. Kuo, Mechanics of living cells measured by laser tracking microrheology, *Biophysical Journal*, 2000, 78, 1736-1747.
22. J. C. Crocker, M. T. Valentine, E. R. Weeks, T. Gisler, P. D. Kaplan, A. G. Yodh and D. A. Weitz, Two-point microrheology of inhomogeneous soft materials, *Physical Review Letters*, 2000, 85, 888-891.
23. D. A. Fletcher and R. D. Mullins, Cell mechanics and the cytoskeleton, *Nature*, 2010, 463, 485-492.
24. D. Discher, C. Dong, J. J. Fredberg, F. Guilak, D. Ingber, P. Janmey, R. D. Kamm, G. W. Schmid-Schönbein and S. Weinbaum, Biomechanics: cell research and applications for the next decade, *Annals of biomedical engineering*, 2009, 37, 847-859.
25. F. Lautenschläger, S. Paschke, S. Schinkinger, A. Bruel, M. Beil and J. Guck, The regulatory role of cell mechanics for migration of differentiating myeloid cells, *Proceedings of the National Academy of Sciences*, 2009, 106, 15696-15701.
26. S. Kumar and V. M. Weaver, Mechanics, malignancy, and metastasis: the force journey of a tumor cell, *Cancer and Metastasis Reviews*, 2009, 28, 113-127.
27. M. J. Paszek, N. Zahir, K. R. Johnson, J. N. Lakins, G. I. Rozenberg, A. Gefen, C. A. Reinhart-king, S. S. Margulies, M. Dembo, D. Boettiger, D. A. Hammer and V. M. Weaver, Tensional homeostasis and the malignant phenotype, *Cancer Cell*, 2005, 8, 241-254.
28. Y. Park, C. A. Best, K. Badizadegan, R. R. Dasari, M. S. Feld, T. Kuriabova, M. L. Henle, A. J. Levine and G. Popescu, Measurement of red blood cell mechanics during morphological changes, *Proceedings of the National Academy of Sciences*, 2010, 107, 6731-6736.

29. D. A. Fedosov, B. Caswell, S. Suresh and G. E. Karniadakis, Quantifying the biophysical characteristics of Plasmodium-falciparum-parasitized red blood cells in microcirculation, *Proceedings of the National Academy of Sciences*, 2011, 108, 35-39.
30. W. H. Grover, A. K. Bryan, M. Diez-Silva, S. Suresh, J. M. Higgins and S. R. Manalis, Measuring single-cell density, *Proceedings of the National Academy of Sciences*, 2011, 108, 10992-10996.
31. J. P. Shelby, J. White, K. Ganesan, P. K. Rathod and D. T. Chiu, A microfluidic model for single-cell capillary obstruction by Plasmodium falciparum-infected erythrocytes, *Proceedings of the National Academy of Sciences*, 2003, 100, 14618-14622.
32. J. D. Shields, M. E. Fleury, C. Yong, A. A. Tomei, G. J. Randolph and M. A. Swartz, Autologous Chemotaxis as a Mechanism of Tumor Cell Homing to Lymphatics via Interstitial Flow and Autocrine CCR7 Signaling, *Cancer Cell*, 2007, 11, 526-538.
33. Y. Boucher, L. T. Baxter and R. K. Jain, Interstitial Pressure Gradients in Tissue-isolated and Subcutaneous Tumors: Implications for Therapy, *Cancer Research*, 1990, 50, 4478-4484.
34. K. Wolf, I. Mazo, H. Leung, K. Engelke, U. H. v. Andrian, E. I. Deryugina, A. Y. Strongin, E.-B. Bröcker and P. Friedl, Compensation mechanism in tumor cell migration:mesenchymal–amoeboid transition after blocking of pericellular proteolysis, *The Journal of Cell Biology*, 2003, 160, 267-277.
35. D. Wirtz, K. Konstantopoulos and P. C. Searson, The physics of cancer: the role of physical interactions and mechanical forces in metastasis, *Nature Reviews Cancer*, 2011, 11, 512-522.
36. Y. Kienast, L. v. Baumgarten, M. Fuhrmann, W. E. F. Klinkert, R. Goldbrunner, J. Herms and F. Winkler, Real-time imaging reveals the single steps of brain metastasis formation, *Nature Medicine*, 2010, 16, 116-122.
37. M. Mak, C. A. Reinhart-King and D. Erickson, Microfabricated Physical Spatial Gradients for Investigating Cell Migration and Invasion Dynamics, *Plos One*, 2011, 6.
38. L. Liu, G. Duclos, B. Sun, J. Lee, A. Wu, Y. Kam, E. D. Sontag, H. A. Stone, J. C. Sturm, R. A. Gatenby and R. H. Austin, Minimization of thermodynamic costs in cancer cell invasion, *Proceedings of the National Academy of Sciences*, 2013, 110, 1686-1691.
39. H. A. Stone, A. D. Stroock and A. Ajdari, Engineering flows in small devices: Microfluidics toward a lab-on-a-chip, *Annu. Rev. Fluid Mech.*, 2004, 36, 381-411.
40. M. Prass, K. Jacobson, A. Mogilner and M. Radmacher, Direct measurement of the lamellipodial protrusive force in a migrating cell, *The Journal of Cell Biology*, 2006, 174, 767-772.
41. C. M. Kraning-Rush, J. P. Califano and C. A. Reinhart-King, Cellular Traction Stresses Increase with Increasing Metastatic Potential, *Plos One*, 2012, 7, e32572.

42. C. A. Lemmon, C. S. Chen and L. H. Romer, Cell Traction Forces Direct Fibronectin Matrix Assembly, *Biophysical Journal*, 2009, 96, 729-738.
43. P. B. Schiff and S. B. Horwitz, Taxol stabilizes microtubules in mouse fibroblast cells, *Proc. Natl. Acad. Sci. USA*, 1980, 77, 1561-1565.
44. M. A. Jordan and L. Wilson, Microtubules as Target for Anticancer Drugs, *Nature Reviews Cancer*, 2004, 4, 253-265.
45. K. E. Gascoigne and S. S. Taylor, How do anti-mitotic drugs kill cancer cells?, *Journal of Cell Sciences*, 2009, 122, 2579-2585.
46. M. Mak, C. A. Reinhart-King and D. Erickson, Elucidating mechanical transition effects of invading cancer cells with a subnucleus-scaled microfluidic serial dimensional modulation device, *Lab on a Chip*, 2013, 13, 340-348.
47. A. Takesono, S. J. Heasman, B. Wojciak-Stothard, R. Garg and A. J. Ridley, Microtubules Regulate Migratory Polarity through Rho/ROCK Signaling in T Cells, *Plos One*, 2010, 5, e8774.
48. M. E. Stearns and M. Wang, Taxol Blocks Processes Essential for Prostate Tumor Cell (PC-3 ML) Invasion and Metastasis, *Cancer Research*, 1992, 52, 3776-3781.
49. P. A. Janmey, U. Euteneuer, P. Traub and M. Schliwa, Viscoelastic properties of vimentin compared with other filamentous biopolymer networks, *The Journal of Cell Biology*, 1991, 113, 155-160.
50. C. Rotsch and M. Radmacher, Drug-induced changes of cytoskeletal structure and mechanics in fibroblasts: an atomic force microscopy study, *Biophysical Journal*, 2000, 78, 520-535.
51. M. Sato, W. H. Schwartz, S. C. Selden and T. D. Pollard, Mechanical properties of brain tubulin and microtubules, *The Journal of Cell Biology*, 1988, 106, 1205-1211.
52. M. A. Tsai, R. E. Waugh and P. C. Keng, Passive mechanical behavior of human neutrophils: effects of colchicine and paclitaxel, *Biophysical Journal*, 1998, 74, 3282-3291.
53. N. Desprat, A. Richert, J. Simeon and A. Asnacios, Creep Function of a Single Living Cell, *Biophysical Journal*, 2005, 88, 2224-2233.
54. O. Thoumine and A. Ott, Time scale dependent viscoelastic and contractile regimes in fibroblasts probed by microplate manipulation, *Journal of Cell Science*, 1997, 110, 2109-2116.
55. S. I. Fraley, Y. Feng, R. Krishnamurthy, D.-H. Kim, A. Celedon, G. D. Longmore and D. Wirtz, A distinctive role for focal adhesion proteins in three-dimensional cell motility, *Nature Cell Biology*, 2010, 12, 598-604.
56. C. M. Kraning-Rush, S. P. Carey, M. C. Lampi and C. A. Reinhart-King, Microfabricated collagen tracks facilitate single cell metastatic invasion in 3D, *Integrative Biology*, 2013, 5, 606-616.
57. G. Lenormand, E. Millet, B. Fabry, J. P. Butler and J. J. Fredberg, Linearity and time-scale invariance of the creep function in living cells, *Journal of The Royal Society Interface*, 2004, 1, 91-97.

58. G. Sagvolden, I. Giaever, E. Pettersen and J. Feder, Cell adhesion force microscopy, *Proceedings of the National Academy of Sciences*, 1999, 96, 471-476.

CHAPTER 5

MECHANICAL DECISION TREES FOR INVESTIGATING AND MODULATING SINGLE-CELL INVASION DYNAMICS

5.1 Introduction

Physical cues exist across all biological scales, from the geometries of molecules to the shapes of complex organisms. Whereas in physics researchers greatly appreciate and analyze in rigorous detail every subtlety in the physical environment, in biology such appreciation is often diminished in favor of biochemically-based effects and molecular signaling cascades. More recently, however, studies in biology and medicine have started to emphasize on form and function in tissue and disease mechanics [1-5]. In particular, cancer is a complex disease that has eluded treatments based on conventional genomics approaches. Cancer dissemination or metastasis, the lethal component in the majority of cancers, is still currently a mystery [6, 7]. Without understanding the fundamental dynamics of metastasis, it will be an overwhelming challenge to develop appropriate therapies. There are many critical elements in the metastatic process that are phenomenologically associated with mechanical transport through a physical environment, including cell navigation through the heterogeneous porous medium of the tumor stromal extracellular matrix (ECM), permeation across endothelial barriers, and circulation and trafficking in microvessels [7-9]. The physical interactions of cancer cells with the mechanical components of these environments are not well understood. Here we demonstrate microsystem designs and implementations that aim to reveal fundamental mechanical factors that modulate single-cell decision making during invasion, and we devise strategies, based purely on mechanical asymmetries, to control this behavior in 3D. For our studies we used the MDA-MB-

231 breast adenocarcinoma cell line, which models highly metastatic cancer cells and thus could provide insights toward aggressively invasive behavior.

5.2 Results and Discussions

5.2.1 Mechanical Cues in Cell Decision Making

To examine cell decision making trajectories in response to local dimensional and directional cues, which are two ubiquitous mechanical features throughout the physiological landscape, we developed microfluidic channels with finely tuned patterns that span two specific ranges: the cell-scale and the subnucleus-scale. Cell-scaled mechanical paths have been shown to promote highly persistent migratory and invasive behavior, and subnucleus gaps and pores rate-limit invasion [10-13]. Microgeometries in 2D studies also have been shown to impact cell behavior, from directed migration to stem cell differentiation [14, 15]. At these scales and with 3D microchannels, here we probed the decision making patterns of invading cells by creating a binary decision tree and observed the affinity of cells towards each of the two paths. Just as chemotaxis and durotaxis studies probe cell affinities toward a chemotactic or substrate stiffness gradient, the decision tree microchannels here enable a means to study cell behavior in response to common mechanical signals in the local environment that are not well understood. As shown in Fig. 5.1, cells are loaded into the microchannel inlet reservoir. They spontaneously migrate unidirectionally in the cell-scaled channels and encounter the decision tree. Decision trees of the same design are serially patterned in each separate channel, and two different designs are incorporated in parallel. Pattern 1 consists of a circular design with two path branches that split at the same angle which is perpendicular to the initial cell path; path 1 has a larger width of 10μm and path 2 has a smaller subnucleus width of 3.3μm. Pattern 2 consists of a semicircular design; the top path (path 1) is larger with a 10μm width and

has an entrance that is perpendicular to the original cell path, and the bottom path (path 2) is subnucleus-scaled with a 3.3µm width and is collinear with the original path.

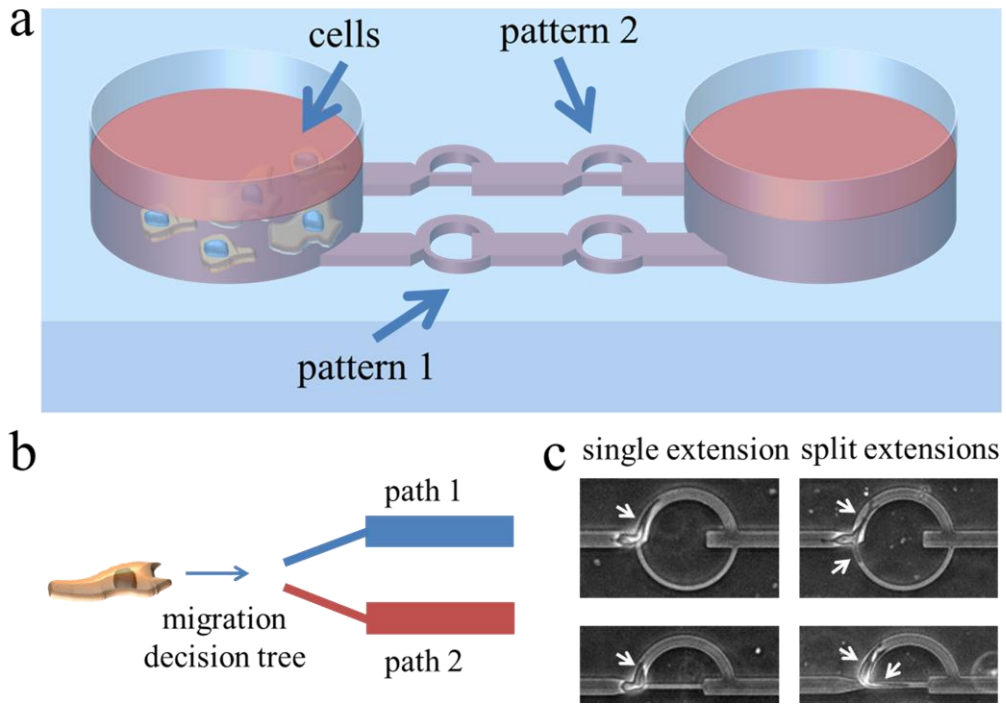

Figure 5.1: Schematics and images illustrating the decision tree microchannel device concept and operations. a) Cells are loaded into the device via pipetting into the reservoir. They will then spontaneously invade into the microchannels. There are two patterns incorporated into our device design. Pattern 1 is a circular design with an arched top path (path 1) that is larger (cell-scaled, 10µm) and an arched bottom path (path 2) that is highly confining (subnucleus-scaled, 3.3µm), and pattern 2 is a semi-circular design with an arched top path (path 1) that is larger (cell-scaled, 10µm) and a straight bottom path (path 2) that is highly confining (subnucleus-scaled, 3.3µm) and collinear with the original cell path. The height of the channels is 10µm. b) Conceptual illustration of a cell migrating along a particular direction and encountering an interface with split paths. The goal is to analyze some under-explored but ubiquitous factors that bias the decision making process in route choosing. c) Typical images of cells in the split path device. This matrix of images shows the possible cell-path interactions at the path junction. In both patterns, cells can exhibit a single extension interaction, in which the cell migrates along one leading edge, or a split extension interaction in which two leading edges, with one in each path, compete for the cell's ultimate decision. Leading edges are marked by arrows.

5.2.2 Dynamics of Cell Decision Making

As shown in Fig. 5.1c, as an individual cell encounters the decision tree, two scenarios can occur. The cell exhibits either a single extension path choice, in which the cell enters the selected path with no contest, or a split extension path choice, in which the cell splits into two competing edges. In the latter case, as demonstrated in Fig. 5.2 a and b and SI videos 5.1 and 5.2, the two competing edges both extend and the cell appears to exhibit a highly tensional state. Eventually, one of the edges collapses and the cell is polarized along the remaining edge. This competing edge phenomenon and the subsequent dynamics elicited in the decision tree microchannels are difficult to recreate and analyze in other cell invasion models, such as with cells embedded in 3D ECMs, where the heterogeneous fibrillar meshwork masks the subtle dynamics in mechanical cell decision making.

Next we treated the cells with Blebbistatin (Bleb) and Paclitaxel (Taxol). Both molecules have been demonstrated previously to have an impact on cell invasiveness. Blebbistatin is an inhibitor of non-muscle myosin IIa, which is implicated in cell contractility and tensional force generation [2, 16-19]. Myosin IIa plays an important role in matrix reorganization in 3D, leading to local matrix alignment and enabling cell invasion [17, 18]. Previous studies have demonstrated that Blebbistatin can inhibit invasion in 3D gels and can alter traction forces [2, 17, 18]. Here we demonstrate that in confined spaces, Blebbistatin alters the migratory mode of cells and changes invasion patterns. Blebbistatin-treated cells exhibit morphologies with long and thin extensions and typically have more rounded cell bodies. This phenotype gives semblance of a tethered ball motile mode, as in a thin string pulling on a tethered ball, as shown in Fig. 5.2 c and d and SI video 5.3.

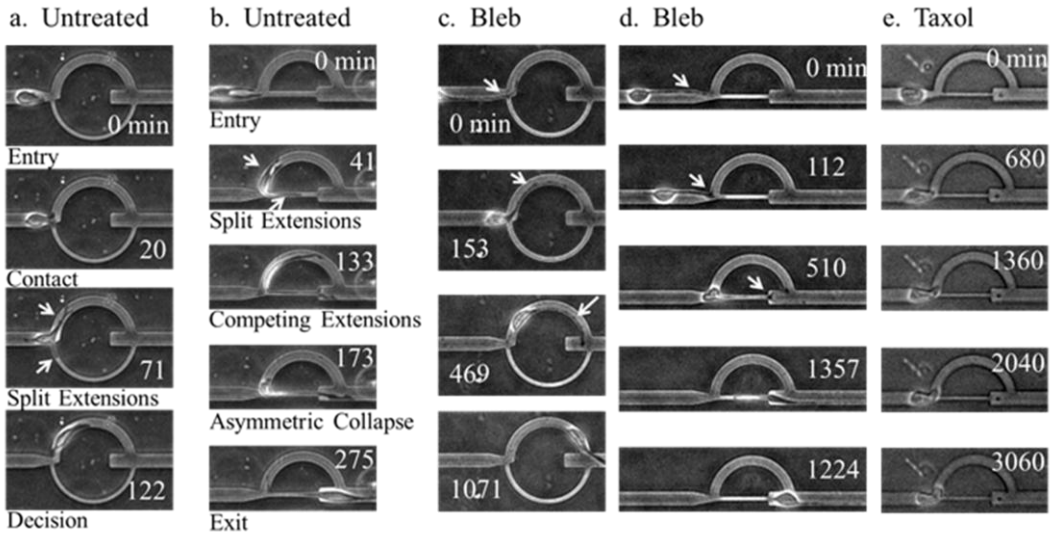

Figure 5.2: Cell invasion dynamics in decision tree microchannels. a) A cell encounters the decision tree of pattern 1. Upon entry, the cell exhibits split extensions. Eventually, one side collapses and the cell is polarized along the other edge. b) A cell encounters the decision tree of pattern 2 and split extensions are formed. The extensions elongate in competing directions until asymmetric collapse occurs, resulting in the cell being polarized along the remaining leading edge. c, d) Blebbistatin-treated cells typically exhibit an altered cell morphology. They have long and thin extensions that drag the cell body along in a motile mode that resembles a tethered ball. Here, the extension drags the cell along the top path of pattern 1 in (c) and along the bottom path of pattern 2 in (d). e) Taxol treated cells tend to be more rounded with less noticeable extensions and have decreased migratory persistence. Arrows point to cell extensions. All time coordinates are in minutes. For scale reference, the width of the top path is 10μm.

Taxol stabilizes microtubules and is a common chemotherapeutic traditionally used for anti-mitotic effects [20]. Microtubule disruption has also been shown to inhibit a cell's ability to permeate through subnucleus-scaled constrictions and impair cell polarity [13, 21, 22]. Taxol-treated cells tend to lose migratory persistence and exhibit a more rounded morphology, as shown in Fig. 5.2e and SI video 5.4.

First, our results show that as the invading cells encounter the decision tree, > 85% of untreated and Blebbistatin-treated cells are able to make a path decision within 5

hours, but most Taxol-treated cells (> 77%) fail to make a decision, as shown in Fig 5.3a. This shows that Taxol (at 10μM) is a decision suppressor. Next, we analyzed the decisions of the untreated and Blebbistatin-treated cells. In Fig. 5.3b, our results from pattern 1 show that untreated invading cells have an overwhelmingly high affinity towards larger channels (path 1) of ≈ 90%. However, when the directionality of the smaller channel is altered to be collinear with the original cell path as in pattern 2, the affinity for path 1 decreases to 68%, demonstrating that migratory polarization effects can bias cell invasion preferences. When the cells are treated with Blebbistatin, the affinity for the collinear route of path 2 in pattern 2 is further increased to 67%, but the affinities are unchanged in pattern 1. These results suggest inhibition of myosin IIa increases the invading cells' sensitivity to directionality, while maintaining the path size affinity when directional biases are not present. Here, we have shown that dimensional and directional factors, which are present along critical steps during cancer metastasis and other phenomena associated with cell motility, can bias cell decision making in a tunable manner, and molecular inhibitors can further modulate those decisions.

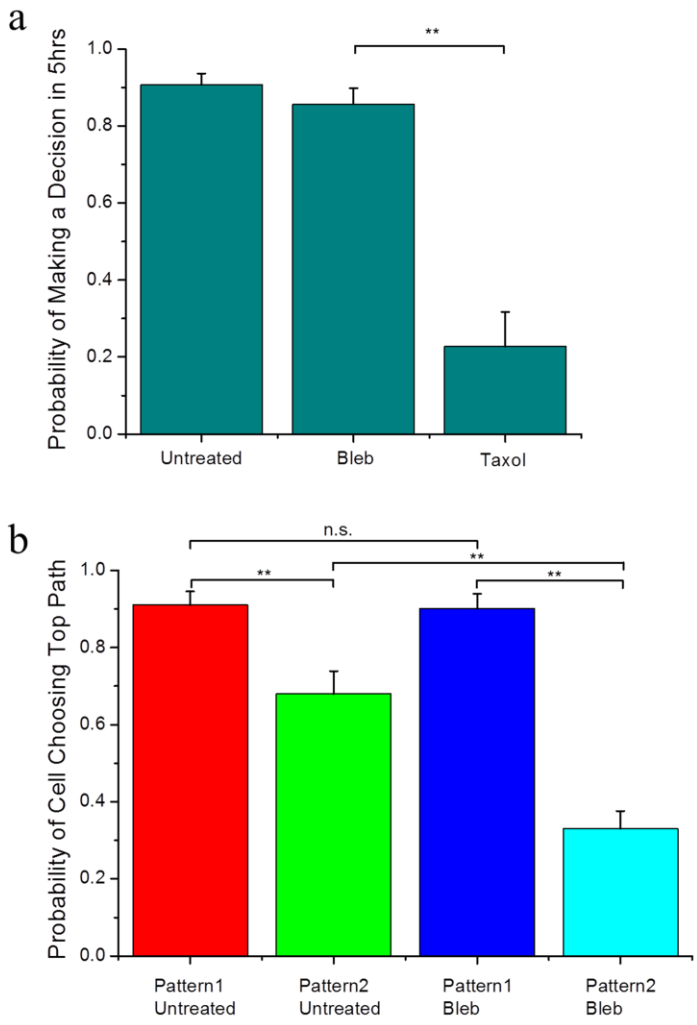

Figure 5.3: Cell decision making statistics. a) Untreated, 50µM Blebbistatin-treated, and 10µM Taxol-treated cells have a probability of making a decision within 5 hours of encountering the decision tree of 0.90 (n = 97), 0.86 (n = 70), and 0.23 (n = 22), respectively, where n is the number of cells. b) The probability of a cell choosing the top path (path 1) for untreated cells in pattern 1, untreated cells in pattern 2, Blebbistatin-treated cells in pattern 1, and Blebbistatin-treated cells in pattern 2 are 0.91 (n = 66), 0.68 (n = 63), 0.90 (n = 59), 0.33 (n = 104), respectively, where n is the number of decisions observed. ** indicates $p < 0.01$ and n.s. indicates not statistically different based on the Chi-square test. Error bars are standard error of the mean (s.e.m.) calculated from the Bernoulli distribution.

5.2.3 Cell Ring Traps

In understanding some of the mechanical and molecular modulators of cell invasive behavior, we can begin to design strategies to manipulate the patterns of invasion. We have shown that cells have an affinity towards cell-scaled paths over subnucleus-scaled paths that can be altered via directional cues and actomyosin activity inhibition. Here, we designed a new mechanical microenvironment that introduces an invasion path, with directional and dimensional asymmetries, that is aimed to bias and prolong cell residence times in localized regions. We call this a ring trap.

As shown in Fig. 5.4a, the trap design consists of a cell-scaled ring region with subnucleus-scaled entrance/exit paths that are perpendicular to the ring. Two trap designs with different exit schemes are incorporated in parallel, one with short constrictions (10μm-long) that are shorter than typical cells and one with long constrictions (60μm-long) that are longer than typical cells, which we call trap10 and trap60, respectively. Since longer traps require permeating cells to undergo larger deformations (and thus require more energy), we hypothesize that this may modulate the trapping stiffness of the rings. The concept is to utilize geometric asymmetry to induce invasive cells to preferentially remain inside the ring and invade in circles.

5.2.4 Symmetry Breaking

Our experiments show that cell-trap interactions exhibit several phenomena. First, as cells invade through the subnucleus-scaled entrance of the ring trap, typically they enter the ring in a symmetric manner, with split edges extending in opposing directions, as shown in Fig. 5.4b and SI video 5.5. After several minutes, the cells undergo spontaneous symmetry breaking, inducing the onset of polarized cell migration. Thus, we have shown here a novel way of inducing spontaneous symmetry

breaking in single-cells by first focusing the cell with a subnucleus barrier, followed by a mechanical barrier upon exit to induce an initial symmetric response. This is essentially a "cell scattering" experiment, analogous to photon scattering experiments in the Rayleigh (subphoton-scaled) and Mie (photon-scaled) regimes that helped uncover the nature of light-matter interactions. Spontaneous symmetry breaking can then be observed and analyzed at the single-cell level, and since symmetry breaking is a fundamental feature that governs the formation and function of all of life [23-25], enabling experimental apparatuses are important for more in depth studies. In particular, symmetry breaking in single-cell migration, especially in 3D, is not well understood. Thus, we have created a way of systematically inducing single-cell scattering experiments and eliciting the dynamics of cell-mechanical environment interactions.

5.2.5 Iteratio ad Nauseam

Next, we show that asymmetries in dimensionality and directionality can indeed be manipulated to suppress cell dissemination by localizing invasion zones. As shown in Fig. 5.4c and SI video 5.6, cells typically remain in the ring trap for an extended period of time and invade in circular and repetitive patterns, which we call *iteratio ad nauseam*. We characterized the trap lifetime and demonstrate in Fig. 5.4d that cells spend over 18 hours in the ring traps. The trap lifetime can be extended by inhibiting myosin IIa with Blebbistatin, which increases the proportion of cells that spend greater than 10 hours in the trap from 55% to 90%, as shown in Fig. 5.4 d and e. The trap lifetime also does not appear to be strongly impacted by the length of the exit constriction. We note here that in our previous studies, we have shown that these aggressive breast cancer cells are highly persistent, maintain speeds on the order of micrometers per minute, and are readily able to permeate through the subnucleus-

scaled barriers when no decision trees are presented [13]. The strategically designed ring trap architectures here are able to confine cells within a region of 50μm radius for an extended period of time simply by catering to natural migratory affinities.

5.2.6 Escape by Division

Finally, we explored the escape mechanisms of cells in the ring traps. We demonstrate in Fig. 5.4f and SI video 5.7 that cell division within or immediately before entering the ring traps promotes cell escape. The trap lifetime after division is reduced to around 4.5 hours, which is significantly less than the 18+ hours of the general population. This is an interesting result, demonstrating that there is an intrinsic connection between invasion and proliferation. Traditionally, cell growth and migration are considered distinct events, and invasive behavior is not presumed to be coupled to cell division. Our results here show the contrary – that cell invasive capacity may be a dynamic property that evolves over the cell cycle.

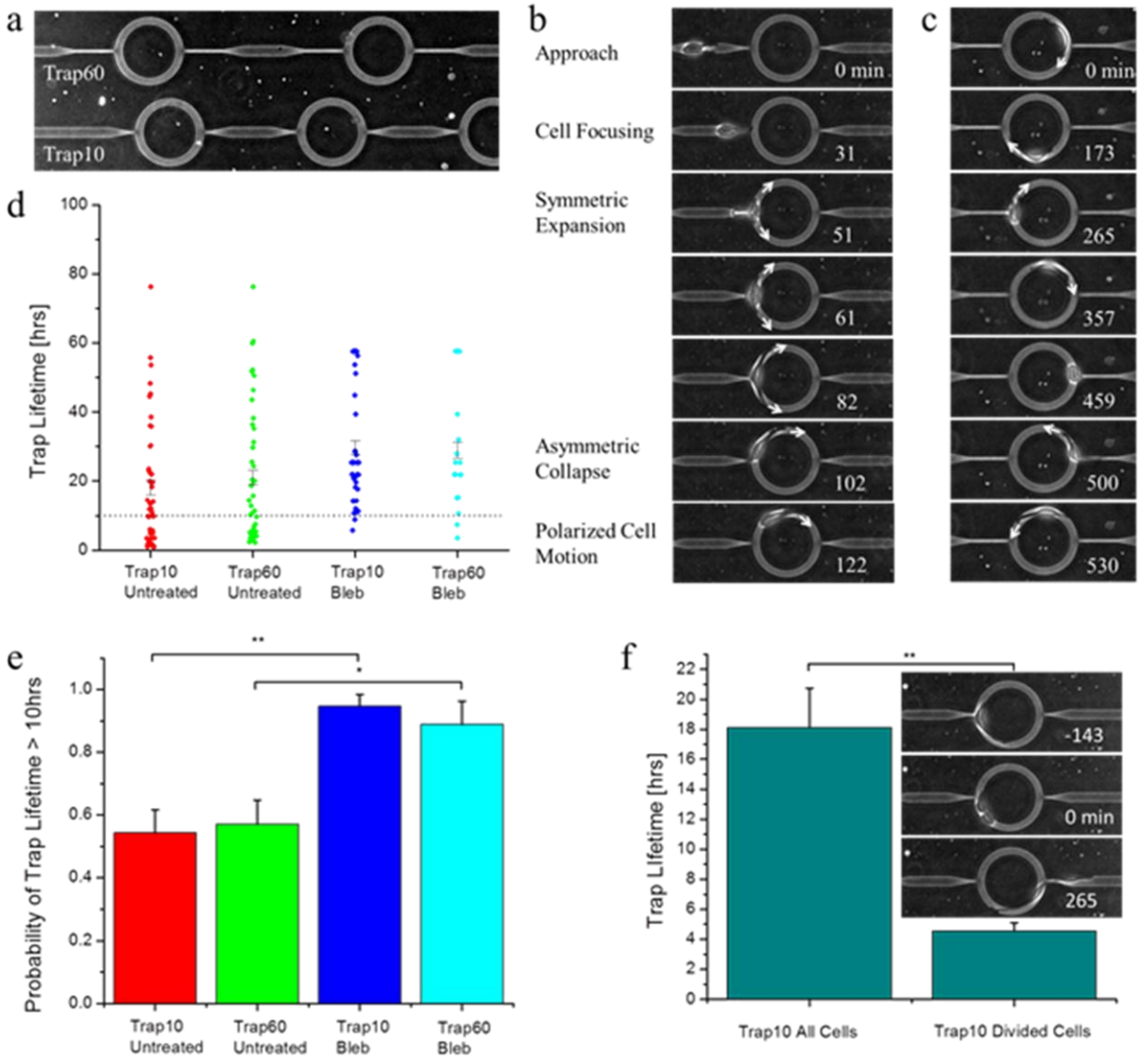

Fig. 5.4: (see caption on next page)

Figure 5.4: (Continued). Cell invasion dynamics in ring traps. a) Two different trap designs are incorporated in parallel, trap10 and trap60 with 10μm-long exits and with 60μm-long exits, respectively. The outer ring has a radius of 50μm. b) As a cell enters the ring trap, it is focused by the subnucleus-scaled constriction. Then it emerges into the trap and expands in a symmetric manner. Next, spontaneous symmetry breaking induces polarized cell migration. Arrows point in the direction of cell extension and migration. c) Cells that enter the trap often exhibit the phenomenon *iteratio ad nauseam*, during which the cells invade in circular patterns in a confined space rather than disseminate. Arrows point in the direction of cell migration. d) The trap lifetime of untreated cells is over 18 hours, and this is extended by Blebbistatin treatment (n = 46, 42, 38, 18 for trap10 untreated, trap60 untreated, trap10 Blebbistatin-treated, and trap60 Blebbistatin-treated cells, respectively, where n is the number of trapping events). The horizontal line denotes the 10 hour mark. Note that this data includes censored data points, *i.e.* the cells are either already in the trap at the beginning of the experiments or are still in the trap at the end of the experiments, so these measurements are under-estimates. e) The probability that a cell spends more than 10 hours in the ring trap is shown for trap10 and trap60 for untreated and Blebbistatin treated cells. This enables an assessment of the statistical difference between untreated and Blebbistatin-treated cells when including censored data. The probabilities are 0.54, 0.57, 0.95, 0.89 for trap10 untreated, trap60 untreated, trap10 Blebbistatin-treated, and trap60 Blebbistatin-treated cells, respectively, for the same data as in (d). Error bars are standard error of the mean (s.e.m.) calculated from the Bernoulli distribution. We note that censored data points under 10 hours (7 out of 151 data points from the raw data) were discarded in order to eliminate arbitrarily short trap lifetimes. f) Cell division promotes escape from the ring traps. Immediately after cell division, the first cell that escapes exhibits a trap lifetime of only around 4.5 hours (n = 21), in comparison to 18+ hours (n = 46) for the overall average in trap10. We again did not include censored data under 10 hours to eliminate arbitrary short trap lifetimes. We note however that for this data set, only 1 out of 68 data points fell in this category, and including that data point did not alter the statistical significance of our results. Also there were no censored data points for the cell escape after division data. * indicates $p < 0.05$ and ** indicates $p < 0.01$. All time stamps on time lapse image stacks are in minutes.

5.3 Conclusion

Cell behavior during invasion is a highly complex process that is not well understood. We created microfluidic devices that elicit the decision making process of cells when encountering mechanical asymmetries on the cell and subnucleus scale. By using well-defined geometries and features, we probed the path affinities of invasive cells and explored mechanical and molecular means of modulating these affinities. We demonstrated that dimensional and directional cues can bias cell invasion patterns, actomyosin inhibition can alter migratory decision making, and properly designed

mechanical asymmetries can promote the phenomenon *iteratio ad nauseam*. The devices and experiments shown here can help reveal more complex factors in the dynamics of invasion at the single-cell level.

Furthermore, we have demonstrated that purely mechanical factors in a 3D environment can induce complex cell behavior. This suggests that mechanically modulating tumor microenvironments may be a potential method in altering cancer invasion patterns, and we have shown a particular type of pattern that could trap invasive cells. Future work in developing tissue engineering methods that can strategically alter the architecture of the fibrillar meshwork of the tumor stroma, particularly based on preconceived modules such as the ring trap presented here, may be a new avenue in cancer therapy aimed at suppressing cancer dissemination. Additionally, the trap micropatterns, with its small footprint, may be converted into a micro-pill or particle format that could be injected into local tumor environments and serve as traps for invasive cells. In particular, previously we have shown that non-metastatic breast epithelial cells are less likely to permeate through subnucleus-scaled barriers than highly metastatic cells [12], so these patterns may be able to selectively trap the most aggressive cells. The devices and designs presented here illustrate a means to rapidly prototype mechanical modules that could impact cell migratory behavior and generate complex and tunable patterns of motility.

5.4 Methods

5.4.1 Cell culture

MDA-MB-231 cells were obtained from the National Cancer Institute Physical-Sciences in Oncology Centers (NCI PS-OC), originally from the American Tissue Culture Collection (ATCC). They were cultured at 37^{o}C without CO_2 supplement in

Leibovitz L-15 media (Life Technologies) with 10% fetal bovine serum (Atlanta Biologicals) and 1% Penicillin-Streptavidin (Life Technologies).

5.4.2 Device Fabrication

Devices were fabricated at the Cornell Nanoscale Science and Technology Facility (CNF). Standard photolithography followed by soft lithography was used to fabricate polydimethylsiloxane (PDMS) microfluidic devices. Briefly, SU8 resist was spun onto a wafer and exposed in a UV stepper aligner under a photomask with the designed patterns to create the mold master. PDMS was cast onto the master, crosslinked, and bonded to glass slides to create the final microfluidic devices.

5.4.3 Experiments and Analysis

Time lapse video microscopy was used to record cell invasion dynamics in the microfluidic channels, which were kept at 37^{o}C via a heating plate. Videos were recorded at 3.4 minutes per frame. Image analysis was performed manually on ImageJ. Data processing was performed using custom MATLAB code. For statistical analysis, Chi-square and student t-tests were used. Statistical significance is indicated by * and ** for $p < 0.05$ and $p < 0.01$, respectively. For Taxol (Cytoskeleton, Inc) studies, cells were incubated in 10μM Taxol for 7 hours prior to experiments. For Blebbistatin (Sigma-Aldrich) studies, cells were incubated in 50μM Blebbistatin for several hours prior to experiments.

5.5 Acknowledgements

The work described was supported by the Cornell Center on the Microenvironment and Metastasis through Award Number U54CA143876 from the National Cancer Institute. This work was performed in part at the Cornell NanoScale Science and

Technology Facility, a member of the National Nanotechnology Network, which is supported by the National Science Foundation (Grant ECS-0335765). Michael Mak is a National Science Foundation Graduate Research Fellow.

5.6 Supplementary Videos

SI Video 5.1: An MDA-MB-231 cell encounters the decision tree in pattern 1. It exhibits extensional dynamics that ultimately result in the cell choosing path 1 (the top path). Each frame is 10000x real time.

SI Video 5.2: As the cell encounters the decision tree in pattern 2, split extensions are generated, asymmetric collapse occurs, and finally the cell is polarized along path 2 (the bottom path). Each frame is 10000x real time.

SI Video 5.3: A Blebbistatin-treated cell navigates through the decision tree. The extensions appear thinner, the cell body is more rounded (likely due to less cell tension), and the cell exhibits a tethered-ball motile state. Each frame is 10000x real time.

SI Video 5.4: Taxol-treated cells typically are more rounded and have less migratory persistence. Here, a Taxol-treated cell struggles at the decision tree interface. Each frame is 10000x real time.

SI Video 5.5: An untreated MDA-MB-231 cell enters the ring trap. The subnucleus-scaled entrance focuses the cell and the cell expands symmetrically into the ring region. Eventually, symmetry breaks and the cell undergoes polarized migration. Each frame is 10000x real time.

SI Video 5.6: Mechanical asymmetries can suppress cell dissemination by confining cell trajectories within the ring region, inducing the phenomenon *iteratio ad nauseam*. Each frame is 10000x real time.

SI Video 5.7: Cells that divide in the ring trap tend to escape soon thereafter, indicating coupling dynamics between cell proliferation and cell invasion. Each frame is 10000x real time.

REFERENCES

1. M. J. Bissell and D. Radisky, Putting tumours in context, *Nat Rev Cancer*, 2001, 1, 46-54.
2. M. J. Paszek, N. Zahir, K. R. Johnson, J. N. Lakins, G. I. Rozenberg, A. Gefen, C. A. Reinhart-king, S. S. Margulies, M. Dembo, D. Boettiger, D. A. Hammer and V. M. Weaver, Tensional homeostasis and the malignant phenotype, *Cancer Cell*, 2005, 8, 241-254.
3. C. S. Chen, M. Mrksich, S. Huang, G. M. Whitesides and D. E. Ingber, Geometric Control of Cell Life and Death, *Science*, 1997, 276, 1425-1428.
4. W. R. Legant, A. Pathak, M. T. Yang, V. S. Deshpande, R. M. McMeeking and C. S. Chen, Microfabricated tissue gauges to measure and manipulate forces from 3D microtissues, *Proceedings of the National Academy of Sciences*, 2009, 106, 10097-10102.
5. Y. Zheng, J. Chen, M. Craven, N. W. Choi, S. Totorica, A. Diaz-Santana, P. Kermani, B. Hempstead, C. Fischbach-Teschl, J. A. López and A. D. Stroock, In vitro microvessels for the study of angiogenesis and thrombosis, *Proc. Natl. Acad. Sci. USA*, 2012.
6. M. H. Zaman, The role of engineering approaches in analysing cancer invasion and metastasis, *Nat Rev Cancer*, 2013, advance online publication.
7. A. F. Chambers, A. C. Groom and I. C. MacDonald, Dissemination and growth of cancer cells in metastatic sites, *Nature Reviews Cancer*, 2002, 2, 563-572.
8. S. Kumar and V. M. Weaver, Mechanics, malignancy, and metastasis: the force journey of a tumor cell, *Cancer and Metastasis Reviews*, 2009, 28, 113-127.
9. K. Wolf, I. Mazo, H. Leung, K. Engelke, U. H. v. Andrian, E. I. Deryugina, A. Y. Strongin, E.-B. Bröcker and P. Friedl, Compensation mechanism in tumor cell migration:mesenchymal–amoeboid transition after blocking of pericellular proteolysis, *The Journal of Cell Biology*, 2003, 160, 267-277.
10. D. Irmia and M. Toner, Spontaneous migration of cancer cells under conditions of mechanical confinement, *Integrative Biology*, 2009, 1, 506-512.
11. P. Friedl, K. Wolf and J. Lammerding, Nuclear mechanics during cell migration, *Current Opinion in Cell Biology*, 2011, 23, 55-64.
12. M. Mak, C. A. Reinhart-King and D. Erickson, Microfabricated Physical Spatial Gradients for Investigating Cell Migration and Invasion Dynamics, *Plos One*, 2011, 6.
13. M. Mak, C. A. Reinhart-King and D. Erickson, Elucidating mechanical transition effects of invading cancer cells with a subnucleus-scaled microfluidic serial dimensional modulation device, *Lab on a Chip*, 2013, 13, 340-348.
14. G. Mahmud, C. J. Campbell, K. J. M. Bishop, Y. A. Komarova, O. Chaga, S. Soh, S. Huda, K. Kandere-Grzybowska and B. A. Grzybowski, Directing cell motions on micropatterned ratchets, *Nature Physics*, 2009, 5, 606-612.

15. K. A. Kilian, B. Bugarija, B. T. Lahn and M. Mrksich, Geometric cues for directing the differentiation of mesenchymal stem cells, *Proceedings of the National Academy of Sciences*, 2010, 107, 4872-4877.
16. A. F. Straight, A. Cheung, J. Limouze, I. Chen, N. J. Westwood, J. R. Sellers and T. J. Mitchison, Dissecting Temporal and Spatial Control of Cytokinesis with a Myosin II Inhibitor, *Science*, 2003, 299, 1743-1747.
17. P. P. Provenzano, D. R. Inman, K. W. Eliceiri, S. M. Trier and P. J. Keely, Contact Guidance Mediated Three-Dimensional Cell Migration is Regulated by Rho/ROCK-Dependent Matrix Reorganization, *Biophysical Journal*, 2008, 95, 5374-5384.
18. R. Poincloux, O. Collin, F. Lizárraga, M. Romao, M. Debray, M. Piel and P. Chavrier, Contractility of the cell rear drives invasion of breast tumor cells in 3D Matrigel, *Proceedings of the National Academy of Sciences*, 2011, 108, 1943-1948.
19. C. M. Kraning-Rush, S. P. Carey, J. P. Califano, B. N. Smith and C. A. Reinhart-King, The role of the cytoskeleton in cellular force generation in 2D and 3D environments, *Physical Biology*, 2011, 8, 015009.
20. M. A. Jordan and L. Wilson, Microtubules as Target for Anticancer Drugs, *Nature Reviews Cancer*, 2004, 4, 253-265.
21. A. Takesono, S. J. Heasman, B. Wojciak-Stothard, R. Garg and A. J. Ridley, Microtubules Regulate Migratory Polarity through Rho/ROCK Signaling in T Cells, *Plos One*, 2010, 5, e8774.
22. R. J. Petrie, A. D. Doyle and K. M. Yamada, Random versus directionally persistent cell migration, *Nature Reviews: Molecular Cell Biology*, 2009, 10, 538-549.
23. L. P. Cramer, Forming the cell rear first: breaking cell symmetry to trigger directed cell migration, *Nat Cell Biol*, 2010, 12, 628-632.
24. A. van Oudenaarden and J. A. Theriot, Cooperative symmetry-breaking by actin polymerization in a model for cell motility, *Nat Cell Biol*, 1999, 1, 493-499.
25. M. Bornens, Organelle positioning and cell polarity, *Nat Rev Mol Cell Biol*, 2008, 9, 874-886.

CHAPTER 6

CONCLUSIONS

6.1 Summary

My research has resulted in the development of microfluidic systems to investigate cancer invasion dynamics and revealed the behavior of single-cells in engineered mechanical microenvironments. Physical spatial gradients in confined environments were demonstrated to induce transition dynamics in the migratory trajectory of invading cells. The MUSIC device and the incorporated subnucleus-scaled barriers were used to elicit interface effects of invasion, such as morphological changes in phenotype, cell division asymmetry, and single-cell invasion strategies. Stabilization of microtubules via taxol was shown to suppress cell permeation across mechanical barriers. Decision tree microchannels were developed that elucidated the impact of dimensionality and directionality in on cell behavior during invasion. Inhibition of myosin IIa in these channels altered the paths that invading cells took and thus can modulate invasion patterns. Ring traps were contrived and implemented that utilizes dimensional and directional asymmetry to induce repetitive motions in invading cancer cells, thus suppressing dissemination via *iteratio ad nauseam*. Additionally, a serial microfluidic micropipette was introduced that adds another dimension towards understanding mechanical cell invasion by probing the passive responsivity of cells to repeated deformations.

All of these efforts now set the stage for exciting future work that can further improve our understanding of cancer metastasis and help strategize new therapeutic mechanisms against cancer progression.

6.2 Future Work

6.2.1 Strategies in Tissue Engineering

Concepts derived from these microfluidic systems, particularly in regard to the mechanical modulation of invasive cells through microenvironmental patterns and physical cues, can be translated into strategies in targeting physiological environments. Physicochemically inducing asymmetric patterns, similar to the ring traps in Chapter 5, in the local tumor environment could potentially suppress the metastatic process. Changing the tumor surroundings, rather than only targeting tumor cells with drugs or therapy, can modulate the behavior of invasive cells and may be a new avenue of suppressing cancer progression. This is consistent with the emergence of studies demonstrating the importance of cell-environment interactions [1, 2].

6.2.2 Drug Screening

Heterogeneity and metastasis are two critical challenges in the treatment of cancer. However there are currently no standardized methods that can gauge these properties in order to discover appropriate therapies. With microfluidics, high throughput single-cell invasion assays can be developed and integrated with current high throughput robotic drug development infrastructures in order to screen for new compounds or repurpose existing drugs. By considering cell-based functional invasion assays at the single-cell level, both heterogeneity and metastasis can be appreciated in much greater depth at the *in vitro* drug screening stage.

6.2.3 Emerging Physics in the Coupling of Cell Invasion and Proliferation

Cell proliferation and invasion have traditionally be separate fields with distinct research efforts. However, as shown in Chapter 5, invasion and escape from "trap

environments" may be strongly influenced by cell division. For instance, when cells divide while they are in the ring trap undergoing *iteratio ad nauseam*, they break from the repetitive motion and exit the trap despite mechanical asymmetries that otherwise bias cell behavior. Additionally, as cells grow and become larger relative to the pore or barrier size, they are mechanically more obstructive during their invasion across subnucleus-scaled barriers. Thus, the invasiveness of any individual cell may be cell cycle-dependent. Cells that are trapped may become free after cell division, and cells that are highly invasive may become suppressed when they are progressing through the growth part of the cell cycle. Next generation device designs that incorporate both growth and invasion chambers can help unveil the dynamic coupling between cell proliferation and invasion. This may help identify additional modulators of cancer dissemination. Increasing the growth phase of cancer cells while prolonging the proliferation rate may suppress invasion by increasing the size of cells over finite time intervals. Strategic dosing dynamics of cell growth and invasion drugs, such as Taxol, may help regulate the dissemination process in a more subtle but potentially more effective manner.

6.2.4 Drug Resistance

Once cancer is disseminated, it requires systemic treatments, particularly chemotherapy. Chemotherapy, however, almost always fails after prolonged treatment due to the cancer cells' acquisition of drug resistance. The fundamental dynamics in the emergence of resistance is not well understood. To begin to uncover this process, we can consider several emerging and related properties about cancer – heterogeneity and evolution. The principles of Darwinian evolution, *i.e.* survival of the fittest, have recently been applied to describe cancer progression and evolution

against treatments. A basic conceptual and mathematical framework has been developed that states:

$$\frac{\partial u}{\partial t} = \sigma^2 \frac{\partial G}{\partial u} \tag{6.1}$$

where u is the cell phenotype, t is time, σ is the phenotypic diversity of the population, and G is the fitness function [3]. Essentially, the evolutionary rate, *i.e.* the change in phenotype over time of the cancer cells, is dependent on the existing diversity in the population and the sensitivity of the fitness function to changes in phenotypes. When a drug is applied, the evolutionary stress is increased such that the fitness function is highly sensitive to changes in phenotypes, so the evolutionary rate is high. This can ultimately lead to the somatic evolution of resistant phenotypes and/or the persistence and proliferation of heterogeneous subpopulations that are not responsive to the given treatment. Additionally, evolution selects for phenotypes, so many different genotypes could confer resistance against a particular chemotherapeutic. All of this suggests that existing genomics-based approaches that identify specific genetic biomarkers for targeted cancer therapy may be fundamentally flawed, as they do not account for heterogeneity, evolution, and drug resistance. For instance, the somatic evolution or pre-existence of subpopulations of cells that do not express a targeted biomarker or are otherwise resistant could eventually render any particular treatment futile. Furthermore, existing methods in studying drug resistance, as with most traditional methods in biology, are based on bulk population studies, which cannot distinguish many fundamental characteristics of evolutionary resistance. For instance, while bulk studies can potentially measure $\partial u/\partial t$ on average for the entire population, they cannot measure it for each single-cell lineage. Thus, the contributions to drug resistance from somatic evolution and pre-existing heterogeneities are difficult to

distinguish. The fundamental dynamics that govern the rise of the dominant resistant phenotype are masked.

These existing gaps in current methods and techniques present a unique opportunity for single-cell microfluidics. By creating highly parallel single-cell microchambers, single-cells and their subsequent single-cell progenies can be tracked independently, enabling the emergence of drug resistance to be measured at its very onset and in high biological resolution, *i.e.* resistant lineages can be identified at their very emergence

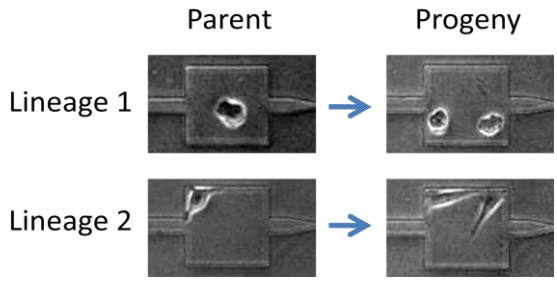

Fig. 6.1: A device design integrating growth and invasion chambers. Certain motile and morphological attributes are passed on from parent to daughter cells. Lineages 1 and 2, both from the same MDA-MB-231 bulk population, display different inheritable phenotypes. Single-cell lineage tracking is facilitated by parallel chambers. The width of the growth chamber is 80µm.

and traced to a single parent cell. These studies can reveal the fundamental dynamics that govern drug resistance, which may be different across different cancer types, and appropriate therapies and dosing schemes can be developed to not only suppress cancer progression but also reduce resistant behavior.

The MUSIC device, developed in chapter 3, and other single-cell microchamber designs can be applied to study single-cell progenies. Heterogeneities in invasive phenotype, proliferation dynamics, and drug responsivity are among the emerging properties that could be elucidated and contribute towards a more comprehensive

understanding of the critical elements in cancer. Figure 6.1 demonstrates an implementation of integrated microfluidic growth and invasion chambers used to track the morphological phenotype of single cell lineages.

6.3 Concluding Remarks

There are many opportunities at the interface between cancer research and microfluidics that can help unveil critical factors in cancer progression that are not fully addressed by conventional techniques, particularly genomics-based approaches. Higher resolution biology in high throughput is required to fully understand the dynamics of cancer, from heterogeneity to metastasis to drug resistance. Microfluidics provides the channel for making this possible. While conventional biology is focused on static and bulk population studies that mask the heterogeneity, plasticity, and dynamicity that are characteristic of cancer, microfluidic approaches can conduct high throughput single-cell studies of critical functional events, such as cell invasion. In the future, the integration of high resolution, high content, and high throughput single-cell, multi-cell, cell-microenvironment, and cell-body-on-chip studies in conjunction with genomics, proteomics, metabolomics, secretomics, and *pan*-omics will ultimately provide the complete picture of cancer that will enable the engineering of the most sophisticated treatments that are humanly possible.

REFERENCES

1. M. J. Bissell and D. Radisky, *Nat Rev Cancer*, 2001, **1**, 46-54.
2. M. J. Paszek, N. Zahir, K. R. Johnson, J. N. Lakins, G. I. Rozenberg, A. Gefen, C. A. Reinhart-king, S. S. Margulies, M. Dembo, D. Boettiger, D. A. Hammer and V. M. Weaver, *Cancer Cell*, 2005, **8**, 241-254.
3. R. J. Gillies, D. Verduzco and R. A. Gatenby, *Nat Rev Cancer*, 2012, **12**, 487-493.